Application of Semianalytic Satellite Theory
to Maneuver Planning

by

Carole Ann Jablonski
B.S. Astronautical Engineering,
United States Air Force Academy
(1989)

Submitted in Partial Fulfillment
of the Requirements for the
Degree of
Master of Science
in Aeronautics and Astronautics
at the
Massachusetts Institute of Technology
June, 1991
© Carole Ann Jablonski, 1991

Signature of Author _____
Department of Aeronautics and Astronautics
May, 1991

Certified by _____
Dr. Paul J. Cefola
Thesis Supervisor, CSDL
Lecturer., Department of Aeronautics and Astronautics

Accepted by _____
Professor Harold Y. Wachman
Chairman, Departmental Graduate Committee

1

Application of Semianalytic Satellite Theory
to Maneuver Planning

by

Carole A. Jablonski

Abstract

The high precision mean element (semianalytic) satellite theory developed at Draper Laboratory is more efficient than conventional numerical methods and more accurate than the current generation of analytic theories. This efficiency, along with its portability to a variety of computing environments makes the semianalytic theory a natural choice for maneuver planning applications. These applications will become more important in the future as the capability of individual platforms to maneuver, the number of platforms in space, and the requirements for rapid response to requests for data all increase. The application of semianalytic satellite theory to an Earth Observation satellite in an orbit similar to that expected for LANDSAT 6 is investigated. Orbit constraints such as sun synchronous, repeat ground track, frozen orbit, and non-impulsive maneuver capabilities are included in this analysis. Applications of maneuver planning to past and future satellite missions that include at least two of the listed orbit constraints are discussed.

Since atmospheric drag is the primary uncertain disturbing acceleration to the nominal satellite orbit, upper and lower limits of a density confidence interval were determined. Two methods were analyzed; it was found that using forecast and actual solar flux and geomagnetic activity data from the years 1986-1990 resulted in a conservative but realistic confidence interval. The upper limit is utilized to compute the time of the orbit adjust burn and the lower limit of the density is used to calculate the magnitude of the orbit adjust burn. These limits are necessary so that the ground track boundaries are not exceeded.

Thesis Supervisor: Dr. Paul J. Cefola
Title: Lecturer, Department of Aeronautics and Astronautics
        Section Chief, The Charles Stark Draper Laboratory, Inc.

3

Acknowledgements

Carole A. Jablonski, Lt., USAF

Dedicated to Francis Rodakowski

Contents

List of Figures

12

List of Tables

Chapter 1

Introduction

1.1 Background

This thesis focuses on the orbital maneuver planning process for Earth Observation satellite missions. Since the launch of the first Earth Observation satellite, TIROS - 1, in April of 1960, over 135 satellites have been launched with specific missions to gain data on the Earth [69]. Typical functions of Earth Observation satellites encompass a broad range including:

- Weather
- Climate
- Meteorology
- Land Survey
- Agriculture
- Forestry
- Disasters (Alarm, Relief Planning)
- Hydrology
- Oceanology

A majority of the measurements needed by these different missions are common. To attain these measurements, there are two basic classes of instruments, passive and active. The basic passive instrument is the radiometer which measures the reflected radiation from the Earth within some frequency band and polarization. The

microwave radiometer detects sea ice conditions and cover in day or night. It is only slightly affected by cloud cover. The medium resolution visible/infrared radiometer can detect sea surface temperatures, sea ice conditions, surface reflectivity, ocean color, and classify vegetation through cloud cover. The high resolution imager/radiometer, like the thematic mapper of LANDSAT 4/5, can determine changes in vegetation, ice motion, terrain mapping, surface melting of snow and ice, and local winds. In the active instrument category, the most common is the radar altimeter, which measures the range to the Earth's surface. The scatterometer determines sea surface wind vectors from the wave pattern generated by the wind. The synthetic aperture radar, like on SEASAT and ERS-1, is not affected by lack of light or cloud cover. It can also penetrate shallow ice or snow to determine surface features below. This precise instrument not only detects ice and fine scale sea surface roughness, but also maps the Earth's surface in all weather and classifies rock, soil, surface wetness, and vegetation. One less common active instrument is the Lidar, a laser altimeter [84]. Some of the instruments used frequently and their functions are listed in Table 1.1 [3,22,89].

Table 1.1. Earth Observation Instrument Function

Instrument	Function
Altimeter	• Surface topography • Wave direction • Ocean wave height
Microwave imager	• Wind speed • Precipitation • Arctic ice cover, thickness, and age
Microwave radiometer	• Surface temperatures
Synthetic aperture radar	• Image of surface
Scatterometer	Surface wind

The general orbital characteristics of these satellites repeat due to the similarity in the instrument constraints. There are trade-offs and relationships between the desired satellite functions, the physical and geometrical constraints in the satellite structure, the specific limitations of the vehicle subsystems, and the properties of orbital motion and satellite dynamics [52].

A general Earth Observation satellite will usually have a mission lifetime of three to five years. The coverage of the Earth is usually global, but may be constrained for coverage up to a specified latitude. Most land observation satellites have coverage constraints between 55° S to 75° N latitude due to the distribution of the Earth's land mass. An orbit of 75° inclination covers the Earth's land mass and leaves only the extreme north and south latitudes unobserved. Other coverage constraints may include a ground track that repeats itself. This allows instruments to return to re-examine a certain point of the Earth. A repeat ground track allows an easily predictable pattern of coverage and an opportunity to make direct comparisons between observations taken at regular intervals for the locations covered. There is a trade-off between the frequency of re-examination and the degree of global coverage. The degree of Earth coverage is also constrained by the instrument observation swath, or field of view, over the Earth's surface as the satellite moves in its orbit. The swath coverage of the Earth is determined by the displacement of the swath, ie. in the ground track, over time. The primary variable in determining the swath width of an instrument is the altitude of the satellite. By raising or lowering the mean altitude of the satellite orbit, the swath width respectively decreases or increases. The size of the orbit may also be determined by the resolution needed. If the instrument, itself, can not be improved to increase resolution, the mean orbit altitude may be decreased to meet the resolution constraints. But because of the trade-off between mission lifetime and instrument resolution, the lowering of the mean orbit altitude increases atmospheric

drag experienced, thus decreasing mission lifetime or increasing orbital maintenance requirements. In addition, lowering the mean altitude of the satellite decreases the ground station contact time, therefore decreasing the amount of data transferred to or from the satellite [54]. The conventional Earth Observation satellite orbit is usually near circular to ameliorate altitude changes that may be sensed by on board instruments over the observation swath. In addition, the various aspect angles needed by instrument observations may be a constraint on the coverage characteristics of an Earth Observation satellite. The instruments that attain these various aspect angles must be placed on board the satellite so that the observations are not contaminated by the spacecraft structure. The illumination of the Earth and/or the satellite may be a deciding factor in determining the orbit. The existence of visible light sensors on the spacecraft may cause a sun synchronous orbit to be desired for constant illumination conditions. As the seasons change, the solar incidence angle has long periodic changes revealing landscape and terrain features on the surface for a sun synchronous orbit. Also, if a satellite's power is solar generated, a sun synchronous orbit can minimize eclipsing of the solar wings. The number and placement of sensors and experiments may constrain the type of booster used, or the booster weight and configuration limits may constrain the instruments themselves. The orbital maintenance predicted for a satellite in orbit may constrain the number of solar cells on the satellite. Since larger solar wings create a greater amount of drag, this may decrease the lifetime or increase the orbital maintenance needed. Another limit in maintenance burns is the maximum velocity of the thrusters given by the Rocket Equation:

$$\Delta v_{max} \approx g I_{sp} \ln \left(\frac{W_{init}}{W_{final}} \right) \tag{1.1}$$

where g is the gravitational acceleration of the Earth, I_{sp} is the specific impulse of the thruster fuel, W_{init} is the initial weight of the spacecraft at the beginning of the

18

maneuver, and W_{final} is the final weight of the spacecraft after the maneuver [52].

To fully understand the orbital requirements of Earth Observation systems, working definitions of the terms sun synchronous, repeat ground track, and frozen orbit concept are needed. The detailed discussion and algorithms associated with these concepts will be addressed in Chapter 4. Here, a brief preview of these concepts is provided.

A sun synchronous orbit keeps the orbit plane at a constant angle to the sun by using the geopotential perturbations of the Earth to move the line of nodes westward along the equator approximately one degree per day. The line of nodes is defined as the intersection of the orbit plane and the Earth's equator. Through the application of the Earth's geopotential to Lagrange's Planetary Equations, the mean nodal rate is calculated by a formula from Kozai where the elements are assumed to be mean elements in a secular sense [18]:

$$\frac{d\bar{\Omega}}{dt} = -\frac{3}{2}J_2 \left(\frac{R_e}{a(1-e^2)}\right)^2 \sqrt{\frac{\mu}{a^3}} \cos i \qquad (1.2)$$

where $\bar{\Omega}$ is the mean longitude of the ascending node, the angle of the line of nodes from the vernal equinox. The variable J_2 is the harmonic coefficient of the Earth's oblateness equal to 1.08263×10^{-3}. The mean equatorial radius of the Earth, denoted R_e, is equal to 6378.135 km and the gravitational parameter of the Earth, μ, is 398601.2 km^3/sec^2 [4]. The exact values of these parameters depend on the gravity model employed; therefore the values stated here are approximate. The semi-major axis, a, the inclination, i, the longitude of the ascending node, Ω, and the eccentricity, e, of the orbit are variables in the common Keplerian orbital element set. For a more detailed description of orbital elements, see Appendix A. By setting the nodal rate equal to 360° per year, the solution for sun synchronous orbital elements can be determined from Equation 1.2. To guarantee that the line of nodes moves at the

correct rate, a sun synchronous Earth Observation satellite is usually in a slightly retrograde orbit with an altitude of approximately 200 to 1000 nautical miles (370 to 1852 km).

A satellite ground track is defined as the locus of points traced out on the Earth's surface directly beneath the spacecraft orbit. This ground track does not normally repeat itself, ie. retrace a previous orbit's ground track, by reason of the Earth rotating underneath the satellite orbit while the line of nodes rotates around the Earth's equator due to perturbations. A commensurability condition for a repeat ground track may be determined by using an equation from Baxter [5]:

$$2\pi N = M(\omega_e - \dot{\Omega})P_N \tag{1.3}$$

where N is the number of nodal days until the ground track repeats, M is the number of orbits in the repeat cycle, ω_e is the approximate constant rotation rate of the Earth, $\dot{\Omega}$ is the rotation rate of the line of nodes, and P_N is the nodal period of the satellite. A nodal day is defined as the time for the Earth to rotate 360° with respect to the line of nodes. A solar day is defined as the time for the Earth to rotate 360° with respect to the Earth-Sun line. If the satellite orbit is sun synchronous, a solar day is approximately the same as a nodal day since the line of nodes is at a constant angle to the sun. The nodal period depends mainly on the Keplerian period, orbit inclination, and to a lesser extent the orbit eccentricity. If the satellite is near circular, ie. eccentricity is approximately zero, the equation for the nodal period is [78,18]:

$$P_N = P_k \left[1 - \frac{3}{4}J_2 \left(\frac{R_e}{a}\right)^2 (6 - 5\sin^2 i)\right] + O(e^2) \tag{1.4}$$

where P_k is defined as the Keplerian (two body) orbital period [4]:

$$P_k = 2\pi\sqrt{\frac{a^3}{\mu}} \tag{1.5}$$

where a is the semi-major axis and i is the inclination and both values are taken at the node crossing. As previously stated in Equation 1.2, the variable J_2 is the harmonic coefficient of the Earth's oblateness equal to 1.08263×10^{-3}, the mean equatorial radius of the Earth, denoted R_e, is equal to 6378.135 km, and the Earth's gravitational parameter, μ, is 398601.2 km^3/sec^2. Again, these values are approximate and dependent on the actual gravity model used. A repeat ground track orbit is advantageous because it allows observations of areas of interest to be regularly scheduled.

The frozen orbit concept sets the argument of perigee to $\pm 90°$ and the eccentricity to a determined small nominal value. This configuration causes the J_2 and odd numbered harmonics of the Earth's gravitational field to cancel one another causing the argument of perigee to oscillate around the nominal value if it is perturbed. By setting the argument of perigee to $\pm 90°$, the eccentricity oscillates around its set nominal value since the lower order geopotential perturbations in the eccentricity depend on the cosine of the argument of perigee. The frozen orbit concept provides passive eccentricity and argument of perigee control. In addition, it minimizes spacecraft altitude variations at all latitudes since the perigee location is nearly constant [61].

The optimal compromise between these parameters to accomplish the Earth Observation mission is created using two body orbital mechanics plus the oblateness of the Earth to identify nominal mission orbits. Then, other orbital perturbations are added in to determine if the candidate orbit will realistically succeed. By determining how this orbit will change over time, the maintenance maneuvers needed may be accurately planned before launch to determine the fuel and maneuver schedule for a successful mission. This candidate orbit must be feasible in terms of the maintenance required and its accessibility for the launch vehicle expected. The maintenance needed must not be too expensive in terms of fuel weight for the desired mission in addition to not interfering with the observations by the instruments on board the

spacecraft. If any one of these constraints is violated, a new nominal orbit must be determined and the orbit analysis cycle repeated.

1.2 Maneuver Planning for Single Satellites

There are several past and future Earth Observation satellite applications that jointly utilize at least two of the following concepts: sun synchronous, repeat ground track, and frozen orbit. Past missions include the 1978 precursor SEASAT, the LANDSAT 4/5 missions in 1982 and 1984 respectively, the NROSS program of 1986 that was killed prematurely, and GEOSAT from 1986 to 1990. Even though NROSS was not launched, it motivated several important analytical efforts and is considered here. In addition, there are several future programs that will follow similar orbits. Among these are ERS-1, LANDSAT 6, TOPEX, and EOS. A more specific outline of these missions follows.

1.2.1 SEASAT

After SEASAT's launch on June 26, 1978, NASA proved that oceanographic parameters could be measured from a satellite observatory. Its accurate observations with a radar altimeter and microwave sensors included ocean surface temperatures, winds, waves, sea ice, currents, and atmospheric water content [21,71,89]. SEASAT was designed for a one year life time with the first two months used to insert the satellite in orbit and calibrate the instruments. This initial orbit was an exact three day repeat ground track, renewing every 43 orbit revolutions. This ground track passed over the laser ranging site on the island of Bermuda to calibrate the altimeter. The rapid global sampling achieved in this orbit also was advantageous for calibrating the other instruments on board SEASAT. In mid-August to accomplish the mission objectives, the orbit was altered to a near 'Cambridge' orbit with a repeat cycle that

lasted 17 nodal days or 244 orbit revolutions [69,89]. Due to a malfunction in the power subsystem, SEASAT failed on October 9, 1978 [3]. The mean orbital elements of SEASAT while it was successfully in orbit are stated in Table 1.2 [21,89].

Table 1.2. Orbital Elements for SEASAT

Mean Keplerian Element	SEASAT Injection	SEASAT Mission
semi-major axis, a	7168.3 km	7173.6 km
eccentricity, e	≈ 0.0008	≈ 0.001045786
inclination, i	108°	108°
argument of perigee, ω	90°	90°

These orbital elements supported the two separate repeat ground tracks in a frozen orbit condition. The mission orbit mapped 95% of the Earth's global oceans every thirty-six hours [69]. The results achieved before SEASAT failed demonstrated the feasibility and necessity of using satellite observations to obtain global information.

1.2.2 LANDSAT 4/5

The Earth observation satellites, LANDSAT 4 and LANDSAT 5, were both launched from the Western Test range on Delta 3920 launch vehicles [42]. Both LANDSAT 4 and 5 had two instruments to make observations of the Earth. The multi-spectral scanning radiometer and the high resolution thematic mapper were used to take surface pictures of the Earth [69]. There were many applications for the observations from the LANDSAT program: agribusiness, geology, forestry, disaster assessment/engineer planning, hydrology, land use and regional planning, range management, and cartography [20]. After LANDSAT 4 encountered difficulties in returning data from its thematic mapper, its multi-spectral scanner was used to obtain data for foreign ground stations while LANDSAT 5 became the global provider for thematic mapping data [69].

LANDSAT 4 was put into orbit first in July of 1982, and then LANDSAT 5 followed on March 1, 1984. LANDSAT 5 was put in the same orbit and phased 180° with LANDSAT 4 so that their period of world coverage was halved. Together LANDSAT 4 and 5 form a two satellite constellation but each is treated as an individual satellite. This is done by maintaining each satellite in a sun synchronous, repeat ground track, frozen orbit [42,69]. The orbit inclination maintenance preserves the sun synchronous orbit which maintains the nodal period needed for a repeat ground track. The repeat ground track maintenance, within ±10 km, preserves the common orbit that the satellites share and the phasing between the two satellites. The frozen orbit concept allows for passive maintenance of the eccentricity and argument of perigee. The frozen orbit concept also favors ideal conditions for the instruments on board since the altitude variations are minimized [49]. Both satellites are in a 16 day repeat ground track cycle. Each satellite achieves global coverage in one 16 day repeat cycle, or every 233 revolutions of the satellite in orbit. Since LANDSAT 5 is phased 8 days from LANDSAT 4, there is global coverage every 8 days if both satellites are operational. The repeat ground track, sun synchronous, and frozen orbit is achieved by the orbital elements shown in Table 1.3 [42].

Table 1.3. Orbital Elements for LANDSAT 4/5

Keplerian Element	LANDSAT 4/5 Value
semi-major axis, a	7077.8 km
mean eccentricity, e	≈ 0.0012
inclination, i	98.2°
argument of perigee, ω	90.0°
equatorial crossing time	0930-1000 hours local time

Orbital perturbations cause these nominal orbital elements to vary from their initial values. To predict the frequency of the altitude and inclination adjust burns,

LANDSAT mission analysis used a Cowell propagator to generate an accurate prediction of the LANDSAT 4/5 orbit [42]. Atmospheric drag is the primary perturbing force for a satellite in a low altitude orbit. Since the in-plane force of drag causes the satellite to lose energy, the satellite loses orbital altitude and the satellite period decreases, see Equation 1.5. This can be viewed as the satellite arriving at its equator crossing too early. This does not allow the Earth enough time to rotate sufficiently for the ground track to exactly repeat, thus the ground track appears to drift eastward. To keep the ground track within its required boundaries of ± 10 km, an altitude adjust burn must be done approximately every 50 days for a median value of atmospheric drag. This median atmosphere was based on the average of the estimated extremes of the solar flux values during the mission. A graphical view of this maneuver estimation can be viewed in the *LANDSAT-D Orbit Adjust Criteria* [49]. The atmospheric drag is determined mathematically through an atmospheric model and the prediction of the solar flux values in the future. These solar flux values are difficult to forecast and are discussed fully in Chapter 5. If the solar flux is less than predicted after the maneuver, the ground track may drift beyond the western boundary requiring a retrograde maneuver (a 180° spacecraft yaw). Therefore, the altitude adjust burns must be conservative in estimating the burn magnitude [42].

The inclination drift is primarily due to solar gravitational forces acting on the satellite. These forces are not in the orbital plane and cause the orbit to become more polar. This change in inclination affects the sun synchronous condition of the orbit, thus necessitating adjustment burns [49]. The orbital inclination after orbit injection was set to a value such that it was 18 months after launch that the first inclination adjustment burn was needed. After that, an inclination burn was anticipated to be needed every 8 months [42].

1.2.3 Navy Remote Ocean Sensing System (NROSS)

The NROSS mission, a derivative of the SEASAT mission, was to map sea surface topography by measuring mesoscale variations in the sea surface height. Sea surface topography is computed as the residual of the reference sea geoid and the ocean surface height detected by the on board altimeter. This altimeter is identical to the altimeter presently on board the GEOSAT spacecraft [3]. The sea geoid is the expected ocean surface affected only by the Earth's gravitational potential. This includes the reference ellipsoidal earth plus the sea height variation due to the tides. An illustration of the definition of sea surface topography can be seen in Figure 1.1. The value, **H**, is the observed altimeter height of NROSS while **alt** is the radial altitude of the satellite independently determined from the altimeter height. The difference between these two values gives the ocean topography [68]. Since the ocean
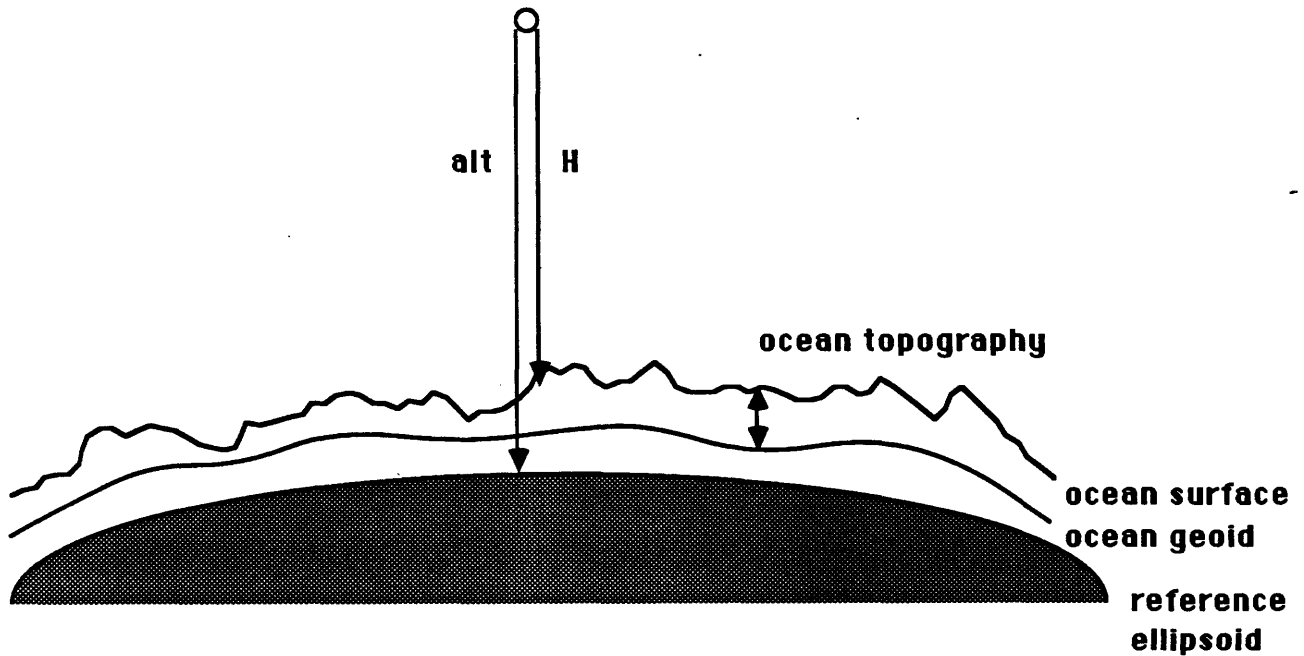
Figure 1.1. Illustration of Sea Surface Topography

geoid is not accurately known over most regions, NROSS was to primarily track changes in rather than the absolute value of the ocean topography [68].

The NROSS spacecraft was a scaled down version of the cancelled National Oceanic Satellite System (NOSS) from 1981. The NOSS participants, ie. NASA, Navy, and National Oceanic and Atmospheric Administration (NOAA), were joined again under the leadership of the Navy to form the NROSS program in 1985. The Air Force also joined in to provide ground station and tracking facilities [71]. In one view, the NROSS spacecraft was to be a NOAA-D platform bus with Defense Meteorlogical Satellite Program (DMSP) communications and telemetry processing subsystems. The NROSS instruments were to be added on this bus to accomplish the mission objectives [22]. The instruments scheduled to be on board NROSS were the altimeter previously mentioned, a modified scatterometer from SEASAT, a new low-frequency radiometer, and a special sensor microwave/imager (SSM/I) from DMSP rather than the synthetic aperture radar from SEASAT [3,69].

The optimal orbit called for a sun synchronous and stringent repeat ground track orbit [18]. The repeat ground track lessened altimeter bias from ocean geoid height at points where the current ground track crossed over a previous ground track [68]. Originally, a 0.001 maximum mean eccentricity constraint was specified. This near circular orbit was to be maintained throughout the mission to avoid unnecessary altitude variations in instrument observations of the sea surface height. The on board altimeter experiment needed the support of a rigorous repeat ground track and the scatterometer required minimal altitude variations to maintain stable locations for the sea surface cells. Using the frozen orbit concept increased the nominal mean eccentricity to 0.00115 but minimized altitude variations throughout all latitudes of the orbit. The frozen orbit concept also had an additional advantage by decreasing the amount of orbit maintenance through passive control of the eccentricity and

27

argument of perigee. Hence, a frozen orbit geometry was adopted, since the frozen orbit advantages pertaining to decreased orbit maintenance and increased instrument performance outweighed the small increase in maximum mean eccentricity. The orbital elements prescribed for the NROSS mission are summarized in Table 1.4. These

Table 1.4. Orbital Elements for NROSS

Keplerian Element	NROSS Value
semi-major axis, a	7198.65 km
mean eccentricity, e	0.00115
inclination, i	98.697°
argument of perigee, ω	90.0°
equatorial crossing time	0530 hours local time

elements insured a frozen, sun synchronous orbit and a repeat cycle of 19 nodal days, or 270 orbit revolutions [61].

NROSS was to be launched on a Titan II launch vehicle near the maximum of the 11 year solar cycle, which was expected in 1990. These maximum solar flux values were expected to create high levels of atmospheric drag during the three to four year mission lifetime of NROSS [34,3,71]. In-plane, along track burns maintain both the semi-major axis and the orbital eccentricity and are designed to simultaneously preserve both the frozen orbit geometry and meet the repeat ground track requirement. Because of high estimated solar activity, the semi-major axis decay due to atmospheric drag was the expected dominant cause of ground track drift. Because of this drift, altitude adjust burns were predicted to take place every 10-25 days [33]. In addition, inclination drift causes ground track error at extreme latitudes. It was determined in the NROSS orbit adjust strategy that a bound on the inclination of ±0.009° would maintain the ground track at the high latitudes [34]. Additional ground track drift was attributed to changes in the nodal rate and the mean eccentricity.

28

The NROSS project had its procurement cancelled in December of 1986, and the entire project cancelled in 1987 [61]. The mission objectives of NROSS have been split up and partitioned to other satellite systems, ie. scatterometer on EOS, altimeter on SPIN satellite, and an altimeter and radar scatterometer on DMSP Block 6 [73].

1.2.4 GEOSAT

The United States Navy GEOSAT spacecraft was launched March 12, 1985, on an Atlas E launch vehicle to complete geoid mapping initialized by SEASAT in 1978 [53]. After this mission was accomplished, GEOSAT performed a transition burn between October 1, 1986 and November 6, 1986, from a geodetic to an oceanographic phase of the mission. This second phase is referred to as the GEOSAT Exact Repeat Mission (ERM) [30]. The only instrument on board was a highly redundant altimeter. Although this instrument had a narrow swath width causing the data collected to be exiguous, the altimeter observed ocean wave height and direction and tracked ocean surface topography. The wind speed and direction could be determined from ground processing of the received back scatter cross section [3,53]. The altimeter data was also used to create a dense grid of observations required to improve the model of the Earth's gravitational potential [69]. The GEOSAT ERM ground track repeated every 244 orbits or every 17 nodal days and was maintained until 1990 within ± 1 km. The research initialized by GEOSAT will be followed on by SALT in 1991 [30].

GEOSAT measured the time dependent oceanographic features, ie. rings and eddies, and the time independent features of circulation, ie. gulf stream, in addition to the sea geoid height. It was necessary to implement a stringent repeat cycle specification to minimize the effects of sea geoid uncertainty on the determination of ocean variability, by allowing the sea geoid to be averaged out of the satellite altimeter data [53]. GEOSAT also utilized the frozen orbit concept resulting in a constant

altitude history from orbit to orbit since the argument of perigee and eccentricity were stable [79].

To maintain the repeatable, frozen orbit condition, the ERM orbital elements are summarized in Table 1.5. These elements gave GEOSAT a nodal rate of 2.0517209°/day

Table 1.5. Orbital Elements for GEOSAT ERM

Keplerian Element	GEOSAT ERM Value
semi-major axis, a	7173.6 km
mean eccentricity, e	0.0007971
inclination, i	108.04397°
argument of perigee, ω	91.493632°
longitude of the ascending node, Ω	49.788597°

and a nodal period of 6037.5601 seconds [79].

GEOSAT maneuver research determined that a change in the semi-major axis is most efficient with an along track burn and can be changed independent of the other Keplerian orbital elements if equal burns are done at any true anomaly, f, and $f \pm 180°$. A change in the eccentricity of the orbit is also most efficient with an along track burn and can be changed independent of the other elements with equal and opposite burns at $f = 0°$ and $f = 180°$. A change in the argument of perigee is also most efficient with a burn in the along track direction and independent of the other elements with equal and opposite burns at true anomalies of $f = \pm 90°$. A simultaneous change in the argument of perigee and eccentricity can be achieved independent of a change in the semi-major axis with along track burns of equal and opposite magnitudes at true anomalies, f and $f + 180°$, where f is determined by the equation:

$$f = -\omega + \arctan\left[(e\sin\omega - e_0)/e\cos\omega\right] \qquad (1.6)$$

where e is the actual eccentricity of the orbit, e_0 is the nominal frozen orbit eccentric-

ity, and ω is the argument of perigee [79]. These general independent element adjust burns are summarized in Table 1.6.

Table 1.6. Independent Element Adjust Burns

Element	True Anomaly, f	Burn Direction
a	f_1; $f_2 = f_1 \pm 180°$	Both posigrade
e	$f_1 = 0°$; $f_2 = 180°$	one posigrade, one retrograde
ω	$f_1 = 90°$; $f_2 = -90°$	one posigrade, one retrograde

Simulations and real time data show that the ground track drift is sensitive to errors in nodal period, node rate, and atmospheric drag, with drag being the least predictable of the three. The average decrease in the semi-major axis during the initial geodetic mission was approximately 0.5 m/day, caused by an $F_{10.7}$ solar flux between 70 and 75. Assuming that the solar flux would be approximately the same for the ERM, the time of arrival at the ascending node, after N revolutions, is reduced in seconds per day by:

$$\Delta t_N = 2.2 \times 10^{-5} N^2 \qquad (1.7)$$

This equation is derived from taking the partial derivative of the nodal period with respect to the semi-major axis and assuming the ERM semi-major axis to be 7167.4 km. To maintain the ERM within one kilometer, the nodal crossing needs to be maintained within ±2.15 sec of the ERM nodal crossing time. This means a theoretical 22 days until the first burn is needed at the eastern boundary. The orbit is then adjusted by overshooting the semi-major axis needed for the exact repeat period and allowing the ground track to drift west. Orbital perturbations, mainly drag, will decrease the semi-major axis and force the ground track through the exact repeat period. Another maneuver will be performed before the ground track violates the eastern 1 km boundary. Mathematically, this would lead to approximately 50 days between follow-

ing orbit adjust maneuvers, even with a 10% error in drag prediction [9]. The actual maintenance maneuvers for the semi-major axis were done approximately every 30 days, since the solar flux varied more than expected [79].

1.2.5 ERS-1

The European Space Agency (ESA) will launch its first remote sensing spacecraft, ERS-1, on May 3, 1991. Its mission is to observe coastal oceans including ice formations, while measuring ocean and wind data to improve global weather information, thus making it an operational successor to SEASAT and NROSS. The information received from this satellite will complement the optical data from the LANDSAT and French SPOT systems. It is expected that ERS-1 will have a gradual transfer from an initial experimental mode to an operational mission to attain usable Earth observations [69,10]. The instruments that ERS-1 will carry to accomplish this mission are listed in Table 1.7. The functions of these instruments can be found in Table 1.1.

Table 1.7. ERS-1 Instrumentation

• Wind scatterometer
• Radar altimeter
• Synthetic aperture radar
• Laser retro-reflector array
• Along-track scanning radiometer
• Precise range and range rate exp.

The ERS-1 synthetic aperture radar (SAR) has two operational modes. The wide swath width of the Image Mode observes all weather images over oceans, polar regions, and land. The Wave Mode of the SAR creates 5 km x 5 km images at regular intervals to determine the length and direction of ocean waves. The European Space Operations Center (ESOC) will determine orbit data within 60 m along track through accurate modelling of atmospheric drag and the Earth's geopotential. The data from

the laser and precise range and range rate experiment (PRARE) will ameliorate this orbit determination and increase autonavigation [41,2,10]. The PRARE, sponsored by the German Federal Ministry for Research and Technology, will have its performance tested on the ERS-1 mission for future utilization on other space missions. The PRARE's space segment, which includes its own data transmission and memory for a more generic system, sends a signal down to an unmanned tracking station. The signal is radiated at frequencies of 8 and 2 GHz. The ground station works as a regenerative transponder for the 8 GHz signal. The primary measurement is performed by the space segment at reception of the returning 7 GHz signal. The accuracy is expected to be within 0.1 - 0.2 m for range and within 0.3 mm/sec for range rate. Since the 2 GHz signal is affected more by the ionosphere, there is a time difference (with the 8 GHz signal) measured at the ground station which is also returned to the satellite. At some central ground station, the time difference is processed to estimate the ionospheric correction to the range and range-rate data to be used in the orbit determination. The PRARE system will function in all weather since the signals are in the microwave band of frequencies [40].

All of the instruments listed in Table 1.7 need to observe the fast changing features over the globe in constant geometric and local time conditions to accomplish their mission. This leads to a trade-off between frequency of re-observation of covered areas and fraction of global coverage. The orbital elements chosen to meet these needs are listed in Table 1.8. This orbit is sun synchronous to provide regular observation times and constant lighting, especially for the along-track scanning radiometer. Three separate repeat ground tracks will be supported by these orbital elements during the 2-3 year life time of ERS-1. The first repeat cycle will be every three days, the second repeat cycle will last 35 days, and the third will last 176 days. All of the ground tracks will be maintained within ±1 km. The altitude adjusts needed to

Table 1.8. Orbital Elements for ERS-1

Mean Keplerian Element	ERS-1 Value
average semi-major axis, a	7153.1439 km
eccentricity, e	≈ 0.001166
inclination, i	98.52146°
argument of perigee, ω	90.0°
descending equatorial crossing time	1030 hrs local

maintain these ground tracks will be provided by thrusters in the posigrade direction. ERS-1 will be yawed 90° to provide an out of plane thrust for periodic inclination adjusts. The central ground station at Salmijaervi, Sweden, will link up with ERS-1 approximately 10 times per day. At least once a day, the ground station will verify satellite operations scheduled for the next 24 hrs, including necessary orbit adjusts. The repeat ground track coverage attained depends upon both the field of view of the instruments and the mean spacing between adjacent, not successive, ground tracks. For the ERS-1 three day repeat ground track orbit, the distance between adjacent ground tracks is predicted to be 932 km. The argument of perigee was set to 90.0° and the eccentricity calculated to attain a frozen orbit to minimize altitude variations and provide passive eccentricity and argument of perigee control [41]. It is expected if solar activity is low, $F_{10.7} = 70$ and $A_p = 8$, maneuvers to maintain these elements will take place approximately every 7 weeks. If the solar activity is high, $F_{10.7} = 210$ and $A_p = 10$, maneuvers are expected every 2-4 weeks [89,35,2].

The follow on, ERS-2, will be launched in 1994 by an Ariane 4 launch vehicle. This satellite will continue the data observed by ERS-1 with the addition of a global ozone monitoring experiment to examine the ozone problem [41].

1.2.6 LANDSAT 6

LANDSAT 6 is an advanced Earth Observation satellite to be placed in orbit in May, 1992, with a Titan II launch vehicle [65]. Like LANDSAT 4/5, LANDSAT 6 will be in a sun synchronous, repeat ground track, frozen orbit. The orbital elements that accomplish these orbit constraints, listed in Table 1.9, are very similar to the LANDSAT 4/5 elements, listed in Table 1.3 [70,62].

Table 1.9. Orbital Elements for LANDSAT 6

Keplerian Element	LANDSAT 6 Value
semi-major axis, a	7077.8 km
mean eccentricity, e	≈ 0.0013
inclination, i	98.2°
argument of perigee, ω	90.0°
equatorial crossing time	0930-0945 hours local time

As in the previous LANDSAT 4/5 satellites, the LANDSAT 6 ground track will repeat every 233 orbits or every sixteen days. Thus, adjacent, not necessarily successive, ground tracks will be separated by approximately 1.54506°. This ground track repeat cycle will be maintained within ±5 km during the desired 5 year lifetime. Since the time of launch places the orbit near the peak of the solar cycle, atmospheric drag will be the primary perturbation to counteract with altitude adjusts to maintain the repeat ground track. The needed change in eccentricity to maintain the frozen orbit condition will most often be corrected at the same time as the altitude adjust. If the change in eccentricity is too large to be completely reset during the altitude adjust, the eccentricity adjust will be of the greatest degree possible given only posigrade burns are allowed. As previously observed in Table 1.6, an independent change in eccentricity is accomplished with burns in equal and opposite directions. Since the LANDSAT 6 spacecraft bus will only have thrusters in the posigrade direction,

the desired retrograde burn to independently change the eccentricity would require a costly 180° yaw or pitch to position the thrusters in the correct burn direction. The yaw maneuver is preferred so that the satellite will not flip over 180° as would occur in the undesirable, but possible, pitch maneuver. In addition, an out of plane burn will require an approximately 90° yaw to correctly position the thrusters to adjust the inclination. The inclination will need to be adjusted periodically to maintain the sun synchronous condition and the repeat ground track at high latitudes. Since the primary perturbation that changes the orbit inclination is due to solar gravity and is nearly constant for a frozen, sun synchronous orbit [65,70,62], the inclination adjusts are simple to predict. The inclination adjust needed will be similar to the LANDSAT 5 adjusts at a Δi less than 0.03°.

Since the government is now commercializing the LANDSAT mission with government funding, LANDSAT 6 is being designed and built by General Electric Astro-Space Division for the Earth Observation Satellite (EOSAT) Company. The National Oceanographic and Atmospheric Administration (NOAA) oversees the LANDSAT 6 project since they managed the LANDSAT 4 and LANDSAT 5 projects for the US government [58,65].

1.2.7 Ocean Topography Experiment (TOPEX)

The joint US/French TOPEX/POSEIDON will be launched in June, 1992, by the National Aeronautics and Space Administration on a French Ariane 4 launch vehicle. The mission profile of TOPEX is to study oceanic sea surface topography using instruments including an advanced radar altimeter, a multi-frequency radiometer, a laser retro-reflector array, a TRANET beacon, and an experimental high-precision radiometric tracking device. The French will supply a precision tracking system and an additional solid state altimeter that will be operational only 5% of the time to avoid

36

interference with the primary altimeter [6,28,89,69]. Its proposed mission length is three years with orbital elements as stated in Table 1.10. The semi-major axis for

Table 1.10. Orbital Elements for TOPEX

Keplerian Element	TOPEX Value
semi-major axis, a	7713.3869 km
mean eccentricity, e	0.0009825
inclination, i	64.606°
argument of perigee, ω	270.0°
longitude of the ascending node, Ω	139.552°

TOPEX is significantly higher than the satellites reviewed previously. This value was chosen to decrease the amount of atmospheric drag on the satellite [69]. To minimize altitude variations throughout the orbit and to maintain an eccentricity less than 0.001, a frozen orbit is planned. In addition, the TOPEX system will have a repeat ground track with a repeat interval of 10 sidereal days, or 127 orbits, which will be maintained within ±1 km [6,28].

The inclination is constrained to meet several mission requirements. The intersection of ascending and descending ground tracks must be nearly orthogonal to determine two orthogonal components of the surface with comparable accuracy. Parallel tracks could accomplish this but would demand a repeat cycle longer than required by the mission specifications. The TOPEX orbit also needs a nodal precession rate far from sun synchronous and not near any integer nodal rate so mean surface topography can be distinguished from major tidal components. This constraint restricts the TOPEX inclination to be between 62° and 65° [32]. By examining repeat ground track orbits in this inclination region, the TOPEX orbital elements were chosen as stated above in Table 1.10.

1.2.8   Earth Observing System (EOS)

EOS consists of three integrated functions: the Scientific Research Program, the
Data and Information System, and the EOS Space Measurement System (EOSSMS).
The EOSSMS includes the EOS satellite system [29]. Conceptual studies, begun in
1982, focused on an optimal four or five satellite constellation, but later changed to
two series of polar orbit platforms, labelled A and B [19]. These satellites, EOS A
& B, will be treated as single satellite systems and will not be dependent on each
other for their individual missions. Each platform series will consist of three satellites
with five year lifetimes, although proposals to separate the B series into several small
satellites are being discussed [25]. These satellites, put up consecutively, will give each
series a fifteen year total mission length. The A series will focus on potential global
warming and other aspects of global change while the B series will extend observations
made by the Upper Atmospheric Research Satellite (UARS) and TOPEX. The delay
in determining the exact instrument complement for each series allows for continuing
research in mission planning and available technology [72]. The first A satellite will
be launched in 1998 followed by the first B launch two and a half years later. The
current plan is to launch all of the satellites from the Western Test Range on Titan
IV rockets [30].

Since the mission constraints call for global coverage every one to three days, a sun
synchronous orbit was chosen with a quasi-two day repeat cycle. Any difficulty with
separating the tides from mean surface topography associated with a sun synchronous
orbit is assumed to be removed by sea geoid measurements from TOPEX [30,19]. The
orbital elements chosen to the present are listed in Table 1.11. Observe that these
orbital elements are very similar to the LANDSAT 4/5/6 orbital elements. The semi-
major axis for EOS is only 5 km higher than the LANDSAT semi-major axis. This

Table 1.11. Orbital Elements for EOS A/B

Keplerian Element	EOS A/B Value
semi-major axis, a	7083.135 km
inclination, i	98.2°
argument of perigee, ω	90° or 270°
equatorial crossing time	1030 hr local time

semi-major axis was chosen to meet both the wide swath-width and high resolution instrument specifications. The inclination was chosen to insure a sun synchronous orbit at the given altitude using equation 1.5. A sun synchronous orbit was chosen to avoid biasing the measurements of EOS with diurnal and seasonal effects of the sun [29]. The crossing time was altered from a 1:30 pm time that complemented LANDSAT's morning crossing times to a 10:30 am time that improved observation conditions in the humid regions of the Earth during their growing season. This new choice of crossing time fails to observe peak surface heating, but the disadvantage of this data lost is still undetermined [31].

The A and B series will be supplemented by future National Oceanic and Atmospheric Administration (NOAA), European, and Japanese polar platforms planned in conjunction with the EOS satellites. EOS will also launch a third series of polar platforms dedicated to a synthetic aperture radar (EOS SAR) as on SEASAT. This instrument, because of its unique requirements, could not be included on either the A or B platform series, and will be launched in 1999. This series will be composed of three individual five year lifetime satellites that will be placed in orbit consecutively for a fifteen year total mission length. The EOS SAR will be in a slightly different orbit than the A or B series with a lower semi-major axis of 6998.135 km but will still retain the 1:30 pm equatorial crossing time [30,29].

1.3 Maneuver Planning for Multiple Satellites

Maneuver planning for satellite constellations is no more than a general application of single satellite theory to many satellites with added constraints. These constraints might be needed to ensure Earth coverage, inter-satellite communication limits, constellation geometry, etc. There are planar constraints, ie. between satellites in the same plane. The different velocities of the satellites at separate parts of the same orbit need to be considered to preserve a certain maximum or minimum angle between satellites in the same plane. There are also inter-planar constraints, ie. between satellites of different planes, which are more difficult to maintain since the perturbations in the separate orbits can be varied. The inter-planar constraints may consist of maintaining phasing between satellites in different planes. A future multiple satellite system that needs to address these difficulties is the Iridium project that has a nominal constellation of 77 satellites. It is obvious to the casual observer that the use of sun synchronous, repeat ground track, and frozen orbits can be applied to more than Earth Observation satellite constellations.

These same problems must be addressed in US Defense-oriented multiple satellite constellation such as Brilliant Pebbles. The Soviet Military EORSAT system is thought to utilize an ocean surveillance satellite constellation of 6 satellites in 2 planes to detect, identify, and track US and Allied naval forces [50]. The two planes are separated by 172° at the equator. The satellites have a mean altitude near 420 km and their orbits are inclined to 65°. All of the satellites are phased to follow the same repeat ground track cycle that lasts three days, or 46 orbit revolutions. This Soviet constellation is an example of how the maintenance of a repeat ground track can maintain the phasing needed by a constellation system. The Soviet EORSAT system has had difficulties with keeping the correct number of satellites up and keeping the

satellites in the repeat ground track because of satellite errors in the maintenance burns. This lack of accuracy in maintenance burns lessens the synchronicity of the constellation [50].

1.3.1   Iridium

The Iridium project sponsored by Motorola Satellite Communications is planned to be a commercial, cellular communications system that is satellite based for worldwide coverage. This system is designed to complement the existing terrestrial cellular telephone system. The constellation composed of 77, small, 320 kg, smart satellites will be internetted to 'cover' the Earth with cells to allow channels to be reused many times. The portable units will communicate with the constellation within a direct line of site on or above the Earth's surface.

These 77 satellites will reside in seven separate polar orbital planes to provide full Earth coverage with a minimum number of satellites determined by Adams and Rider [1]. These orbits are not sun synchronous, but to minimize orbit maintenance a frozen orbit along with a repeat ground track requirement are prescribed, but the final decision is still to be determined (TBD). As in the LANDSAT 4 and 5 projects, the satellites of a constellation may be treated individually by maintaining each satellite in a repeat ground track and frozen orbit. Orbit inclination maintenance will preserve the ground track at higher latitudes and will maintain the nodal period needed for a repeat ground track. Semi-major axis maintenance, within some prescribed boundaries, will preserve the orbit that each satellite is expected to follow. In addition, the phasing between the satellites in the same plane and other planes will also be upheld with maintenance of each individual repeat ground track. The frozen orbit concept would allow for passive maintenance of the eccentricity and argument of perigee of each individual satellite. If all the satellites follow this method, the interplanar con-

straints may be easier to uphold since orbit maintenance would only have to focus on the ground track and not how the other planes are perturbed. Thus by keeping the individual ground tracks intact for each orbital plane, inter-planar angles would be preserved without any complicated comparison between the planes. This may not be optimal in terms of stationkeeping maneuvers but this possible solution does require some examination.

The Iridium satellites in the odd numbered planes are in phase with each other and half out of phase with those in the even numbered planes. Most of the planes are co-rotating, ie. moving in the same direction about the Earth. Only the seam between the first and seventh planes is counter-rotating. The co-rotating planes will be separated by 27° and the counter-rotating planes separated by 17.5°. The distance is smaller between the first and seventh planes because Earth coverage is more difficult to achieve with counter-rotating planes. These satellites will all be in polar orbits with a mean semi-major axis of 7143 km so that the local elevation of a satellite to a portable user will be greater than 10°.

The maintenance of this satellite constellation will be difficult, as discussed above, because of the many constraints in and between the planes in addition to the cellular set up of the communication linkage [56].

1.4 Summary

SEASAT, GEOSAT, and TOPEX are repeat ground track and frozen orbit missions that do not utilize the sun synchronous condition. Conversely, EOS, LANDSAT 4/5, NROSS and the European Space Agency (ESA) ERS-1 all utilize the three concepts mentioned above. This is summarized in Table 1.12.

This thesis will focus on maneuver planning for a sun synchronous, frozen orbit, repeat ground track orbit applied to the LANDSAT 6 mission constraints. Instead

Table 1.12. Satellite Orbit Summary

Satellite System	Repeat Ground Track	Sun Synchronous	Frozen Orbit
SEASAT	YES	NO	YES
LANDSAT 4/5	YES	YES	YES
NROSS	YES	YES	YES
GEOSAT ERM	YES	NO	YES
ERS-1	YES	YES	YES
TOPEX	YES	NO	YES
EOS	YES	YES	YES
Iridium	TBD	NO	TBD

of using more common propagation methods as in past satellite systems, this thesis takes a new approach to maneuver planning by suggesting the employment of a high precision mean element orbit propagator, called the Draper Semianalytic Satellite Theory (DSST) to predict how the orbit changes from the nominal elements over time.

This propagation method is not only accurate and computationally efficient, but it is also singularity free through the usage of equinoctial orbital elements rather than the more common Keplerian elements. The DSST Standalone Orbit Propagator is small and its modern architecture allows it to be portable to many computer systems including IBM and CDC Mainframes, a VAX, an IBM PC, a Sun SPARCstation, and a Macintosh PC.

Chapter 2 reviews the mean element theory and program flow used in the DSST Orbit Propagator. Chapter 3 discusses an existing software tool, MEANELT, that applies the DSST propagation techniques to maneuver planning for maintaining the nominal orbit. Chapter 4 states the specific algorithms necessary for sun synchronous, repeat ground track, and frozen orbit maneuver planning and specifies the impulsive and finite burn models used in the LANDSAT 6 mission software. Chapter 5 discusses

43

ground track motion forecasting using solar flux and geomagnetic activity predictions and the confidence interval of the density calculated form these values. Chapter 6 asserts the results and conclusions of this thesis and gives recommendations for future work. A review of the Keplerian and equinoctial elements sets can be found in Appendix A. Appendix B discusses the porting of the Draper Semianalytic Satellite Theory Standalone Propagator from the IBM mainframe to other computing environments, ie. VAX, Sun SPARCstation, IBM PC, and Macintosh PC.

Chapter 2

Review of Semianalytic Theory

To determine a satellite orbit precisely in time and to insure that it meets the mission specifications, the orbit must be propagated through time using perturbation methods from two basic categories: Special and General Perturbation Theories. The first, called the Numerical Method or the Special Perturbation Theory, constructs the perturbed orbit through direct integration of the equations of motion. This method is very precise but computationally inefficient; to retain accuracy, the high frequency perturbations constrain the integration step size to be very small. In addition, the large number of steps taken increase the truncation and round-off error in many orbit determination applications. The Special Perturbation Method does not provide general physical insight into orbit dynamics. A Cowell propagator is an example of a Special Perturbation Theory. On the other hand, the General Perturbation Theory or the Analytic Model, transforms the equations of motion into exact differentials that can be analytically integrated. To realize these closed form analytic expressions, the Keplerian orbit including all perturbations is generalized through assumptions, ie. simplified perturbation models, approximations, ie. small terms in series expansions are neglected, and restricted ranges of theoretical validity. This method is not very accurate because of the many simplifications, but it is computationally efficient after the algorithms have been defined. If any additional perturbations are desired, another

tedious derivation must take place to construct the new analytic expressions [4,23].

An alternative to, or combination of, these two classes of perturbation methods is a semianalytic theory that is both accurate and computationally efficient. Potential, or conservative, perturbations are put in Lagrangian Variation of Parameters (VOP) form and non-potential, or nonconservative, perturbations are put in Gaussian Variation of Parameters form. The long period and secular components of the perturbations are separated from the short period components of satellite motion. In the mean element theory used in this thesis, this is done through the application of the Generalized Method of Averaging to the VOP equations of motion. The simple conservative perturbations are analytically averaged. These conservative perturbations could be numerically averaged, but this method is not computationally efficient, thus it is reserved for the more complex, non-conservative perturbations. Through these averaged equations of motion, integration of the mean element (long period and secular) motion is achieved efficiently by applying large step sizes. The magnitude of this step size is constrained by the magnitude of the next higher frequency oscillations [87,23]. In this thesis, the step size is one day or larger [27]. Accuracy is achieved by adding in the short periodic terms at the output time. In the Draper Semianalytic Satellite Theory Standalone, these short periodic terms are determined on a grid and if the output time is not on the grid, the short periodic terms are interpolated. The only difficulty with the mean, semianalytic theory is that it requires a procedure to determine the initial mean elements to start the integration at the same osculating elements as a numerical integrator. This problem only arises when the semianalytic theory is to be compared to a numerical integration of the same satellite orbit. In normal orbit determination operations, convergence of the semianalytic method rapidly eliminates errors in the mean initial conditions. For comparison testing, the initial mean elements are determined through a least squares fit of the semianalytic theory

to the desired osculating trajectory. This mean initial state could also be achieved by numerically averaging the osculating state over one orbit [87,23]. A more rigorous mathematical summary is stated below.

There is ongoing research into new methodologies for the development of analytical and semianalytical theories. These new methods explore the use of algebraic software and hardware to decrease the work in deriving the analytic expressions [24].

2.1 Mathematical Summary

2.1.1 Variation of Parameters

Newton's second law may be applied to the equations of motion of two point mass particles, ie. the Earth and the satellite, to determine the fundamental differential equation of the two-body Keplerian orbit [4]:

$$\ddot{\mathbf{r}} + \frac{\mu}{r^3}\mathbf{r} = 0 \tag{2.1}$$

where $\mathbf{r}$ is the position vector of the satellite with magnitude r, μ is the gravitational parameter of the Earth, and over dots denote time differentiations. The solution to this equation leads to six constants of integration:

$$\mathbf{c} = \begin{bmatrix} c_1 & c_2 & c_3 & c_4 & c_5 & c_6 \end{bmatrix}^T \tag{2.2}$$

which can be represented:

$$\mathbf{r} = \mathbf{r}(\mathbf{c}, t) \tag{2.3}$$

$$\dot{\mathbf{r}} = \mathbf{v}(\mathbf{c}, t) = \frac{\delta \mathbf{r}}{\delta t} \tag{2.4}$$

where $\mathbf{r}$ and $\mathbf{v}$ represent the transformations between the position/velocity vectors and the orbital elements of c. The most common of these orbital elements are the Keplerian orbital elements, but a variation of these are the equinoctial elements; both

described in Appendix A. These orbital elements describe the two body, osculating, orbit that would exist in a system only affected by the law of gravitation with the bodies involved defined as point masses. But, a satellite orbiting the Earth is not influenced only by the gravitational attraction of the Earth, meaning that the orbit is also affected by perturbations to this two-body orbit. This is denoted by the following equation:

$$\ddot{\mathbf{r}} + \frac{\mu}{r^3}\mathbf{r} = \mathbf{a}_d \tag{2.5}$$

where $\mathbf{a}_d$ is the perturbing acceleration acting on the satellite. If the perturbing acceleration, $\mathbf{a}_d$, is very small compared to the primary gravitational acceleration, the solution to Equation 2.5 would closely approximate the solution to the unperturbed case in Equation 2.1. Under the additional perturbations, $\mathbf{a}_d$, the orbital elements in $\mathbf{c}$ change slowly over time. The purpose of the Method of Variation of Parameters (VOP) is to construct differential equations which give the motion of these orbital elements over time.

Lagrangian Variation of Parameters

The Lagrange VOP equations express the perturbing acceleration as the gradient a conservative disturbing function, R:

$$\mathbf{a}_d = \left[\frac{\delta R}{\delta \mathbf{r}}\right]^T = \left[\begin{array}{ccc} \frac{\delta R}{\delta r_1} & \frac{\delta R}{\delta r_2} & \frac{\delta R}{\delta r_3} \end{array}\right] \tag{2.6}$$

where r_1, r_2, and r_3 are the coordinates of the position vector, $\mathbf{r}$. Differencing Equation 2.3 and allowing the orbital elements of $\mathbf{c}$ to vary with time gives:

$$\mathbf{v} = \dot{\mathbf{r}} = \frac{\delta \mathbf{r}}{\delta t} + \frac{\delta \mathbf{r}}{\delta \mathbf{c}}\frac{d\mathbf{c}}{dt} \tag{2.7}$$

By substituting the latter part of Equation 2.4 into the above equation, the first three constraints on the orbital elements c are derived:

$$\frac{\delta \mathbf{r}}{\delta \mathbf{c}} \frac{d\mathbf{c}}{dt} = 0 \tag{2.8}$$

Next by differencing Equation 2.4, an expression for the second derivative of the position vector, r, is determined and can be substituted into the perturbed equation of motion giving:

$$\frac{\delta^2 \mathbf{r}}{\delta t^2} + \frac{\delta \mathbf{v}}{\delta \mathbf{c}} \frac{d\mathbf{c}}{dt} + \frac{\mu}{r^3}\mathbf{r} = \left[\frac{\delta R}{\delta \mathbf{r}}\right]^T \tag{2.9}$$

Since c is the solution for the unperturbed case, Equation 2.1 is restated in the following form and substituted into Equation 2.9 to give the final three conditions on the orbital elements c:

$$\frac{\delta^2 \mathbf{r}}{\delta t^2} + \frac{\mu}{r^3}\mathbf{r} = 0 \tag{2.10}$$

$$\frac{\delta \mathbf{v}}{\delta \mathbf{c}} \frac{d\mathbf{c}}{dt} = \left[\frac{\delta R}{\delta \mathbf{r}}\right]^T \tag{2.11}$$

The six constraints, or differential relations, of the orbital elements, c, of Equations 2.8 and 2.11 can be placed in matrix form:

$$\left[\begin{array}{c}\frac{\delta \mathbf{r}}{\delta \mathbf{c}} \\ \frac{\delta \mathbf{v}}{\delta \mathbf{c}}\end{array}\right] = \left[\begin{array}{c}0 \\ \frac{\delta R}{\delta \mathbf{r}}\end{array}\right]^T \tag{2.12}$$

By pre-multiplying this equation by the 6 × 6 matrix:

$$\left[-\left[\frac{\delta \mathbf{v}}{\delta \mathbf{c}}\right]^T \left[\frac{\delta \mathbf{r}}{\delta \mathbf{c}}\right]\right] \tag{2.13}$$

and using the chain rule of partial differentiation:

$$\frac{\delta R}{\delta \mathbf{c}} = \frac{\delta R}{\delta \mathbf{r}} \frac{\delta \mathbf{r}}{\delta \mathbf{c}} \tag{2.14}$$

a convenient and more familiar expression for the transformation between the variables r, ṙ and the orbital elements, c is provided:

$$L\frac{d\mathbf{c}}{dt} = \left[\frac{\delta R}{\delta \mathbf{c}}\right]^T \tag{2.15}$$

where the skew-symmetric Lagrangian matrix is defined:

$$L^T = -L \tag{2.16}$$

$$L \equiv \left[\frac{\delta \mathbf{r}}{\delta \mathbf{c}}\right]^T \frac{\delta \mathbf{v}}{\delta \mathbf{c}} - \left[\frac{\delta \mathbf{v}}{\delta \mathbf{c}}\right]^T \frac{\delta \mathbf{r}}{\delta \mathbf{c}} \tag{2.17}$$

To achieve the orbital element rates directly from Equation 2.15, the inverse of the Lagrangian matrix L must be determined. The proof given by de Lafontaine [23] shows that the skew symmetric Poisson matrix, P, is the negative inverse of L. This gives the Lagrangian VOP equations of motion [4]:

$$\frac{d\mathbf{c}}{dt} = P^T \frac{\delta R}{\delta \mathbf{c}} \tag{2.18}$$

where the Poisson bracket, P is defined:

$$P \equiv \left[\frac{\delta \mathbf{c}}{\delta \mathbf{r}}\left[\frac{\delta \mathbf{c}}{\delta \mathbf{v}}\right]^T - \frac{\delta \mathbf{c}}{\delta \mathbf{v}}\left[\frac{\delta \mathbf{c}}{\delta \mathbf{r}}\right]^T\right] \tag{2.19}$$

Gaussian Variation of Parameters

The Gaussian form of Variation of Parameters is developed with no assumptions made concerning the perturbing accelerations. This differs from the Lagrangian form where the perturbing acceleration is defined as the gradient of some disturbing function, R. The Gaussian VOP equations of motion are used for perturbations that can not be expressed in terms of R, ie. non-conservative forces like atmospheric drag. By no longer allowing the substitution of Equation 2.6, Equation 2.18 is now stated:

$$\frac{d\mathbf{c}}{dt} = P^T \left[\frac{\delta \mathbf{r}}{\delta \mathbf{c}}\right]^T \mathbf{a}_d \tag{2.20}$$

By expanding the Poisson bracket, the following equation is achieved:

$$\frac{d\mathbf{c}}{dt} = \frac{\delta \mathbf{c}}{\delta \mathbf{v}}\left[\frac{\delta \mathbf{r}}{\delta \mathbf{r}}\right]^T \mathbf{a}_d - \frac{\delta \mathbf{c}}{\delta \mathbf{r}}\left[\frac{\delta \mathbf{r}}{\delta \mathbf{v}}\right]^T \mathbf{a}_d \tag{2.21}$$

50

Since the components of the position and velocity vectors are considered independent, the following equations hold true:

$$\frac{\delta \mathbf{r}}{\delta \mathbf{r}} = \mathbf{I} \qquad (2.22)$$

$$\frac{\delta \mathbf{r}}{\delta \mathbf{v}} = \mathbf{O} \qquad (2.23)$$

where $\mathbf{I}$ is the identity matrix and $\mathbf{O}$ is the zero matrix. These equations may be substituted into Equation 2.21 to result in the final form of the Gaussian VOP equations of motion [4]:

$$\frac{d\mathbf{c}}{dt} = \frac{\delta \mathbf{c}}{\delta \mathbf{v}} \mathbf{a}_d \qquad (2.24)$$

This Gaussian form may be applied to determine the rates of change of the singularity free equinoctial element set [57]:

$$\frac{da}{dt} = \frac{2\mathbf{v}}{n^2 a} \mathbf{a}_d \qquad (2.25)$$

$$\frac{dh}{dt} = \left[\frac{1}{\mu}[(2\dot{X}_1 Y_1 - X_1 \dot{Y}_1)\hat{f} - X_1 \dot{X}_1 \hat{g}] + \frac{k}{G}(qIY_1 - pX_1)\hat{w} \right] \mathbf{a}_d \qquad (2.26)$$

$$\frac{dk}{dt} = \left[-\frac{1}{\mu}[Y_1 \dot{Y}_1 \hat{f} - (2X_1 \dot{Y}_1 - \dot{X}_1 Y_1)\hat{g}] - \frac{h}{G}(qIY_1 - pX_1)\hat{w} \right] \mathbf{a}_d \qquad (2.27)$$

$$\frac{dp}{dt} = \left[\frac{1 + p^2 + q^2}{2G} Y_1 \hat{w} \right] \mathbf{a}_d \qquad (2.28)$$

$$\frac{dq}{dt} = \left[\frac{I(1 + p^2 + q^2)}{2G} X_1 \hat{w} \right] \mathbf{a}_d \qquad (2.29)$$

$$\frac{d\lambda}{dt} = \left[n - \frac{2}{na^3}\mathbf{r} + \beta \left(k\frac{\delta h}{\delta \mathbf{v}} - h\frac{\delta k}{\delta \mathbf{v}} \right) + \frac{1}{na^2}(qIY_1 - pX_1)\hat{w} \right] \mathbf{a}_d \qquad (2.30)$$

The parameter, G, is determined by the following equation:

$$G = na^2 \sqrt{1 - h^2 - k^2} \qquad (2.31)$$

The satellite mean motion, n, is calculated with the equation:

$$n = \sqrt{\frac{\mu}{a^3}} \qquad (2.32)$$

The variables, X_1, Y_1, $\dot{X}_1$, and $\dot{Y}_1$, are the position and velocity coordinates of the satellite in the equinoctial orbit frame. They are determined with the following equations:

$$X_1 = a[(1 - h^2\beta)\cos F + hk\beta \sin F - k] \tag{2.33}$$

$$Y_1 = a[(1 - k^2\beta)\sin F + hk\beta \cos F - h] \tag{2.34}$$

$$\dot{X}_1 = \frac{na^2}{r}[hk\beta \cos F - (1 - h^2\beta)\sin F] \tag{2.35}$$

$$\dot{Y}_1 = \frac{na^2}{r}[(1 - k^2\beta)\cos F - hk\beta \sin F] \tag{2.36}$$

where the parameter, β, is equated:

$$\beta = \frac{1}{1 + \sqrt{1 - h^2 - k^2}} \tag{2.37}$$

The eccentric longitude, F, can be determined through an iterative solution of the following equation:

$$\lambda = F + h\cos F - k\sin F \tag{2.38}$$

The unit vectors $\hat{f}$ and $\hat{g}$ both lie in the orbit plane while the unit vector $\hat{w}$ is perpendicular to the orbit plane. This orthogonal coordinate system is determined through the transformation:

$$[\,\hat{f} \quad \hat{g} \quad \hat{w}\,] = \frac{1}{1 + p^2 + q^2}\begin{bmatrix} 1 - p^2 + q^2 & 2pqI & 2p \\ 2pq & I(1 + p^2 - q^2) & -2q \\ -2Ip & 2q & I(1 - p^2 - q^2) \end{bmatrix} \tag{2.39}$$

The position and velocity vectors are now determined in this coordinate system:

$$\mathbf{r} = X_1\hat{f} + Y_1\hat{g} \tag{2.40}$$

$$\mathbf{v} = \dot{X}_1\hat{f} + \dot{Y}_1\hat{g} \tag{2.41}$$

Since the DSST Standalone uses both the Lagrangian and the Gaussian VOP methods, the perturbing acceleration is separated into conservative and non-conservative

parts. This leads to a general form of the VOP equations of motion [23].

$$\mathbf{a}_d = \mathbf{a}_{d_{NC}} + \mathbf{a}_{d_C} = \mathbf{a}_{d_{NC}} + \left[\frac{\delta R}{\delta \mathbf{r}}\right]^T \qquad (2.42)$$

$$\frac{d\mathbf{c}}{dt} = P^T \frac{\delta R}{\delta \mathbf{c}} + \frac{\delta \mathbf{c}}{\delta \mathbf{v}} \mathbf{a}_{d_{NC}} \qquad (2.43)$$

2.1.2 Generalized Method of Averaging

The equations of motion in both the Lagrangian and Gaussian VOP forms include the secular and the long and short periodic perturbations that disturb the orbit from a two-body Keplerian orbit. The Generalized Method of Averaging eliminates the short periodic terms from these expressions to form mean element equations of motion. These mean element equations may be integrated using a larger time step, thus decreasing the amount of computational time. The short periodic terms can be added in at the requested time to recall the accurate osculating state of the satellite.

To determine the mean element equations of motion, the orbital elements must be separated into a group of slow osculating orbital elements, $\mathbf{c}$, and a fast variable, c_6. This separation in the VOP equations of motion can be shown functionally in the following form [60]:

$$\frac{d\mathbf{c}}{dt} = \epsilon \mathbf{G}(\mathbf{c}, c_6) \qquad (2.44)$$

$$\frac{dc_6}{dt} = h(\mathbf{c}) + \epsilon G_6(\mathbf{c}, c_6) \qquad (2.45)$$

The functions $\mathbf{G}$ and G_6 represent the perturbing accelerations from the right hand side of the equations of motion while the function h represents the Keplerian motion of the fast parameter, see Equation 2.43. A near identity first order transformation from the mean to osculating elements is determined with the following expressions [88]:

$$\mathbf{c} = \bar{\mathbf{c}} + \epsilon \eta(\bar{\mathbf{c}}, \bar{c}_6) \qquad (2.46)$$

$$c_6 = \bar{c}_6 + \epsilon \eta_6(\bar{\mathbf{c}}, \bar{c}_6) \qquad (2.47)$$

53

where the over bar denotes the averaged elements and the functions $\epsilon\eta$ and $\epsilon\eta_6$ denote the short periodic functions, and are the first order terms in an asymptotic series for the original dynamics. The rates of the mean elements can not depend on the variables c_6 or $\bar{c}_6$ because these are fast changing values and are eliminated in the averaging. Therefore, the mean element rates can be written:

$$\dot{\bar{\mathbf{c}}} = \epsilon\mathbf{A}(\bar{\mathbf{c}}) \tag{2.48}$$

$$\dot{\bar{c}}_6 = h(\bar{\mathbf{c}}) + \epsilon A_6(\bar{\mathbf{c}}) \tag{2.49}$$

where again the variable ϵ denotes the small magnitudes of the disturbing accelerations, $\mathbf{A}$ and A_6. The mean element rates and short periodic functions are determined by first assuming an asymptotic matching between the original VOP equations and equations resulting from the differentiation of Equations 2.46 and 2.47. This matching is usually done to first and second order in the variable ϵ. The expressions for the mean element rates and short periodic functions are realized with the the substitution of the mean element rates, Equations 2.48 and 2.49, into the asymptotic expansion. One important constraint is that the short periodic functions, η and η_6, are periodic in the fast variable, c_6, with a period of 2π; ie. the following constraints apply [88]:

$$\epsilon\eta(\bar{\mathbf{c}}, \bar{c}_6 + 2\pi) = \epsilon\eta(\bar{\mathbf{c}}, \bar{c}_6) \tag{2.50}$$

$$\int_0^{2\pi} \epsilon\eta(\bar{\mathbf{c}}, \bar{c}_6)d\bar{c}_6 = 0 \tag{2.51}$$

This assumption allows simplification of the mean element rates so that first order coefficients, $\mathbf{A}$, are calculated [60]:

$$\mathbf{A}_i = \frac{1}{2\pi}\int_0^{2\pi} G_i(\bar{\mathbf{c}}, \bar{c}_6)d\bar{c}_6 \tag{2.52}$$

where the integer i is from 1 to 6.

2.1.3 Mean Element Equations of Motion

For conservative forces, like the Earth's geopotential zonal harmonics, the mean element equations of motion are found through an analytical averaging of the Lagrangian VOP equations of motion over the fast variable for one full orbital period [60,88]:

$$\epsilon A_i = \frac{1}{2\pi} \int_0^{2\pi} P^T \frac{\delta R}{\delta \mathbf{c}} dc_6 \qquad (2.53)$$

But, the Poisson matrix, P, depends only on the slowly varying elements, $\mathbf{c}$, so it may be pulled through the integral.

$$\epsilon A_i = P^T \frac{1}{2\pi} \int_0^{2\pi} \frac{\delta R}{\delta \mathbf{c}} dc_6 \qquad (2.54)$$

By interchanging the order of the integral and the differential, the right hand sides of the mean element equations of motion are expressed in terms of the averaged potential and the partial derivatives of the averaged potential:

$$\epsilon A_i = P^T \frac{\delta}{\delta \mathbf{c}} \left[\frac{1}{2\pi} \int_0^{2\pi} R dc_6 \right] \qquad (2.55)$$

The average of the potential and the derivatives of the averaged potential have been constructed for the zonal harmonics, tesseral harmonics, and the third body point mass effects. Detailed mathematical expressions for the averaged geopotential zonal harmonics can be found in reference [16], the effects of J_2^2 in reference [8], the averaged geopotential tesseral harmonics (resonance) can be found in references [76,14], and the averaged effects of solar-lunar point masses in reference [16].

For non-conservative perturbations, like atmospheric drag and solar radiation, the Draper Semianalytic Theory applies the general first-order averaging method to the singularity free equinoctial element equations of motion described in Equations 2.25 through 2.30. The Method of Averaging is still applied but now the Gaussian VOP equations of motion are averaged using a Gaussian quadrature method [60,88].

In the Keplerian element set, the fast element is represented by the mean anomaly and in the equinoctial element set it is the mean longitude. To uniformize the integrand and increase computational efficiency, the integration variable is transformed from the mean longitude, λ, to the eccentric longitude, F, with the following expression [57]:

$$\frac{d\bar{F}}{d\bar{\lambda}} = (1 - \bar{k}\cos\bar{F} - \bar{h}\sin\bar{F})^{-1} \tag{2.56}$$

2.1.4 Short Periodic Perturbations

If only the mean element equations of motion are integrated, accuracy is lost. Therefore, the short periodic terms must be recalled and added in to determine the true osculating state at the requested output time. If the short periodic terms are calculated at every output time, there is a loss of computational efficiency if the desired output times are at many closely spaced points in time. The Draper Semianalytical Satellite Theory Standalone (DSST Standalone) determines the coefficients of the short periodic Fourier series expansions on a grid. This grid is closely tied to the integration of the mean element equations of motion. If the request time is in between the grid points, the short periodic coefficients are determined with a three point Lagrangian interpolator formula. If the request time is not spanned by coefficients already calculated, the program determines the correct interpolation interval and calculates the coefficients and uses these to interpolate the short periodics at the request time. This formulation allows a high execution speed for many closely spaced request times [27].

As stated above, the short periodics are determined through a Fourier series expansion in the fast variable with C_i and D_i representing the series coefficients [88]:

$$\epsilon\eta(\bar{c}, \bar{c}_6) = \sum_{i=1}^{N} \epsilon C_i(\bar{c})\sin i\bar{c}_6 - \epsilon D_i(\bar{c})\cos i\bar{c}_6 \tag{2.57}$$

56

$$\epsilon\eta_6(\bar{c}, \bar{c}_6) = \sum_{i=1}^{N} \epsilon C_{6,i}(\bar{c}) \sin i\bar{c}_6 - \epsilon D_{6,i}(\bar{c}) \cos i\bar{c}_6 \qquad (2.58)$$

In the DSST Standalone, the fast variable, c_6 is either the mean longitude, λ, eccentric longitude, F, or true longitude, L [27]. The choice of which longitude to use as the expansion variable is different for various perturbations. The central body zonal harmonics are in a closed form expression if the expansion variable is the true longitude, L. The same is true for the slow moving third body perturbations with the eccentric longitude, F. A more detailed examination of the mathematical expressions is given for the zonal harmonics in references [51,81], third body short periodic effects in references [80,51], and the tesseral harmonics in references [51,77,17,76,14].

The central body gravitational sectoral and tesseral harmonics short periodics are determined through two expansions. The first expansion is in the longitude of the central body's prime meridian, θ, which is measured from the equinoctial origin of longitudes in the satellite orbit. These periodics require a separate expansion since they are of medium period, ie. $\frac{1}{m}$ times the rotational period of the central body where m is a small integer. The second expansion is in both the mean longitude, λ, and the longitude of the prime meridian, θ. This expansion leads to short periodic terms with a much higher frequency than the satellite period. This double expansion may result in some very long periodic terms resulting from tesseral resonance. These long periodic terms are removed from the short periodic expansion and added to the averaged equations of motion.

For third body point mass perturbations, there is a choice of two formulations to determine the associated short periodics. The first formulation employs an expansion in the eccentric longitude of the satellite, F [80]. The second formulation employs both the mean longitude of the satellite, λ, and the mean longitude of the third body, λ', as trigonometric variables. This last formulation is particularly useful for high

altitude satellites whose mean motion is not large relative to the mean motion of the perturbing third body. An Earth Observation satellite has a relatively short period and the third body can be assumed to have a constant position over the satellite orbital period [27].

2.2 Draper Semianalytic Satellite Theory Standalone Orbit Propagator (DSST Standalone)

The Draper Semianalytic Satellite Theory Standalone Orbit Propagator is a descendant of the Goddard Trajectory Determination System (GTDS) Averaged Orbit Generator. The GTDS program was modified by Draper Laboratory to include more perturbations, interpolator choices, models for the short periodic variations, and partial derivatives of the current mean elements with respect to the solve for parameters [27]. The DSST Standalone is a straight orbit propagation program version of the Draper GTDS program which is a full orbit determination system. The DSST Standalone is portable to different host programs and to different computing environments. This thesis will focus on the DSST Standalone because of its application to a maneuver planning simulation.

The Draper Semianalytic Satellite Theory Standalone Orbit Propagator initializes and propagates orbital elements, or ephemeris data, over a period that is maneuver free. If a maneuver takes place, the DSST Propagator reinitializes the ephemeris data and continues the propagation scheme. The driver program, **SEMIANAL**, utilizes five basic subroutines shown in Figure 2.1. Subroutine **SETELM** initializes the epoch time, epoch elements, and the duration of the propagation. **INTANL** initializes the mean element propagator. A call to **BEGANL** sets the direction of integration and starts the integrator at the epoch time. If the user requests output at specified times, subroutine **ORBANL** will propagate to that time and output
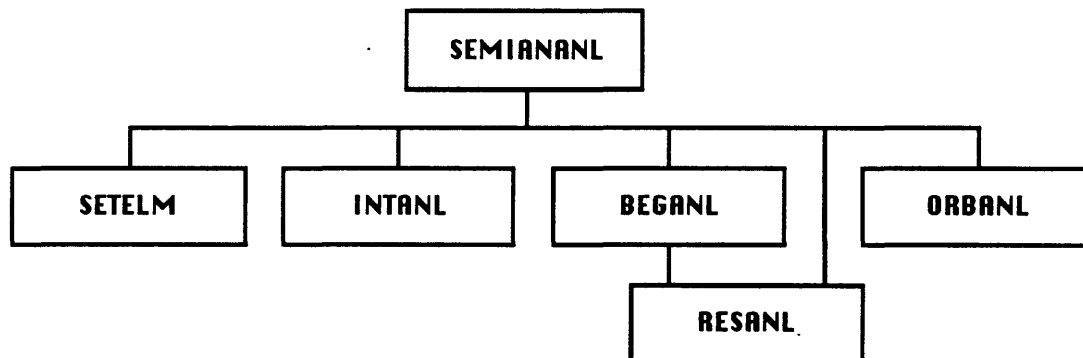
Figure 2.1. DSST Driver SEMIANAL

the ephemeris. Subroutine **RESANL** restarts the integration after an impulsive maneuver takes place. If the maneuver is not modeled as impulsive, calls to **INTANL** and **BEGANL** will restart the integrator to set the new epoch ephemeris to the orbital elements after the maneuver. Calls to **ORBANL** will continue until the end of the propagation period is reached.

2.2.1 SETELM

Subroutine **SETELM** sets the initialization parameters needed by the DSST Propagator to start the integration. The parameters which should be set in this subroutine and their definitions are listed in Table 2.1.

2.2.2 INTANL

Subroutine **INTANL** is called at the beginning of an orbit propagation to initialize the integrator parameters and force models. The parameters input into this subroutine are listed in Table 2.2.

Subroutine **INTANL** calls three subroutines to initialize the integrator parameters and force models. This is shown in Figure 2.2. Subroutine **SETANL** first calls

Table 2.1. SETELM Output

Variable	Definition
ELMINT	Mean orbital elements at epoch. If Keplerian, angular values are in deg a, e, i, Ω, ω, M If Equinoctial, angular values are in rad a, h, k, p, q, λ
RETINT	Retrograde factor if ELMINT is equinoctial
ITYPE	Type of input orbital elements = 1, Cartesian (position, velocity) = 2, Keplerian = 3, Equinoctial
ICOORD	Coordinate system of orbital elements = 1, Mean 1950 = 2, True of Date
IOSCU	Are elements osculating or mean? = 1, osculating = 2, mean
YMDINT	Calendar date of epoch YYYYMMDD.
HMSINT	Time of epoch HHMMSS.SSSSS
YMDEND	Calendar date of end YYYYMMDD.
HMSEND	Time of end HHMMSS.SSSSS
PRTSTP	Print interval in UTC seconds
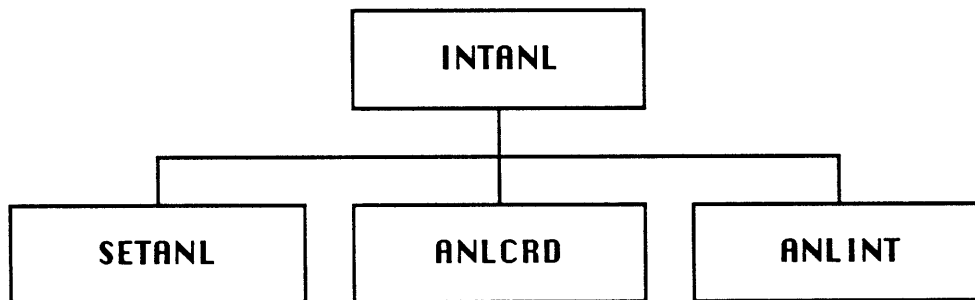
Figure 2.2. Subroutine INTANL

Table 2.2. INTANL Input

Variable	Definition
ELMINT	Mean orbital elements at epoch. If Keplerian, angular values are in deg $a,\ e,\ i,\ \Omega,\ \omega,\ M$ If Equinoctial, angular values are in rad $a,\ h,\ k,\ p,\ q,\ \lambda$
RETRO	Retrograde factor if ELMINT is equinoctial
ITYPE	Type of input orbital elements = 1, Cartesian (position, velocity) = 2, Keplerian = 3, Equinoctial
ICOORD	Coordinate system of orbital elements = 1, Mean 1950 = 2, True of Date
IOSCU	Are elements osculating or mean? = 1, osculating = 2, mean
YMDINT	Calendar date of epoch YYYYMMDD.
HMSINT	Time of epoch HHMMSS.SSSSS

SETFRC to initialize the force model parameters. Then a call to **SETAVR** sets the parameters relevant to the mean element equations of motion. **SETANL** then calls **SETSP** to set the parameters related to the model of the short-periodic perturbations. Finally, **SETANL** calls **SETDRV** to set flags related to the computation of partial derivatives. Then **INTANL** calls subroutine **ANLINT** to determine the parameters that are needed to initialize the integrator. **ANLCRD** is presently an empty subroutine; in the future, **ANLCRD** will process card inputs to the program.

2.2.3   BEGANL

Subroutine **BEGANL** is called at the beginning of an orbit propagation to start the integrator at the desired epoch. This is accomplished by setting the integration direction and the interpolation time step parameters. The propagator is able to propagate forwards or backwards in time, but it may not switch directions in the middle of a propagation. It then initializes the partial derivatives at epoch. Subroutine **RESANL** is called to start the integrator. **BEGANL** must be preceded by a call to **INTANL**. One of the needed input parameters, **DIRINT**, is input through **BEGANL**'s argument listing and the rest are input through **COMMON** blocks denoted by surrounding slashes. The input parameters are described in Table 2.3. The output of **BEGANL** is all through **COMMON** blocks and is listed in Table 2.4.

2.2.4   ORBANL

Subroutine **ORBANL** is called to return the satellite state corresponding to the requested time. The subroutines called by **ORBANL** can be viewed in Figure 2.3. If the requested time is not within the interval of calculated coefficients, subroutine **STPANL** is called to propagate the mean orbital elements, calculate the mean element rates and determine the short periodic interpolator coefficients for the

Table 2.3. BEGANL Input

Variable	Definition
DIRINT	Direction of integration = 1, forward = -1, backward
/ANLFIL/	
NPRINT	Standard output unit
/ANLPRM/	
ELMEPO	Mean equinoctial elements at epoch
NSOLVE	Number of solve for parameters
NSTATE	Number of state solve for parameters
NDYNAM	Number of dynamic solve for parameters
/AVRHST/	
HAFWID	Half-width of interpolator interval
STEP	Integrator step size, negative if backwards
/SPREAL/	
PVSTEP	Interval between successive interpolator points
PVWID	Half-width of interpolator interval
SPSTEP	Interval between successive interpolator points
SPWID	Half-width of interpolator interval

Table 2.4. BEGANL Output

Variable	Definition
/AVRHST/	
HAFWID	Half-width of interpolator interval
STEP	Integrator step size, negative if backwards
AVRDRV	Partials of current mean elements with respect to solve for parameters
/SPREAL/	
PVSTEP	Interval between successive interpolator points
PVWID	Half-width of interpolator interval
SPSTEP	Interval between successive interpolator points
SPWID	Half-width of interpolator interval
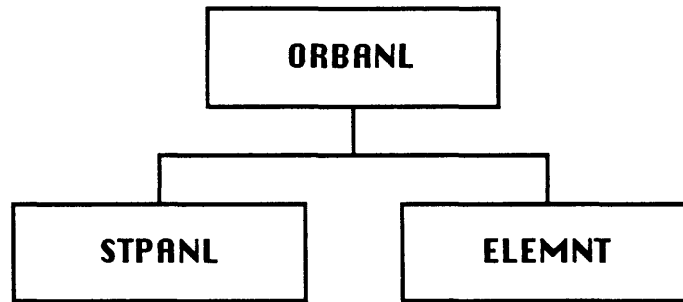
Figure 2.3. Subroutine ORBANL

new interval. Subroutine **ELEMNT** determines the short periodic terms that need to be added to the mean elements to get the osculating satellite state at the output time. Subroutine **ELEMNT** is called much more frequently than subroutine **STPANL** since the mean elements and the short periodics can be interpolated from one integration interval's coefficients for several output times.

If an external event prematurely ends the propagation, the time of the propagation stop is returned with the satellite state and partial derivatives at that time. The input parameters needed by **ORBANL** are listed in Table 2.5. The satellite state at the request time is output in part through **ORBANL**'s argument listing and the rest through **COMMON** blocks. The exact output is listed in Table 2.6.

2.2.5 RESANL

Subroutine **RESANL** restarts the orbit generator through a call to subroutine **RESRNK**, a Runge-Kutta integrator, and through initializing interpolators. The needed incoming parameters are input through **RESANL**'s argument listing or **COMMON** blocks. They are described in Table 2.7. All of **RESANL**'s output is through **COMMON** blocks. These variables are listed in Table 2.8 [55,15]. Subroutine **RESANL** is called by **BEGANL** at the beginning of the program to initialize the integrator. Subroutine **RESANL** can also be called by the main program

Table 2.5. ORBANL Input

Variable	Definition
OBSTIM	Request time from epoch, A.1 sec
/ANLPRM/	
NSOLVE	Number of solve for parameters
/AVRHST/	
DIRECT	Direction of integration = 1, forward = -1, backward
/SPINTG/	
INTPOS	Interpolate for position/velocity? = 1, yes = 2, no
/SPREAL/	
PVEND	End of short-arc interpolator interval, sec

Table 2.6. ORBANL Output

Variable	Definition
POS	Position vector of satellite
VEL	Velocity vector of satellite
OSCELM	Osculating equinoctial elements of satellite
AVRELM	Mean equinoctial elements of satellite
PVDRV	Partial derivatives of current position/velocity with respect to solve for parameters
AVRDRV	Partial derivatives of current mean equinoctial elements with respect to solve for parameters
ENDORB	Does external event stop propagation?
OBSTIM	Request time from epoch, A.1 sec
/SPREAL/	
PVEND	End of short-arc interpolation interval

Table 2.7. RESANL Input

Variable	Definition
ELEMNT	Commanded new mean equinoctial orbital elements
PARDRV	Partial derivatives of the mean equinoctial elements with respect to solve for parameters
RESTIM	Time elapsed from epoch
/AVRHST/	
DIRECT	Direction of integration = 1, forward = -1, backward
/MACHINE/	
DBLNUL	Null value
DBLMAX	Maximum value
DBLMIN	Minimum positive value

Table 2.8. RESANL Output

Variable	Definition
/SPREAL/	
SPBEG	Beginning of auxiliary interpolator interval
SPEND	End of auxiliary interpolator interval
PVBEG	Beginning of position/velocity interpolator interval
PVEND	End of position/velocity interpolator interval

after an impulsive burn to restart the integrator. If the burn model is not impulsive, then the main program must start with a call to **BEGANL** which will then call **RESANL** to restart the integrator.

Chapter 3

The MEANELT Program

The MEANELT computer program is an existing stationkeeping tool received from Aerospace Corporation. It provides a long term simulation of a satellite's stationkeeping capability. This program utilizes the Draper Semianalytic Satellite Theory Standalone Orbit Propagator (DSST Propagator) to propagate the satellite orbit in time until the satellite needs to expend an impulsive maintenance burn. Then, the propagator is reinitialized and propagation continues until the stop time is reached or the fuel budget is depleted. The original MEANELT program was written by R. G. Hopkins of the Aerospace Corporation Astrodynamics Department. It is written in FORTRAN 77 in 51 modules (3, 661 lines of code) in addition to the DSST Standalone subroutines described in Chapter 2.

3.1 Current Capabilities

The stationkeeping capabilities of MEANELT include maintaining the longitude of perigee, apogee, or ascending node, or maintaining the semi-major axis. The program can maintain any one of the longitude variables within a time period of up to ten years. The nominal value of the maintained element is allowed to change over time and the actual maintained longitude will be a linear change from one nominal value

to the other. This program is robust in that it can tolerate stable and unstable points of an orbit, as for a geosynchronous satellite, where perturbing accelerations change sign. There are no assumptions in MEANELT in calculating the nodal period or rate of the longitude drift [44].

MEANELT also has the ability of long term semi-passive eccentricity control. This is attained through varying where impulsive changes in velocity are expended and the magnitude of the impulsive maneuver to maintain the longitude of perigee, apogee, or ascending node, or the semi-major axis. The default is to minimize the change in velocity for longitude maintenance, but there is also a capability to minimize the change in eccentricity or to keep the eccentricity from exceeding a nominal value of eccentricity, e_0 [45].

3.2   Description of Original Software

Only the program flow for maintaining the longitude of the ascending node will be discussed since that capability applies to maintenance of an Earth Observation satellite in a sun synchronous, repeat ground track, and frozen orbit. By maintaining the longitude of the ascending node of every M satellite orbits, or every N nodal days, a repeat ground track orbit can be maintained using the program MEANELT. The total complexity of MEANELT is much too great for the scope of this thesis.

3.2.1   MAIN

The main program for MEANELT first calls two subroutines, **SETDAF** and **SETINP**, to initialize the parameters needed by the orbit propagator, ie. the DSST Standalone, and the stationkeeping portion of the program. These two subroutines are analogous to the DSST Standalone subroutine **SETELM** described in Section 2.2.1. The main program then sets variables to their default values and then reads nine

namelist input files to adjust the input variables of the default case to the desired case simulation. These namelist files parallel the function of subroutine **INTANL** of the DSST Standalone. The nine input namelist files are **FRCSET**, **AVRSET**, **SPSET**, **DVRSET**, **STKPSET**, **MEANSET**, **PROPSET**, **OUTSET**, and **FUELSET**. The namelist **FRCSET** specifies the geopotential, spacecraft physical, solar radiation pressure, and atmospheric drag constants. It also includes the force model used for the orbital perturbations. **AVRSET** contains parameters for the averaged equations of motion including propagation error, resonant terms, and J_2 gravitational potential effects. **SPSET** indicates the parameters that determine if osculating elements will be calculated from evaluated short-periodic terms. **DVRSET** determines if partial derivatives of the current mean state with respect to the epoch mean state, in equinoctial elements, will be calculated. **STKPSET** sets the stationkeeping parameters. **MEANSET** defines the initial mean elements, coordinate system, and reference frame for the repeat orbit and stationkeeping portion of the program, while the namelist **PROPSET** defines the epoch mean elements, coordinate system, reference frame, and output format for the propagation portion of the program, ie. the DSST Standalone. **OUTSET** specifies the printed and plotted output to be produced. Lastly, the namelist **FUELSET** determines if a fuel budget is to be kept and what the fuel initial conditions are.

The main MEANELT program finally calls subroutine **SYNKRO**. It is subroutine **SYNKRO** that acts as the simulation driver.

3.2.2 SYNKRO

Subroutine **SYNKRO** is the main driver for the orbit maintenance simulation. **SYNKRO** first converts the inputs from the namelists to units needed by MEANELT and the DSST Standalone Propagator. This driver then calls two separate compo-

nents, **REPEAT** and **STKEEP** (see Figure 3.1).
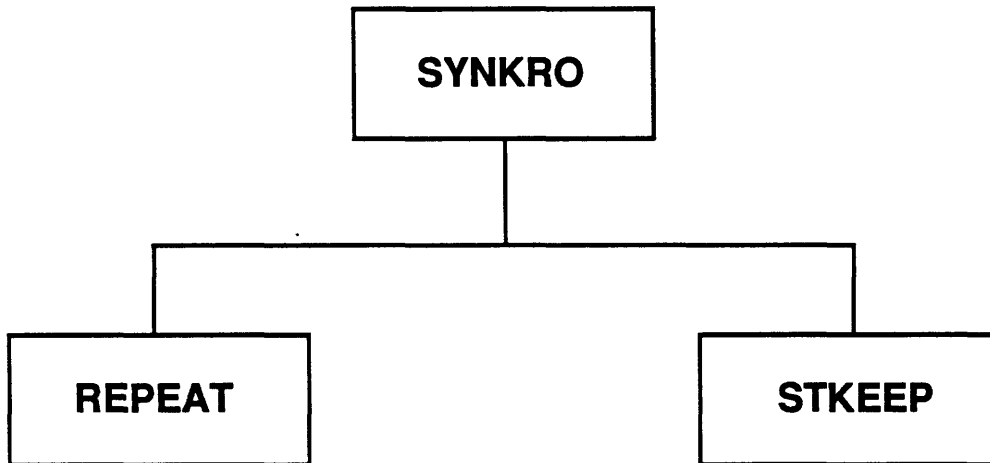
Figure 3.1. Top Level Driver

Subroutine **REPEAT** adjusts the epoch time and epoch elements, input from the namelists, to satisfy user-imposed repeatability requirements and initial perigee altitude. After **REPEAT** is finished, the driver **SYNKRO** calls subroutine **STKEEP** to coordinate the orbit propagation, print the output, and perform stationkeeping maneuvers when required. Subroutine **STKEEP** is the real 'meat' of the MEANELT stationkeeping program [44].

3.2.3 REPEAT

Subroutine **REPEAT** adjusts the epoch time, epoch elements, and input from the namelists to satisfy user-imposed repeatability requirements and initial perigee altitude. To determine these changes, **REPEAT** calls subroutines **TNJECT** and **WIEDER** (see Figure 3.2). Subroutine **TNJECT** initializes the DSST Standalone and adjusts the initial epoch time to achieve the desired Earth fixed longitude at the ascending node. It is subroutine **TNJECT** that calls the DSST Standalone interface
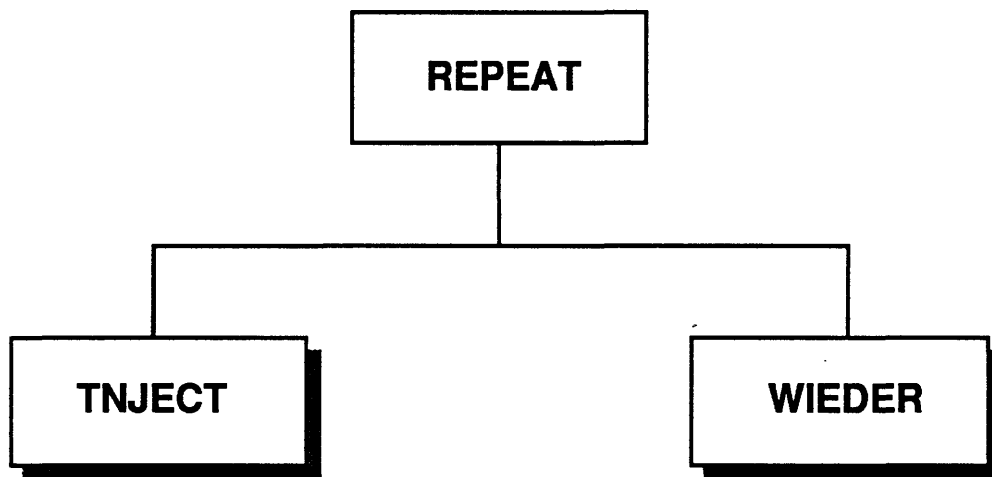
Figure 3.2. Subroutine REPEAT

subroutine **BEGANL**. A subroutine with a shadowed box in the flow diagram signifies a probable site of major modifications in MEANELT for a simulation similar to LANDSAT 6. If the desired orbit is not only constrained by a repeat ground track but also by sun synchronous and frozen orbit constraints, then adjustment of the initial epoch time in **TNJECT** is not needed since the epoch time given will already achieve the needed orbital elements. Subroutine **WIEDER** should be stubbed out all together for the same reasons. Using **WIEDER** iteratively, the semi-major axis can be adjusted to fit the repeatability requirements with a Newton-Raphson technique. If an initial value of perigee altitude is specified by the user, further iteration in **WIEDER** can be performed to adjust both the semi-major axis and eccentricity [44].

3.2.4 STKEEP

Subroutine **STKEEP** coordinates the orbit propagation, prints the output, and performs maintenance maneuvers when required. This is the real 'meat' of the MEANELT stationkeeping program. To accomplish these functions, **STKEEP** calls

subroutines **APOELM**, **OUTPR**, **BDLAM**, and **COREKT**, refer to Figure 3.3.

Subroutine **APOELM** uses Lagrangian interpolation in the z-coordinate to deter-
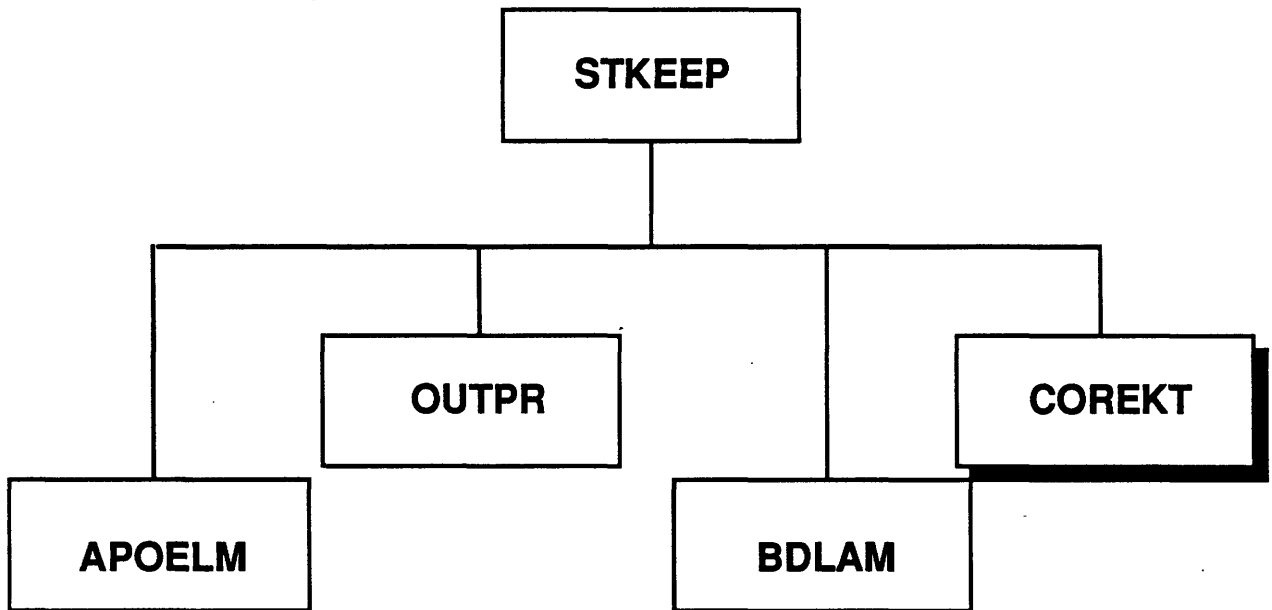
Figure 3.3. Subroutine STKEEP

mine the time of the ascending node crossing. Inside of this subroutine, the DSST Standalone determines the mean orbital elements at that node crossing time through a call to the DSST Standalone **ORBANL**. The subroutine **APOELM** also makes a call to the DSST Standalone subroutine **RESANL** if an impulsive maneuver was just completed. Subroutine **OUTPR** outputs the data concerning orbit propagation and stationkeeping maneuvers to a file and writes various data to arrays for later plotting. The subroutine that compares the geographic longitude of the ascending node to the range of allowed values is **BDLAM**. If no stationkeeping is needed, propagation continues. Subroutine **COREKT** performs the actual stationkeeping maneuver if needed and maintains the fuel consumption of the spacecraft. **COREKT** along with **WIEDER** iteratively determine the value of the semi-major axis and eccentricity to produce the desired variation in the longitude of the ascending node. Here again, subroutine **WIEDER** could be stubbed out and a more direct calculation of

determining the new semi-major axis substituted [44].

It is in subroutine **COREKT** that the long term passive eccentricity control takes place if desired. **COREKT** computes the magnitude of the maintenance burn needed to adjust the semi-major axis to maintain the repeat ground track, ie. the longitude of the ascending node. This burn may occur at many places in the orbit to achieve the change in the semi-major axis desired. Through varying where this impulsive maneuver takes place and varying the magnitude of the burn, subroutine **COREKT** is able to either minimize the velocity expended for longitude maintenance, minimize the change in eccentricity, or keep the eccentricity from exceeding a nominal value of e_0. In the default case, **IALT** $= 0$, where the change in velocity is minimized, the change in eccentricity is approximately:

$$\Delta e \approx (1 - e)\Delta a/a \tag{3.1}$$

In this case, the change in velocity is expended at perigee to adjust the orbit altitude and also affect the eccentricity. This type of maneuver, that changes both the semi-major axis and the eccentricity, is not suitable for an orbit with a small eccentricity when the change in the semi-major axis due to perturbations is less than zero, ie. drag is the dominant perturbation. In this case where the semi-major axis is decreasing, the burn tries to force the eccentricity to a value less than zero. Therefore, the following two capabilities were added to accommodate orbits with small eccentricities. If the change in eccentricity during a burn is to be minimized, **IALT** $= 1$, the semi-major axis will be changed approximately independently of the other orbital elements, see Table 1.6. Half of the ΔV for the altitude adjust will be spent at perigee and half at apogee for small $\Delta a/a$. The change in eccentricity for this case is approximately:

$$\Delta e \approx -e(\Delta a/a) \tag{3.2}$$

This alternate burn will cause only slightly more fuel to be used than in the default

option. If the eccentricity is to be kept from exceeding a set nominal value of eccentricity, **IALT** $= 2$, a combination of the above two cases will be used. If the current eccentricity is less than the nominal value, then the minimum change in eccentricity burn will be simulated. If the eccentricity is greater than the nominal value, then the change in velocity will be expended at perigee if $\Delta a < 0$ or at apogee if $\Delta a > 0$. The latter will lead to a change in eccentricity of:

$$\Delta e \approx -(1+e)\Delta a/a \qquad (3.3)$$

This third option will succeed if the needed change in the semi-major axis is small or maneuvers are made infrequently. In addition, maintaining the eccentricity below a nominal value leads to a substantial increase in the velocity expended and the simulation computational time needed if the change in the semi-major axis due to orbit perturbations is less than zero.

Subroutine **COREKT** assumes an impulsive burn model which may be replaced by actual burn models dependent on time that are discussed further in Section 4.2. In addition, the original repeatability requirements can be replaced with Bruce Baxter's algorithms, see Section 4.1.2 for a specific mathematical discussion of his concepts.

After the new orbital elements and required impulsive Δv are calculated, orbit propagation continues. This is accomplished by **STKEEP** making the necessary call to **APOELM** to restart the orbit propagator through subroutine **RESANL**.

Chapter 4

Maneuver Planning Algorithms

4.1 Orbit Design Concepts

Earth Observation satellites use many common orbit design techniques to improve their instrumentation capabilities. Three of the most common orbit design concepts, sun synchronous orbit, repeat ground track, and frozen orbit, were introduced in Chapter 1 and are discussed in more mathematical detail here.

4.1.1 Sun Synchronous Orbit

A sun synchronous orbit keeps the orbit plane at a constant angle to the sun by using the geopotential perturbations of the Earth to force the line of nodes westward along the equator approximately one degree per day. The line of nodes is defined as the intersection of the orbit plane and the Earth's equator. This line of nodes is often stated as the nearly constant local time of ascending node crossing rather than an angular measurement of longitude. The o'clock angle is the nearly constant angular value between the line of nodes and the Earth/sun line.

Through the application of the Earth's geopotential to Lagrange's Planetary Equations, the mean nodal rate is calculated [18]:

$$\frac{d\bar{\Omega}}{dt} = -\frac{3}{2}J_2 \left(\frac{R_e}{a(1-e^2)}\right)^2 \sqrt{\frac{\mu}{a^3}} \cos i \qquad (4.1)$$

where $\bar{\Omega}$ is the mean longitude of the ascending node, the angle of the line of nodes from the vernal equinox. The variable J_2 is the harmonic coefficient of the Earth's oblateness equal to $1.08263\text{x}10^{-3}$ and the gravitational parameter of the Earth, μ, is equal to 398,601.2 km^3/ sec^2. The mean equatorial radius of the Earth, denoted R_e, is equal to 6378.135 km. These values are approximate and they depend on the actual gravity model used. The semi-major axis, a, the inclination, i, and the eccentricity, e, of the orbit are variables in the common Keplerian orbital element set. By setting the mean nodal rate to sun synchronous:

$$\frac{d\bar{\Omega}}{dt} = \frac{360°}{year}\frac{\pi}{180°}\frac{year}{365.25day}\frac{day}{24hr}\frac{hr}{3600sec}$$

$$= 1.991021 \times 10^{-7} rad/sec \tag{4.2}$$

and assuming that the orbit is near circular, ie. $e \approx 0$, Equation 4.1 may be altered to solve for the sun synchronous relationship between the inclination and the semi-major axis:

$$i = \arccos\left(-4.773621 \times 10^{-15}a^{7/2}\right) \tag{4.3}$$

The graph of this relationship is shown in Figure 4.1.

One of the primary perturbations not considered in the design of the sun synchronous orbit is the third body effects due to the point mass of the sun. The effect of solar gravity on a sun synchronous spacecraft causes the orbital inclination to increase or decrease depending on whether the ascending node is PM or AM, respectively. This change in the inclination creates a change in the nodal precession rate (Equation 4.1) which causes a shift in the expected ground track. This can cause an increase in ground track maintenance if the ground track is to repeat [26].
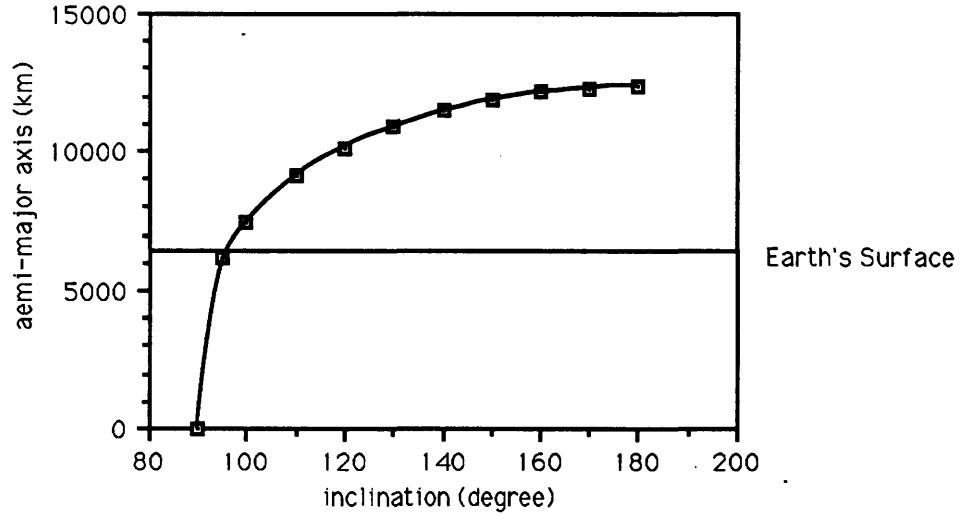
Figure 4.1. Sun Synchronous Orbit: a vs. i

4.1.2 Repeat Ground Track

A satellite ground track is defined as the locus of points traced out on the Earth's surface directly beneath the spacecraft orbit. This ground track does not normally repeat itself, ie. retrace a previous orbit's ground track, by reason of the Earth rotating underneath the satellite orbit while the line of nodes rotates around the Earth's equator due to perturbations. A commensurability condition for a repeat ground track may be determined by using an equation from Baxter [5]:

$$2\pi N = M(\omega_e - \dot{\Omega}_0)P_{N_0} \qquad (4.4)$$

where N is the number of nodal days until the ground track repeats, M is the number of orbits in the repeat cycle, ω_e is the approximately constant rotation rate of the Earth, $\dot{\Omega}_0$ is the initial mean rotation rate of the line of nodes, and P_{N_0} is the initial mean nodal period of the satellite. A nodal day is defined as the time for the Earth to rotate 360° with respect to the line of nodes. A solar day is defined as the time for the Earth to rotate 360° with respect to the Earth-Sun line. If the satellite orbit

is sun synchronous, a solar day is approximately the same as a nodal day since the line of nodes is at a constant angle to the sun. If the satellite is near circular, ie. eccentricity is approximately zero, the equation for the nodal period is [78,18]:

$$P_N = P_k \left[1 - \frac{3}{4} J_2 \left(\frac{R_e}{a} \right)^2 (6 - 5 \sin^2 i) \right] + O(e^2) \qquad (4.5)$$

where P_k is defined as the Keplerian (two body) orbital period [4]:

$$P_k = 2\pi \sqrt{\frac{a^3}{\mu}} \qquad (4.6)$$

where a is the semi-major axis and i is the inclination and both values are taken at the node crossing. As previously stated in Equation 4.1, the variable J_2 is the harmonic coefficient of the Earth's oblateness equal to 1.08263×10^{-3}, the mean equatorial radius of the Earth, denoted R_e, is equal to 6378.135 km, and the Earth's gravitational parameter, μ, is 398601.2 km^3/sec^2. Again, these values are approximate and they depend on the actual gravity model used.

By observing the commensurability condition for a repeating ground track in Equation 4.4, the variable ω_e represents the eastward drift of the Earth while the variable $\dot{\Omega}_0$ represents the natural westward drift of the line of nodes from orbital perturbations, primarily J_2. The cumulative drift difference must be some integer multiple of 2π after M revolutions for the ground track to exactly repeat itself. By manipulating Equation 4.4, an equation for the longitudinal shift of the line of nodes per orbital revolution, $S(0)$, is calculated from the mean nodal period and nodal rate at epoch [5].

$$S(0) = (\omega_e - \dot{\Omega}_0) P_{N_0} = \frac{2\pi N}{M} = \frac{2\pi}{Q} \qquad (4.7)$$

where Q is the number of revolutions per day of the satellite. An illustration of this longitudinal node drift with a non-rotating Earth can be viewed in Figure 4.2. The variable N in this coordinate system can now be viewed as the number of times

80
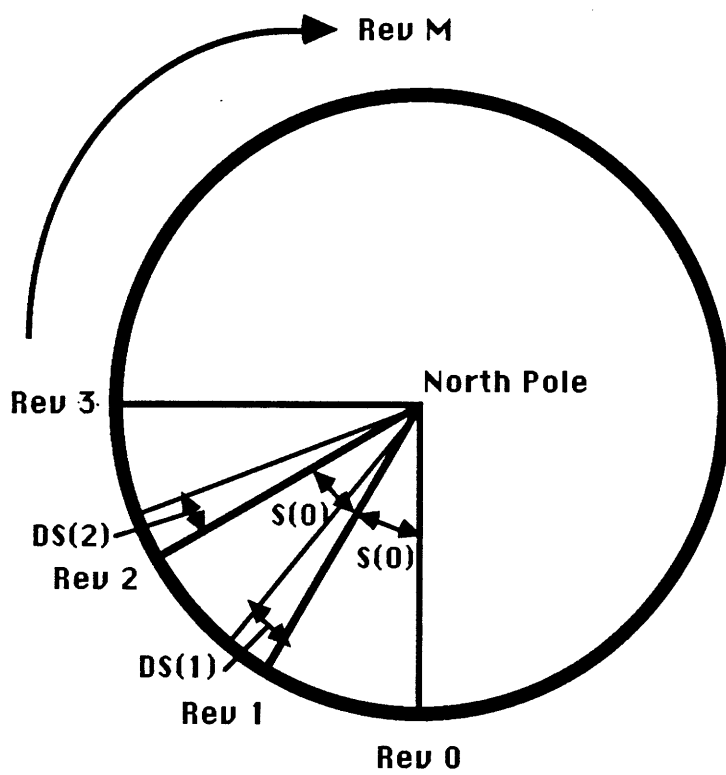
Figure 4.2. Node Drift

that the line of nodes will drift around the equator of a stationary Earth until it returns to its original position. If the variable $S(j)$ is the true longitude drift per orbital revolution for the jth revolution, then the value $DS(j)$ is the instantaneous differential drift in longitude from the original longitudinal drift defined by:

$$
\begin{aligned}
DS(j) &= S(j) - S(0) \\
&= (\omega_e - \dot{\Omega}_j)P_{N_j} - (\omega_e - \dot{\Omega}_0)P_{N_0} \\
&= \omega_e(P_{N_j} - P_{N_0}) - \dot{\Omega}_j P_{N_j} + \dot{\Omega}_0 P_{N_0}
\end{aligned}
\tag{4.8}
$$

By assuming that the longitudinal rate is linear over the time of one orbit revolution, the nodal rate can be equated:

$$
\dot{\Omega}_j = \frac{\Omega_j - \Omega_{j-1}}{P_{N_j}}
\tag{4.9}
$$

Now, substitute Equation 4.9 into Equation 4.8:

$$
DS_j = \omega_e(P_{N_j} - P_{N_0}) - [(\Omega_j - \Omega_{j-1}) - \dot{\Omega}_0 P_{N_0}]
\tag{4.10}
$$

From this equation, the value DS_j can be easily determined from the satellite ephemeris file. An ephemeris is a log of the past positions of the satellite in orbit. Given the longitude of the ascending node, the time of crossing can be interpolated from the ephemeris file. Using this time, the whole satellite state can be found from the ephemeris file. From this satellite state, the nodal period and nodal rate can be calculated, thus the value DS_j is determined. By letting:

$$
\delta P_N = P_{N_j} - P_{N_0}
\tag{4.11}
$$

$$
\delta\Omega = (\Omega_j - \Omega_{j-1}) - \dot{\Omega}_0 P_{N_0}
\tag{4.12}
$$

the instantaneous differential drift in longitude of the ascending node, DS, is now equated:

$$
DS = \omega_e \delta P_N - \delta\Omega
\tag{4.13}
$$

The variable DS can also be viewed as a derivative, therefore:

$$S = S_0 + \int_0^N (DS)dR \qquad (4.14)$$

where S is the cumulative drift, R is the revolution number and S_0 is the initial displacement of the longitude of the ascending node with respect to the nominal value. This value, S_0, is calculated:

$$S_0 = \sum_{i=1}^N S(0) = NS(0) \qquad (4.15)$$

The variable DS is approximately a linear function of time, ie. the rev number, because it is primarily a function of the value δP_N which is an almost linear function of the slowly changing semi-major axis principally due to atmospheric drag. Since the change in the longitude of the ascending node is small compared to the value for the longitude of the ascending node, the value DS can expressed linearly:

$$DS = \alpha_0 + \alpha_1 R \qquad (4.16)$$

where the α coefficients are real numbers. When this linear model is substituted into Equation 4.14 and integrated, the cumulative drift is now a quadratic:

$$\begin{aligned} S &= S_0 + a_1 R + a_2 R^2 \\ &= a_0 + a_1 R + a_2 R^2 \end{aligned} \qquad (4.17)$$

The values for cumulative drift, S, may be smoothed with a sequential Least Squares filter to remove the medium and short periodics and to calculate the coefficients: a_0, a_1, a_2. Now, the equation for DS is solved with $\alpha_0 = a_1$ and $\alpha_1 = 2a_2$.

If S_{ref} is the reference longitude about which the ground track is to be maintained, then the values $S_{ref} \pm S^*$ are the upper and lower boundary longitudes where S^* is the ground track boundary region around S_{ref}. Equation 4.17 gives the station keeping

83

ability within $S_{ref} \pm S^*$, or S_{up} and S_{low}. Since atmospheric drag decreases the semi-major axis, a ground track correction will always be on the lower boundary. For example, by allowing $S = S_{low}$, Equation 4.17 may be solved for the number of orbit revolutions for the ground track to drift from the lower boundary, reach the maximum drift, and return to the lower boundary, ie. let $R = R_{low}$.

$$S_{low} = a_0 + a_1 R_{low} + a_2 R_{low}^2$$
$$a_2 R_{low}^2 + a_1 R_{low} + a_0 - S_{low} = 0$$
$$R_{low} = \frac{-a_1 \pm \sqrt{a_1^2 - 4a_2(a_0 - S_{low})}}{2a_2} \qquad (4.18)$$

To find the number of orbit revolutions until the maximum or minimum of the cumulative drift, S, the partial derivative of S with respect to R is set equal to zero.

$$\frac{\delta S}{\delta R} = 0$$
$$a_1 + 2a_2 R = 0$$
$$R = \frac{-a_1}{2a_2} \qquad (4.19)$$

Now the cumulative drift extremum, S_e, is determined by substituting Equation 4.19 into Equation 4.17:

$$S_e = a_0 + \frac{a_1(-a_1)}{2a_2} + \frac{a_2 a_1^2}{4a_2^2}$$
$$= a_0 - \frac{a_1^2}{4a_2} \qquad (4.20)$$

Since the instantaneous drift rate is the slope of S at that point, the drift rate at R_{low} where the orbit correction is to take place will equal:

$$\left(\frac{\delta S}{\delta R} \right)_{R=R_{low}} = a_1 + 2a_2 R_{low} \qquad (4.21)$$

This drift rate must not only be stopped but reversed so that the drift will approach

84

the extrema value, S_e, again. Therefore, the drift correction, DC, can be calculated:

$$DC = -2\left(\frac{\delta S}{\delta R}\right)_{R=R_{low}} = -2(a_1 + 2a_2 R_{low}) \qquad (4.22)$$

Now, the drift correction must be related to the orbital elements so that the amount of ΔV may be calculated to maintain the ground track. This relationship is furnished by Equation 4.8 since it defines the instantaneous drift rate in terms of the perturbations in the nodal period, δP_N, and the value $\delta\Omega$. A first order Least Squares fit to:

$$\delta\Omega = b_0 + b_1 R \qquad (4.23)$$

using ephemeris data with Equation 4.12 to attain values for $\delta\Omega$ will remove the linear trend caused by $\delta\Omega$ from the quadratic drift correction equation. This is possible since a small change in the nodal period will have a negligible effect of $\delta\Omega$. To induce the necessary drift rate set $DS = DC$:

$$DC = DS = \omega_e \delta P_N - \delta\Omega = -2(a_1 + 2a_2 R_{low})$$

$$DC = \omega_e \delta P_N - b_0 - b_1 R_{low} = -2(a_1 + 2a_2 R_{low})$$

$$\delta P_N = \frac{b_0 - 2a_1 - (4a_2 - b_1)R_{low}}{\omega_e} \qquad (4.24)$$

From Equation 4.5, the nodal period is primarily a function of the semi-major axis, and to a lesser order the inclination and eccentricity. Since the nodal period is basically a function of the semi-major axis, especially for a sun synchronous orbit where the inclination is near polar, a valid assumption to be made is that the nodal period can be approximated by the Keplerian period, ie. $P_N \approx P_k$ where P_k is given in Equation 4.6. Differentiating the Keplerian period determines δP_N:

$$\delta P_N \approx 2\pi\frac{1}{2}\left(\frac{a^3}{\mu}\right)^{-\frac{1}{2}}\frac{1}{\mu}3a^2\delta a \qquad (4.25)$$

$$\approx \frac{3}{2}P_N\frac{\delta a}{a} \qquad (4.26)$$

Recalling the vis-viva integral:

$$v^2 = \mu \left(\frac{2}{r} - \frac{1}{a} \right) \tag{4.27}$$

By assuming a circular orbit where the radial distance, r, equals the semi-major axis, a, the vis viva integral is now:

$$v^2 = \frac{\mu}{a} \tag{4.28}$$

Now differentiate and rearrange Equation 4.28:

$$2v\delta v = \frac{\mu(-1)}{a^2}\delta a$$

$$\frac{\delta a}{a} = -2\frac{a}{\mu}v\delta v = 2\frac{\delta v}{v} \tag{4.29}$$

Now substitute this definition for $\frac{\delta a}{a}$ into Equation 4.25 and solve for ΔV:

$$\delta P_N \approx \frac{3}{2}P_N \left(-2\frac{\delta v}{v} \right)$$

$$\delta v \approx -\frac{v}{3}\frac{\delta P_N}{P_N}$$

$$\Delta V = |\delta v| \approx \frac{v}{3P_N\omega_e}[b_0 - 2a_1 - (4a_2 - b_1)R_{low}] \tag{4.30}$$

This is an approximate value for the magnitude of ΔV needed to correct the semi-major axis since the nodal period was approximated with the Keplerian period.

From Equation 4.17, the parabolic relationship between the orbit revolutions and the amount of longitudinal drift can be graphed, thus showing the orbit correction cycle.

From this illustration, it is easy to see that the decrease in the semi-major axis from atmospheric drag causes the ground track adjust to always occur at the lower boundary. As the ΔV produces a positive δP_N, the line of nodes drifts west, but as P_N decreases due to drag the orbit will reach a point where $P_N = P_e$ at the extremum and the line of nodes will then drift east until the orbit is corrected again.
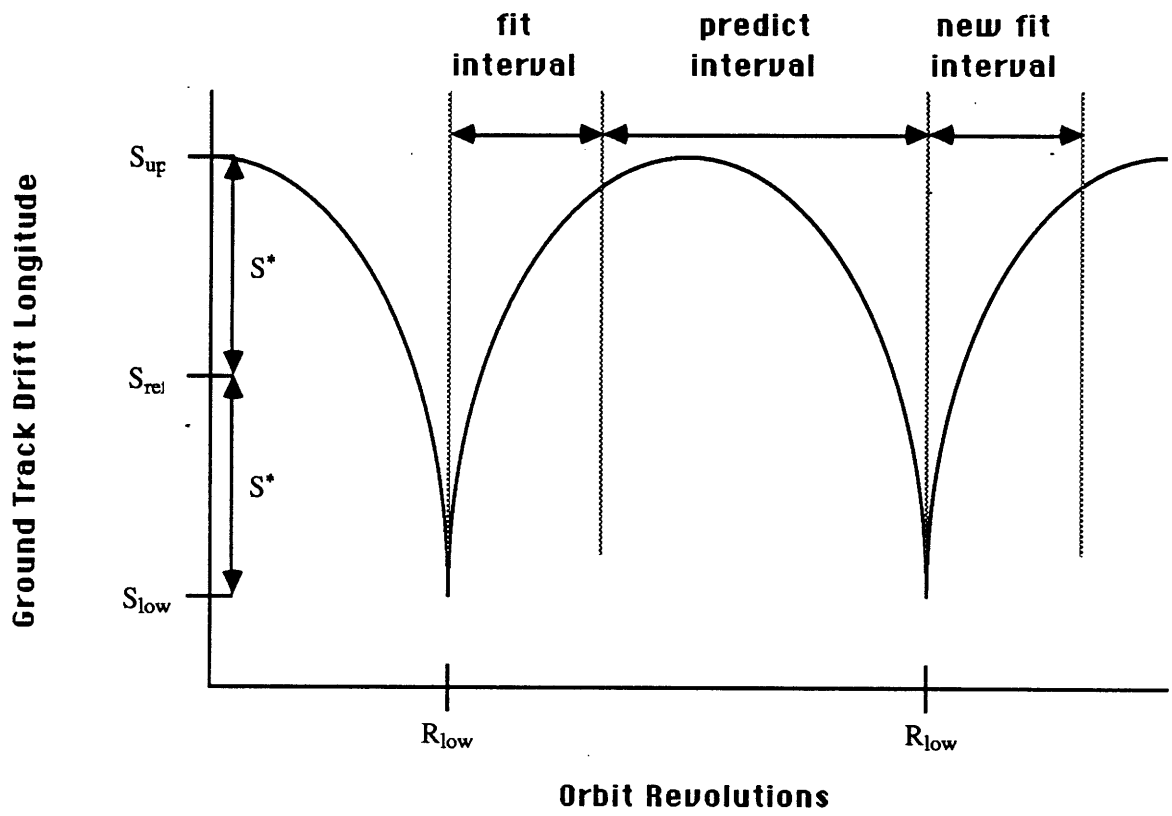
Figure 4.3. Orbit Correction Cycle

It would be an optimal burn if the maximal cumulative drift, S_e, was the same as the upper boundary, S_{up}. But because of the computational lag for the data fit in the beginning of the parabolic arc and uncertainties in the future atmospheric drag, the burn needs to under-correct a bit to avoid having to correct again at the upper bound, usually needing a 180° yaw or pitch attitude maneuver. Therefore, an absolute calculation of ΔV is impossible [5].

There are two types of errors that can destroy the repeating ground track. Primarily, there is atmospheric drag that decreases the semi-major axis and causes the ground track drift trend to be eastward. An illustration of this drift can be viewed in Figure 4.4 [18].
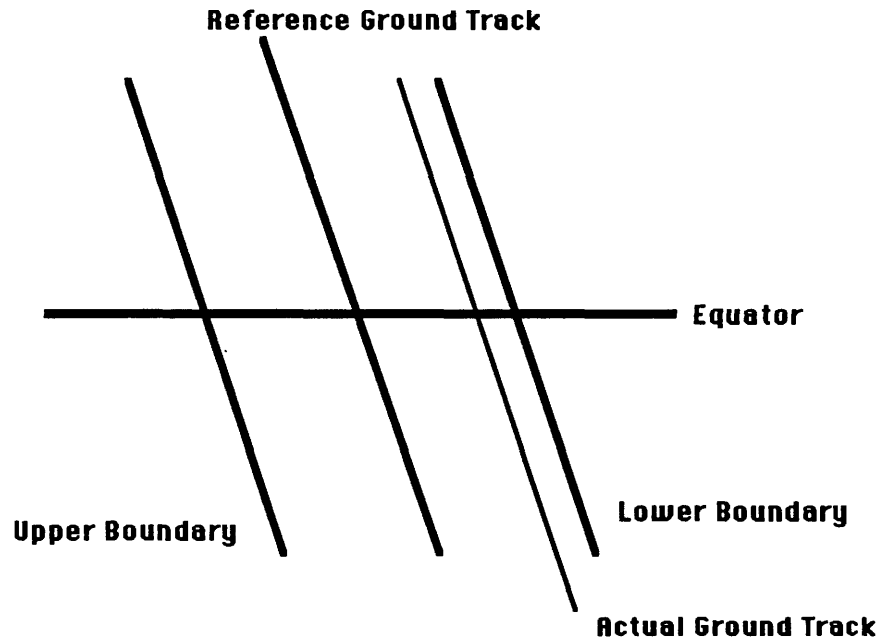
Figure 4.4. Ground Track Drift due to Semi-major Axis Decay

The second type of ground track drift, due to changes in inclination, affects the

nodal period and ground track errors at higher latitudes. A typical AM sun synchronous orbit will have a slow decrease in inclination which will cause a slight decrease in the rate of node regression and a slight increase in the nodal period [48]. Inclination drift will also cause ground track error at higher latitudes. The orbit inclination is perturbed mainly by solar third body gravitational effects, thus slanting the orbit more and upsetting the repeat ground track at the upper latitudes. An example of this type of ground track drift can be viewed in Figure 4.5 [18]. An illustration
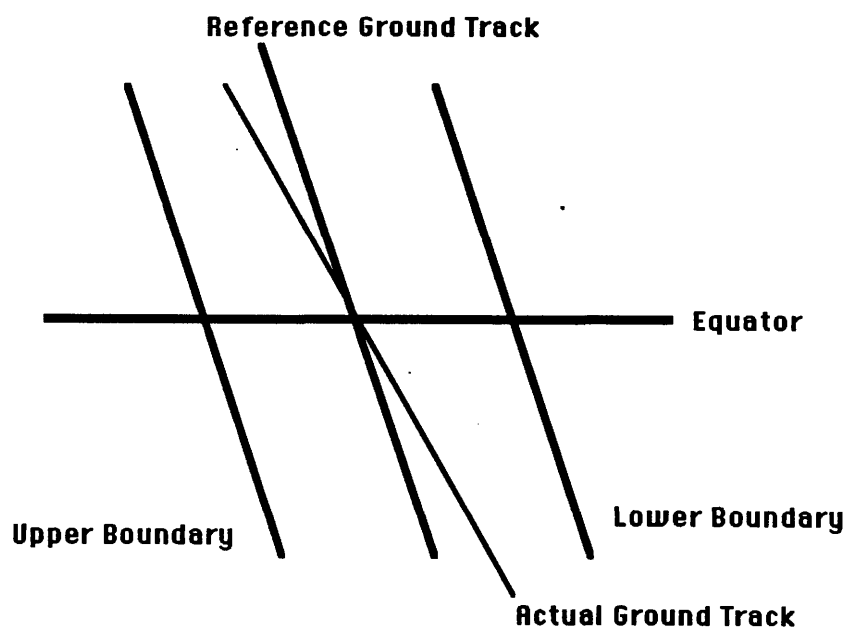
Figure 4.5. Ground Track Drift due to Inclination Decay

of the cumulative effect of the two types of ground track errors can be viewed in Figure 4.6.

The semi-major axis is periodically boosted with a burn in the posigrade direction
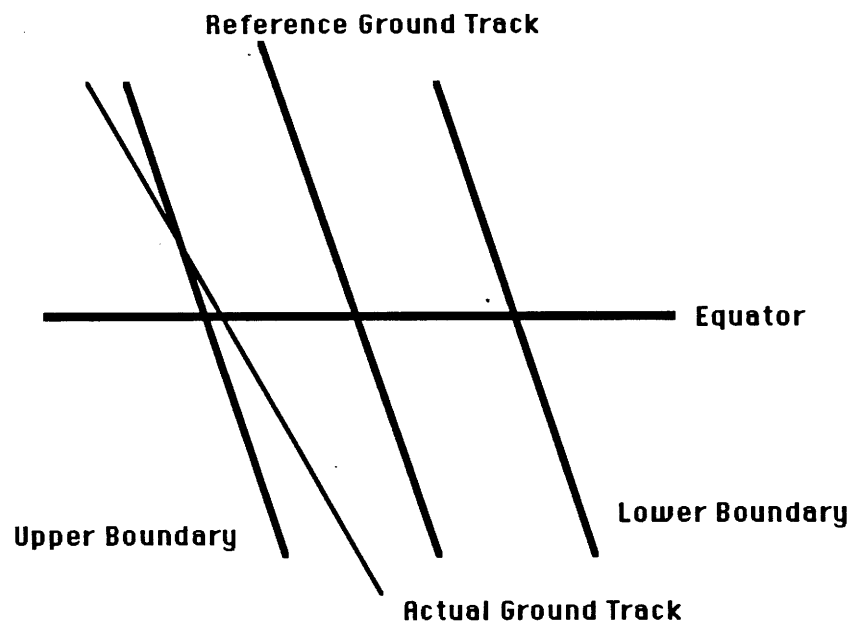
Figure 4.6. Cumulative Ground Track Drift

using the ΔV determined previously is Equation 4.30. The inclination is boosted with an out-of-plane maneuver, but this type of boost is done less frequently than the semi-major axis adjust. As mentioned in Section 4.1.1, the inclination drift in a sun synchronous orbit not only needs to be adjusted to maintain the sun synchronous condition but it also needs to be adjusted to maintain the ground track at the upper latitudes. The out-of-plane maneuver needed for this inclination adjust may be costly because of the attitude maneuver necessary to place the thrusters in the correct position. For a sun synchronous orbit, the satellite may have its inclination biased such that the inclination will drift towards and then away from the desired inclination value, thus elongating the time to an inclination adjust maneuver. The inclination change per day of a sun synchronous satellite can be estimated [26]:

$$\dot{I} = \frac{\Delta \bar{i}}{day} = \frac{3Q\pi}{8n^2} \frac{\mu_s}{r_s^3} (1 + \cos i_s)^2 \sin i_0 \sin 2\Omega_{oc} \tag{4.31}$$

where Q is again the number of orbits per day, n is the satellite mean motion equal to $\sqrt{\frac{\mu}{a^3}}$, μ_s is the solar gravitational parameter, r_s is the mean distance to the center of the sun from the Earth's center, i_0 is the satellite inclination at epoch, Ω_{oc} is the o'clock angle, and i_s is the solar obliquity angle approximately equal to $23.45°$. This change in inclination is very slow, thus it is reasonable to make a first order approximation of the inclination:

$$i = i_0 + \dot{I}T \tag{4.32}$$

Thus the cosine of the inclination can be calculated:

$$\cos i = \cos i_0 \cos \dot{I}T - \sin i_0 \sin \dot{I}T$$

$$\approx \cos i_0 - \dot{I}T \sin i_0 \tag{4.33}$$

The latter equation comes from the assumption that the time multiplied by the rate of change of the inclination in radians is very small. Now substituting Equation 4.33

91

into the equation for the nodal rate, Equation 4.1 and the assumption that the orbit is near circular:

$$
\begin{aligned}
\dot{\bar{\Omega}} &= -\frac{3}{2}J_2\left(\frac{R_e}{a}\right)^2 n\cos i \\
&= -\frac{3}{2}J_2\left(\frac{R_e}{a}\right)^2 n[\cos i_0 - \dot{i}T\sin i_0] \\
&= \dot{\bar{\Omega}}_0 + \frac{3}{2}J_2\left(\frac{R_e}{a}\right)^2 n\dot{i}T\sin i_0
\end{aligned}
\tag{4.34}
$$

If it is assumed that the mean node rate is a linear approximation:

$$
\dot{\bar{\Omega}} = \dot{\bar{\Omega}}_0 + \ddot{\bar{\Omega}}T
\tag{4.35}
$$

then the acceleration of the line of nodes is calculated:

$$
\ddot{\bar{\Omega}} = \frac{3}{2}J_2\left(\frac{R_e}{a}\right)^2 n\dot{i}\sin i_0
\tag{4.36}
$$

By integrating Equation 4.35, an equation for the line of nodes can be found:

$$
\begin{aligned}
\Omega &= \Omega_0 + \dot{\bar{\Omega}}_0 T + \frac{\ddot{\bar{\Omega}}_0}{2}T^2 \\
\Omega = \Omega_{ss} + \delta\Omega &= \Omega_0 + (\dot{\bar{\Omega}}_{ss} + \delta\dot{\bar{\Omega}}_0)T + \frac{3}{4}J_2\left(\frac{R_e}{a}\right)^2 n\dot{i}T^2\sin i_0
\end{aligned}
\tag{4.37}
$$

where $\dot{\bar{\Omega}}_{ss}$ is the node regression rate for a sun synchronous orbit, $\delta\dot{\bar{\Omega}}_0$ is the initial error in the node regression rate, and Ω_{ss} is the instantaneous line of nodes for a sun synchronous orbit which equals $\Omega_0 + \dot{\bar{\Omega}}_{ss}T$. The initial error in the line of nodes, $\delta\Omega$, is calculated:

$$
\delta\Omega = \delta\dot{\bar{\Omega}}_0 T + \frac{\ddot{\bar{\Omega}}_0}{2}T^2
\tag{4.38}
$$

where the first term in this equation is due to launch vehicle and orbit injection errors and the second term is due to solar gravitational effects. The maintenance requirements for the inclination drift can be reduced by injecting the satellite into an orbit with an inclination bias of an opposite polarity of inclination change than that caused by solar gravity [26].

4.1.3   Frozen Orbit Concept

The frozen orbit concept is based on minimizing the mean eccentricity and argument of perigee rates of change due to the Earth's geopotential perturbations. A frozen orbit, where the eccentricity and argument of perigee remain approximately stable, establishes a balance between the secular and long periodic contributions caused by the even zonal harmonics and the long periodic contributions caused by the odd zonal harmonics. The primary harmonics that affect the rates of change for the eccentricity, e, and argument of perigee, ω, are the J_2 and J_3 zonal harmonic terms [61]. In the orbit analysis for SEASAT, the mean element rates for the eccentricity and argument of perigee are calculated [21]:

$$\frac{de}{dt} = -\frac{3nR_e^3 J_3 \sin i}{2a^3(1-e^2)^2} \left(1 - \frac{5}{4}\sin^2 i\right) \cos\omega \qquad (4.39)$$

$$\frac{d\omega}{dt} = \frac{3nJ_2 R_e^2}{a^2(1-e^2)} \left(1 - \frac{5}{4}\sin^2 i\right) \Theta \qquad (4.40)$$

$$\Theta = 1 + \frac{J_3 R_e}{2J_2 a(1-e^2)} \left(\frac{\sin^2 i - e\cos^2 i}{\sin i}\right) \frac{\sin\omega}{e} \qquad (4.41)$$

where n is the mean motion of the satellite and R_e is the Earth's mean equatorial radius. The elements in these equations are assumed to be mean elements. Inspecting Equation 4.39, the mean eccentricity rate will approach zero for an equatorial orbit (ie. $i = 0, 180°$), an orbit at critical inclination (ie. $i_{crit} = 63.4°, 116.6°$), or an orbit which has an argument of perigee, ω, at $\pm 90°$. If the orbit inclination is constrained, as for sun synchronous orbits or Earth coverage constraints, the only variable available to minimize the mean eccentricity rate is the argument of perigee. By inspecting Equation 4.40, the mean argument of perigee rate vanishes when the orbit is at critical inclination or when the variable Θ goes to zero. For the same reasons as in the eccentricity, only Θ is available for orbit selection. By setting Θ to zero, the nominal eccentricity, e_0, that will minimize the rate of argument of perigee can be

determined:

$$e_0 \approx -\frac{J_3}{2J_2}\frac{R_e}{a}\sin i \sin \omega + O(e) \qquad (4.42)$$

If the orbit is not near the critical inclination, this equation is mainly driven by the J_2 term, even when higher zonal harmonics are added. This means that the nominal eccentricity will be nearly equal to $|\frac{J_3}{J_2}| \approx J_2 \approx .001$. Although the eccentricity does change when higher zonals are added to the gravity model, the eccentricity never changes more than twenty percent. If the orbital inclination is near critical, the eccentricity is no longer approximately equal to J_2 and can reach values much larger.

Other perturbations, such as drag, cause the eccentricity to drift from this nominal value. Therefore, the eccentricity must be periodically adjusted with maintenance burns. In orbit analysis for NROSS, it was determined that the change in eccentricity would be very small over time from perturbations other than the Earth's geopotential, and this small change could be easily counteracted during the required semi-major axis adjustment burns. An additional advantage to the frozen orbit concept, besides passive control of the eccentricity and argument of perigee, is that all global and local altitude variations are minimized. The global altitude variation is minimized through the damping of the long period motion of the eccentricity. The local altitude variation is minimized since the argument of perigee oscillates around its stable value of $\pm 90°$ instead of rotating about the orbit [61].

4.2 Maneuver Models

4.2.1 Impulsive Targeting Model

Ground track drift necessitates thruster burns to maintain the perturbed orbital elements, specifically the semi-major axis, a, and the orbital inclination, i. The thruster models used in the LANDSAT 6 mission profile are not modelled as impulsive

94

burns, but an impulsive model can be used initialize the burn parameters of the burn model. These parameters can be refined in numerical or analytical integration of the equations of motion for a continuous thrust model.

Inclination Maintenance

As discussed above, the inclination is mainly perturbed in a sun synchronous orbit by solar gravity. This change in orbit inclination not only causes displacement of the ground track at higher latitudes, but it also affects the nodal period, see Equation 4.5. The inclination burns to correct the perturbations are expected to take place every 6 months if the ground track is maintained within ±1 km, or every 30 months if the ground track is maintained within ±5 km [62]. Since the LANDSAT 6 spacecraft will have thrusters in only one direction, an inclination adjust maneuver will require an approximately 90° yaw to position the thrusters in the correct direction. The change in inclination, i, to first order in the eccentricity can be determined from the equation [62]:

$$\Delta i = \frac{1}{na} \Delta v_N \cos u + \mathcal{O}(e^2) \qquad (4.43)$$

where n is the mean motion of the satellite, Δv_N is the magnitude of the change in velocity in the positive normal direction, and u is the argument of latitude which equals the sum of the true anomaly, f, and the argument of perigee, ω. This equation can be inverted to determine the impulsive value of the velocity needed in the normal direction to achieve the desired change in the inclination [62]:

$$\Delta v_N = \frac{na}{\cos u} \Delta i \qquad (4.44)$$

According to McClain [62], this yaw angle to position the thrusters for an inclination burn is not exactly 90°. Since an exact out of plane burn would result in a change in the semi-major axis, an unnecessary drift in the ground track could be

caused which could even require a retrograde maneuver to correct the semi-major axis. A simple way to observe this phenomenon in the yaw angle is to examine the velocity vectors in the normal and tangential planes, see Figure 4.7. In this figure, the
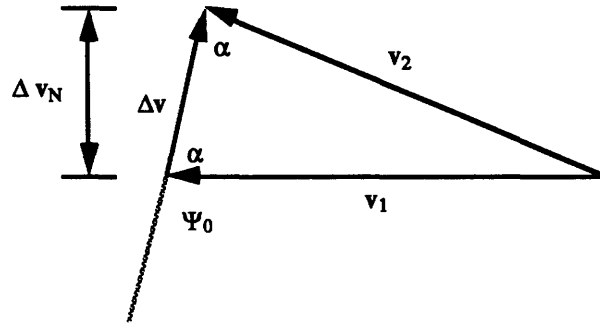
Figure 4.7. Velocity Vectors in Normal and Tangential Planes

velocity vectors before and after the burn, v_1 and v_2, must be of equal magnitude, thus following the expression:

$$\mathbf{v_2} = \mathbf{v_1} + \Delta \mathbf{v} \tag{4.45}$$

$$|\mathbf{v_2}| = |\mathbf{v_1}| = v \tag{4.46}$$

This constraint on the velocity vectors of the satellite before and after the burn create an isosceles triangle allowing the yaw angle, ψ_0, to be determined with the law of cosines:

$$\psi_0 = \frac{\pi}{2} + \arcsin \frac{1}{2} \frac{\Delta v}{v} \tag{4.47}$$

The placement of the actual burn may also effect a change in the longitude of the ascending node, which is not desired. This change may be nulled by performing the burn at the equator crossing, which can be seen by the equation:

$$\Delta \Omega \sin i = \frac{1}{na} \Delta v_N \sin u + \mathcal{O}(e^2) \tag{4.48}$$

The yaw angle must also account for possible errors. There are factors such as the uncertainty of the actual yaw angle, the yaw maneuver bias, thruster misalignment, attitude uncertainty, and a deliberate yaw bias to achieve a small decrease in the semi-major axis with the inclination adjust maneuver since the inclination also affects the nodal period. This bias, approximately 2° for LANDSAT 5, avoids an immediate retrograde maneuver to correct the semi-major axis for the new nodal period. The total impact of the uncertainties affecting the yaw angle, can be determined:

$$\Delta\psi = \sqrt{\sum_k (\Delta\psi_k)^2} \qquad (4.49)$$

Now the actual yaw angle, ψ, can be related to the ideal yaw angle, ψ_0, with the equation:

$$\psi = \psi_0 + \Delta\psi \qquad (4.50)$$

From Figure 4.7, the magnitude of the impulsive velocity needed to change the inclination is determined:

$$\Delta v = \frac{\Delta v_N}{\sin\psi} \qquad (4.51)$$

This value of the impulsive velocity can be used to initialize the burn parameters in the actual finite burn model for the change in inclination [62].

Ground Track Maintenance

As reviewed previously, the ground track drift, in kilometers, is determined with the following commensurability condition [5]:

$$S = (\omega_e - \dot{\Omega})P_N R_e \qquad (4.52)$$

where S is the spacing between consecutive ascending equator crossings, ω_e is the mean rotation rate of the Earth, $\dot{\Omega}$ is the rate of the longitude of the ascending node, P_N is the nodal period, and R_e is the equatorial radius of the Earth. According to

McClain [64], the ground track drift after one orbit revolution, ΔS, can be displayed as a truncated Taylor series expansion if the perturbations are assumed to be small; this is true if mean elements are used.

$$\Delta S = \frac{\delta S}{\delta a}\Delta a + \frac{\delta S}{\delta i}\Delta i \qquad (4.53)$$

where

$$\frac{\delta S}{\delta a} = R_e(\omega_e - \dot{\Omega})\frac{\delta P_N}{\delta a} - R_e P_N \frac{\delta \dot{\Omega}}{\delta a} \qquad (4.54)$$

$$\frac{\delta S}{\delta i} = R_e(\omega_e - \dot{\Omega})\frac{\delta P_N}{\delta i} - R_e P_N \frac{\delta \dot{\Omega}}{\delta i} \qquad (4.55)$$

$$\Delta a = \Delta a_0 + \frac{da}{dt}(t - t_0) \qquad (4.56)$$

$$\Delta i = \Delta i_0 + \frac{di}{dt}(t - t_0) \qquad (4.57)$$

The average rate of drift over one day, also the average rate of the total ground track drift, is determined:

$$\frac{d}{dt}(\Delta S) = \frac{dS}{dt} = \frac{\Delta S}{P_N} \qquad (4.58)$$

$$= \frac{1}{P_N}\left[\frac{\delta S}{\delta a}\Delta a_0 + \frac{\delta S}{\delta i}\Delta i_0\right] + \frac{1}{P_N}\left[\frac{\delta S}{\delta a}\frac{da}{dt} + \frac{\delta S}{\delta i}\frac{di}{dt}\right](t - t_0) \qquad (4.59)$$

$$= K_1 + K - 2(t - t_o) \qquad (4.60)$$

where

$$K_1 = \frac{1}{P_N}\left[\frac{\delta S}{\delta a}\Delta a_0 + \frac{\delta S}{\delta i}\Delta i_0\right] \qquad (4.61)$$

$$K_2 = \frac{1}{P_N}\left[\frac{\delta S}{\delta a}\frac{da}{dt} + \frac{\delta S}{\delta i}\frac{di}{dt}\right](t - t_0) \qquad (4.62)$$

By integrating the expression for the total ground track drift, the quadratic expression is yielded:

$$S - S_0 = K_1(t - t_0) + \frac{1}{2}K_2(t - t_0)^2 \qquad (4.63)$$

98

where S and S_0 are the values of the ground track drift from the nominal ground track at their respective times of t and t_0. By allowing S to equal the maximum longitude, S_{max} in this equation, the basis to calculate the necessary Δv to cause the ground track to drift to its maximum longitude, S_{max}, is provided. First the partial derivatives of S with respect to the semi-major axis and the inclination must be calculated from Equations 4.54 and 4.55. Then the value for the quadratic coefficient K_2 must be calculated from Equation 4.62. From this value of K_2, the value for the coefficient K_1 can be determined by inverting Equation 4.63:

$$K_1 = \sqrt{2K_2(S_0 - S_{max})} \qquad (4.64)$$

The desired value for the semi-major axis adjust is determined by inverting Equation 4.61:

$$\Delta a = K_1 P_N \left(\frac{\delta S}{\delta a}\right)^{-1} \qquad (4.65)$$

The impulsive change in velocity to change the semi-major axis will be in the tangential direction and is computed:

$$\Delta v_T = \frac{n^2 a}{2v} \Delta a \qquad (4.66)$$

If the orbit eccentricity is assumed to be very small, as in the LANDSAT 6 case, the impulsive change in velocity can be more simply expressed:

$$\Delta v_T = \frac{n}{2}\Delta a + \mathcal{O}(e) \qquad (4.67)$$

This value of the impulsive velocity can be used to initialize the burn parameters in the actual finite burn model for the change in the semi-major axis [64].

Frozen Orbit Maintenance

As discussed above, the frozen orbit condition is a function of the calculated nominal values of eccentricity, e_0, and argument of perigee, ω_0. An additional way of

representing these parameters is to combine them to represent an eccentricity vector in polar coordinates, where [61]:

$$e_x = e \cos \omega \qquad (4.68)$$

$$e_y = e \sin \omega \qquad (4.69)$$

The actual eccentricity vector will be displaced from the nominal eccentricity vector because of orbit perturbations that were not modeled in the frozen orbit condition. The actual eccentricity vector will be displaced from the nominal eccentricity vector by the vector Δe with components [63]:

$$\Delta e_x = e \cos \omega - e_0 \cos \omega_0 \qquad (4.70)$$

$$\Delta e_y = e \sin \omega - e_0 \sin \omega_0 \qquad (4.71)$$

The magnitude of the displacement eccentricity vector is calculated:

$$d^2 = |\Delta e| \qquad (4.72)$$

$$= \sqrt{(\Delta e_x)^2 + (\Delta e_y)^2} \qquad (4.73)$$

and the direction of the displacement eccentricity vector is calculated:

$$\theta = \arctan \left(\frac{\Delta e_y}{\Delta e_x} \right) \qquad (4.74)$$

These polar coordinates of the eccentricity vector are sensitive to changes in the velocity in the tangential direction. The effects of these changes are determined [61]:

$$\delta e_x = \frac{2}{na} \cos u \Delta v_T + \mathcal{O}(e) \qquad (4.75)$$

$$\delta e_y = \frac{2}{na} \sin u \Delta v_T + \mathcal{O}(e) \qquad (4.76)$$

where n is the satellite mean motion, a is the semi-major axis, and u is the argument of latitude equal to the sum of the true anomaly and the argument of perigee. The

100

argument of latitude where the burn takes place determines the effect that the burn will have on the eccentricity vector. As observed from Equation 4.67, the tangential velocity needed to adjust the semi-major axis is independent of the latitude of the burn. Thus, the burn may be planned in its location to adjust not only the semi-major axis but also the frozen orbit parameters back to their nominal values with no more fuel expended than was previously necessary by the independent semi-major axis adjust.

The magnitude of the displacement of the eccentricity vector can be combined from Equations 4.75 and 4.76 in the following expression [63]:

$$D^2 = |\delta \mathbf{e}|^2 \tag{4.77}$$

$$= \left(\frac{2}{na}\right)^2 (\Delta v_T)^2 \tag{4.78}$$

where the value of the change in velocity in the tangential direction, Δv_T is determined from the needed change in velocity for the semi-major axis adjust. If the needed change in the eccentricity vector, d, is less than the change in the eccentricity vector due to the change in tangential velocity, D, then two separate burns are needed to correctly adjust both the semi-major axis and the frozen orbit parameters. This is called **Case 1**. If the needed change is greater than or equal to the change in the eccentricity vector due to the change in tangential velocity, only one orbit burn is needed. This is called **Case 2** [63]. In **Case 1**, the two burns will take place at:

$$u_1 = \theta \pm \pi \tag{4.79}$$

$$u_2 = u_1 + \pi \tag{4.80}$$

where u is the argument of latitude where the burn is to take place and θ is defined in Equation 4.74. The magnitude of impulsive velocity expended at each of the two

burns is determined:

$$\Delta v_{T_1} = \frac{\Delta v_T}{2} + \frac{na}{4}d \tag{4.81}$$

$$\Delta v_{T_2} = \frac{\Delta v_T}{2} - \frac{na}{4}d \tag{4.82}$$

where d is determined by Equation 4.73, Δv_T is determined from Equation 4.67, n is the satellite mean motion, and a is the semi-major axis. In **Case 2**, the one impulsive burn will take place at an argument of latitude:

$$u = \theta + \pi \tag{4.83}$$

where θ is determined in Equation 4.74. The magnitude of the burn in **Case 2** is equal to the impulsive burn calculated in Equation 4.67 for the change in the semi-major axis. These values of the impulsive velocities can be used to initialize the burn parameters in the actual finite burn model for the change in the semi-major axis [63]

4.2.2 Finite Burn Models

As discussed in the previous section, the LANDSAT 6 mission profile has finite burn models that are to be initialized by the impulsive changes in velocity to adjust the orbital elements to maintain the repeat ground track, sun synchronous, and frozen orbit conditions. The finite burn model over time is expressed [59]:

$$\epsilon(t) = \epsilon_0 \begin{cases} \left[e^{k(t-t_0)} - 1\right] & 0 \leq t - t_0 \leq 40 \text{ msec} \\ A\{\ln[L(t - t_0)] + C\} & 40 \text{ msec} < t - t_0 < 867 \text{ msec} \\ 1 & 867 \text{ msec} \leq t - t_0 \leq t_b - t_0 \\ e^{-d(t-t_b)} & 0 \leq t - t_b \leq 104 \text{ msec} \end{cases} \tag{4.84}$$

where

$\epsilon(t)$ = thrust acceleration magnitude normalized by the gravitational acceleration at the Earth's surface

ϵ_0 = maximum value of the normalized thrust acceleration

t_0 = burn acceleration initiation epoch

t_b = burn acceleration cut-off epoch

k, A, L, C, d = thruster dependent parameters

This model for the thrust acceleration may be added as a perturbation to the equations of motion and integrated either analytically or numerically to determine how the mean elements change with respect to time during the maneuver. Numerical integration would require step sizes on the order of fractions of a second. This is inconsistant with the general approach in the semianalytical theory. An analytical integration would assume an upper limit of 16 minutes to the burn time, or approximately 60° of orbit motion. These analytical models were applied to a finite burn lasting longer than the 16 minute limit, ie. 18 min. and 30 min. These burns calculated a semi-major axis that differed from the more accurate numerical integration scheme by $2.5 \times 10^{-3}\%$ for the 18 minute burn and $6 \times 10^{-3}\%$ for the thirty minute burn. These errors are very small [66]. The analytical equations used in the LANDSAT 6 mission design for the actual thrust profile are determined by McClain in references [67,59].

Chapter 5

Ground Track Motion Forecasting

Forecasting the ground track is a difficult task. An orbit propagator can be used to determine to a certain accuracy the perturbations affecting the orbit and how these changes affect the ground track. The most difficult of the perturbations to forecast is the atmospheric drag. Complex equations for drag dependent on the spacecraft model exist, but a simple equation for determining atmospheric drag is [23]:

$$\mathbf{a}_{drag} = -\frac{1}{2}\frac{C_D A}{m}\rho v_{rel}\mathbf{v}_{rel} \tag{5.1}$$

where $\mathbf{a}_{drag}$ is the perturbing acceleration due to drag, C_D is the coefficient of drag dependent on the spacecraft structure and material, A is the area of the satellite perpendicular to the satellite velocity relative to the atmosphere, $\mathbf{v}_{rel}$, and m is the spacecraft mass. The upper atmospheric density, ρ, is affected by a complex interaction between the sun, the solar wind, and the Earth's geomagnetic field. Thus, the atmospheric density is a function on the satellite's altitude, latitude, longitude, local time, as well as geomagnetic and auroral activity, and solar flux levels [75]. The solar flux affects the atmospheric density through direct and instantaneous heating by extreme ultraviolet radiation. The geomagnetic activity affects the atmosphere through delayed indirect heating of atmospheric energetic particles from collisions with charged particles emitted from the sun. This heating of the atmosphere causes

105

the density to increase at higher altitudes. The solar flux level and the geomagnetic activity are difficult to predict but are two main inputs into current models of the atmosphere. These two factors are discussed further below.

5.1 Solar Activity

As stated in Prochaska [75], solar flux, the amount of heating that the upper atmosphere experiences through the absorption of extreme ultraviolet (euv) solar radiation, is impossible to measure since the atmosphere does not allow the euv radiation to pass through. There are no current space born systems to measure euv flux nor atmospheric density models to use these space based measurements. Investigation of new models and new parameters such as the precipitation index is currently being done [37,38]. Therefore, the euv measurement must be inferred from the closely correlated Earth based measurements of 10.7 cm length radio waves ($F_{10.7}$). Both radiation types, euv and $F_{10.7}$, originate in the same layers of the sun's chromosphere. The Earth's atmosphere is transparent to the $F_{10.7}$ radiation; its value has been routinely measured since 1940. The $F_{10.7}$ radiation is measured in solar flux units (SFU), $1\ SFU = 1 \times 10^{-22} \frac{watt}{m^2 Hz}$; typical values range from less than 70 to more than 300 SFU [74].

The solar flux exhibits two superimposed cyclic variations. The primary factor is an approximate 11 year cycle that roughly parallels, but lags a few years behind the sun spot cycle. The minimum of this cycle is not halfway between the two maximums since the decreasing phase of the cycle is 6-7 years. The actual peak of the 11 year cycle varies from cycle to cycle.

The secondary solar flux period lasts approximately 6 months and is related to the varying distance of the Earth from the sun during its slightly elliptical orbit. In addition to these two cycles, there are irregular changes to the solar flux that are

related to the growth and decay of active solar regions. These active regions not only have many different patterns of growth, stability, and decay, but also rotate with the sun, approximately 27 days per rotation, thus causing an uncertain cyclic pattern. These patterns are difficult to predict. It is also difficult to determine how they will contribute to the heating of the Earth's atmosphere. It is this uncertainty that affects the accuracy of solar flux predictions [74].

Another characteristic of the density is the diurnal bulge, or local atmospheric expansion, created by the constant heating of the atmosphere on the sunlit side of the Earth. The bulge axis has a local time.of approximately 2-2:30 pm. The bulge is centered on the equator at the equinoxes but moves to higher latitudes than the sun's declination at the solstices. The diurnal bulge makes the atmospheric density dependent on latitude, local time, and time of year [23]

The most commonly accepted measurement of $F_{10.7}$ is distributed by the National Oceanic and Atmospheric Administration (NOAA) at the National Geophysical Data Center in Boulder, Colorado. The actual measurement is made at the Algonquin Radio Observatory in Ottawa, Ontario, Canada [82].

5.2   Geomagnetic Index

Direct collisions of the solar wind with air particles interacting with the Earth's geomagnetic field heat the atmosphere. Geomagnetic activity must be measured to determine the heat generated. The planetary geomagnetic index, k_p, is a quasi-logarithmic worldwide average of geomagnetic activity below the auroral zones. This value is measured every three hours. The geomagnetic planetary amplitude, a_p, is the linear equivalent of this index. Eight values are measured daily and averaged to create the commonly used daily planetary amplitude, A_p [23,36]. The daily planetary amplitude A_p is measured in units of 2 gammas, where 1 gamma $= 10^{-9}$ Tesla. A

typical range of A_p is from 0 to 400; values greater than 100 are rare. The daily planetary amplitude tends to follow the 11 year sun spot cycle, although there are consistently large maximums of A_p in the declining phase of each 11 year cycle. There is also a secondary semi-annual cycle due to the variable position of the solar wind with respect to the Earth's magnetosphere. This cycle is just as variable and as hard to predict as the sun spot cycle. Variations of A_p from the sun spot and semi-annual cycles are mainly due to solar flares, coronal holes, disappearing solar filaments, and the near Earth solar wind environment [36,74]. Intense geomagnetic activity at the auroral zones affects the shape of the atmosphere and makes atmospheric density dependent on latitude [23].

Planetary geomagnetic indices k_p and a_p are compiled using measurements from eleven observatories which lie between 46 N and 63 S latitudes; 3 of these in the United Kingdom, 2 are in Canada, 2 are in the USA, and the remaining four in New Zealand, Australia, Sweden, and Denmark. The most accepted compilation of the measurements from these observatories is created by the Institut fur Geophysik, at Gottingen University, Germany [39].

5.3   Confidence in Forecast

Upper and lower confidence limits for the acceleration due to atmospheric drag are required to determine a conservative time and magnitude of an orbit maintenance burn. When calculating the epoch of a maintenance burn, it is good to assume an upper bound for drag to ensure that the ground track of the satellite does not go beyond the lower ground track boundary before the maintenance burn takes place. In addition, it is wise to use a lower bound of the atmospheric drag to determine the magnitude of the burn. If the actual atmospheric density is less than the density used in calculating the magnitude of the burn, then the ground track will exceed its upper

boundary and an unplanned and unwanted retrograde burn would be required to set the ground track within its nominal bounds.

As seen in Equation 5.1, the acceleration due to drag is proportional to the coefficient of drag, C_D, and the atmospheric density, ρ. In principle, confidence limits of the forecasted atmospheric drag could be inferred from statistics on $F_{10.7}$ and A_p, but this approach is difficult since atmospheric models are complicated and the independence of the variables $F_{10.7}$ and A_p can not be assumed. Research for the TOPEX/POSEIDON mission assumes that k_p variations are independent of $F_{10.7}$ variations. Reference [6] infers this from observing actual values for the solar flux and geomagnetic activity. It is not stated, however, if this assumption is possible because of the high altitude of TOPEX. In an alternative method, nominal density predictions could be used together with upper and lower estimates for the drag coefficient; C_D could be varied using $1\,\sigma$ estimates from current orbit determination or longer term statistics on C_D. Neither of these methods seems very reliable. The method used in this thesis to determine upper and lower confidence limits of atmospheric drag is to use long term statistics of the atmospheric density as modeled to determine upper and lower estimated limits of the forecasted density.

5.3.1 Soviet Density Model

The LANDSAT 6 mission will use a Jacchia-Roberts density model in determining the maintenance burns needed for stationkeeping. Currently, there is not a standalone program for Jacchia-Roberts density evaluation at Draper Laboratory. A simple Soviet density model [85] is used in this thesis to determine a first approximation to the density confidence interval. This Soviet density model was successfully used in previous LANDSAT 6 research. The variability in the Soviet model gave a 1σ prediction error similar to the position error of actual data calculated with a Harris-

Priester density model [13]. This Soviet model was also compared to the Jacchia 1971 density model and found to differ only 5-10% [86]. A future study will employ the method used here with the Jacchia-Roberts density model. The difference between the confidence interval determined here and that determined by the Jacchia-Roberts model is not anticipated to exceed 10%.

The Soviet model was constructed from observations of the orbit motion of the Soviet Kosmos satellites. This model includes the dependence of the density on solar flux and geomagnetic activity as well as the diurnal and semi-annual density variations. This model is recommended for satellites in the altitude range of 160-600 km. Since the LANDSAT 6 mission altitude is 700 km, the application to this mission is necessarily tentative.

The Soviet formula models the actual atmospheric density as a product of five factors, where each factor corresponds to a particular density variation [85]:

$$\rho = \rho_n k_1 k_2 k_3 k_4 \tag{5.2}$$

where ρ_n is the night time density profile assumed to be exponentially decreasing with respect to altitude:

$$\rho_n = \exp[a_1 - a_2(h - a_3)^{\frac{1}{2}}] \tag{5.3}$$

The coefficients in this expression were determined empirically and are listed in Table 5.1. The altitude of the satellite in km is listed as the variable h.

The k_1 factor in Equation 5.2 represents the dependence of the atmospheric density on the solar flux $F_{10.7}$. The factor k_2 accounts for the diurnal effect and k_3 takes into account the semi-annual effect of the density variation. The factor k_4 represents the effect of geomagnetic activity index a_p [85]. In determining the confidence interval, only daily averages of the density are needed and the dependence on the semi-annual cycle is not needed if the error of the predicted density is normalized by the predicted

nominal density. This normalization not only makes the density a stationary process, but also removes the need for the inclusion of the night-time density, ρ_n, in the calculations [13]. The k_1 and k_4 factors given below were the only factors used in this thesis:

$$k_1 = 1 + \frac{(b_1 + b_2 h)(F_{10.7} - \bar{F})}{\bar{F}} \tag{5.4}$$

$$k_4 = 1 + (e_1 + e_2 h) \ln\left(\frac{a_p}{\bar{a}_p}\right) \tag{5.5}$$

where the e and b coefficients are listed Table 5.1. The variable $\bar{F}$ represents the mean solar flux for the period looked at. The Soviet density model only allows for a mean solar flux of 75, 100, 125, or 150. Thus, the actual average solar flux must be rounded to one of these values. The term $\bar{a}_p$ represents the mean geomagnetic index dependent on the mean solar flux which is shown in Table 5.1.

Table 5.1. Soviet Density Model Parameters

	Value with $\bar{F} =$			
	75	100	125	150
a_1	-14.030	-15.095	-17.028	-16.072
a_2	0.9108	0.8299	0.7198	0.7155
a_3	59.77	68.92	93.36	70.33
b_1	-0.630	-0.750	-0.710	-0.765
b_2	0.00506	0.00560	0.00562	0.00571
e_1	-0.132	-0.130	-0.128	-0.115
e_2	0.00108	0.00104	0.00095	0.00089
$\bar{a}_o$	2	2	3	4

5.3.2 Algorithm for Upper and Lower Bounds of Interval

In the Draper version of the Goddard Trajectory Determination System (Draper GTDS), the magnitude of the acceleration due to drag is calculated:

$$a_{drag} = \frac{1}{2}C_D(1 + \epsilon)\rho\frac{A}{m}|v_{rel}|^2 \qquad (5.6)$$

where the variables are the same as in Equation 5.1 with the exception of ϵ which is a correction factor. Often orbit determination runs are done with the coefficient of drag, C_D, held constant and the density, ρ, given by a fixed atmospheric model; the correction factor, ϵ, which is nominally zero, can be solved for in the differential correction to better approximate the actual density encountered. The proposed mission planning software for LANDSAT 6 will use the variable ϵ as an instrument to adjust the density to the upper and lower confidence limits.

$$\rho_{up} = (1 + \epsilon_{up})\rho_{nom} \qquad (5.7)$$

$$\rho_{low} = (1 + \epsilon_{low})\rho_{nom} \qquad (5.8)$$

where ρ_{nom} is the nominal predicted density, ϵ_{up} and ϵ_{low} are the upper and lower confidence limits for the *normalized density error*, and ρ_{up} and ρ_{low} are the resulting upper and lower confidence limits for the density. Note that is is assumed that the value ϵ_{low} is negative.

The normalized density error is calculated:

$$\epsilon_l^{norm} = \frac{\rho_{act} - \rho_l}{\rho_l} \qquad (5.9)$$

where ρ_l is the atmospheric density calculated from the predicted solar flux and geomagnetic activity indices for a particular number of days in the future, l, and ρ_{act} is the density calculated from the actual measured solar flux and geomagnetic data for that day. The National Oceanic and Atmospheric Administration (NOAA) publishes

the predicted solar flux and geomagnetic activity index pairs weekly for up to 27 days in the future. Thus, the possible latency of a forecast, l, ranges from 1 to 27. The predicted values of the solar flux can often be normalized to account for the varying distance of the Earth from the sun. This thesis uses *un-normalized* values of the solar flux since the omission of the k_3 factor in the Soviet density model averages out that semi-annual cycle and it was decided that double averaging would not ameliorate the calculated output. It can be seen from Equation 5.9 that the absolute lower limit of the normalized error is negative one and the absolute upper limit is not defined.

To determine the density confidence interval, the upper bound would be set so that some percentage, P, of the normalized errors lie below that bound. The lower bound would be set so that the same percentage, P, would lie above that bound. This method does not ensure that the bounds will be symmetric about the mean normalized error. In LANDSAT 6, the percentage, P, is required to be 97.3% and is the value used here in this thesis.

One undetermined variable of the method discussed above is the length of time over which the density will be looked at to determine the upper and lower bounds. A long sample period is recommended to increase the reliability of the statistics, but the solar cycle upon which the solar flux and geomagnetic indices are dependent is not a stationary process, ie. the error of the predictions will change over the time of the cycle. In this non-stationary case, the use of a small sample size is recommended.

Method 1, which assumes that the normalized error creates a stationary solar cycle, examined solar flux and geomagnetic data from 1986-1990. For the non-stationary case, Method 2, only data for 1990, the most recent completed previous year, was analyzed, since this year has the closest ties to 1992, the first year of the LANDSAT 6 mission.

5.4 Results

The actual solar flux and all predicted values were received from the Jet Propulsion Laboratory (JPL). The actual solar flux values were compiled for the years 1986-1990 from the *Preliminary Report and Forecast of Solar Geophysical Data (PRF)* published weekly by the National Oceanic and Atmospheric Administration (NOAA). Data was given for previous years but the year 1985 was missing many data points due to magnetometer outages, therefore 1984 and 1985 were not included. The 27 day forecast solar flux data is also predicted weekly by NOAA in the same publication and was compiled by JPL. The actual values for the geomagnetic daily planetary amplitude, A_p, used in this thesis were received from the National Geophysical Data Center, a division of NOAA. This data was deemed more accurate than the data from JPL, since the A_p averages from NOAA included measurements from remote stations and the geomagnetic index used, A_p, was consistent throughout all of the years. The information from JPL began with actual values for the A index, which is determined from the high latitude observations from Anchorage. This index is similar but not identical to the planetary amplitude, A_p, needed by the Soviet density model. This data was placed in files as flat matrices, ie. the same number of columns in each row, for access by a MATLAB script file.

The Soviet density model was programmed as a function to be used by a MATLAB script file.

5.4.1 Method 1

This method assumes that the normalized error is stationary over the solar cycle. Therefore, more reliable statistics can be taken by using a longer time period. In this thesis, all of the available data was used, ie. 1986 - 1990. This method determines

114

the normalized errors for all of the data and then chooses the upper and lower bounds for each latency day to match the required percentages.

There was a small problem with the Soviet density model in the year of 1988. This year started with fairly low values of the solar flux and then reached extremely high values towards the end of the year as the solar maximum approached. This caused negative values of density to be calculated in the beginning of 1988. Hence, 1988 was split and the densities calculated for each half using the appropriate mean solar flux value for that half. This resolved the problem.

The graph of the normalized error limits can be viewed in Figure 5.1. This data
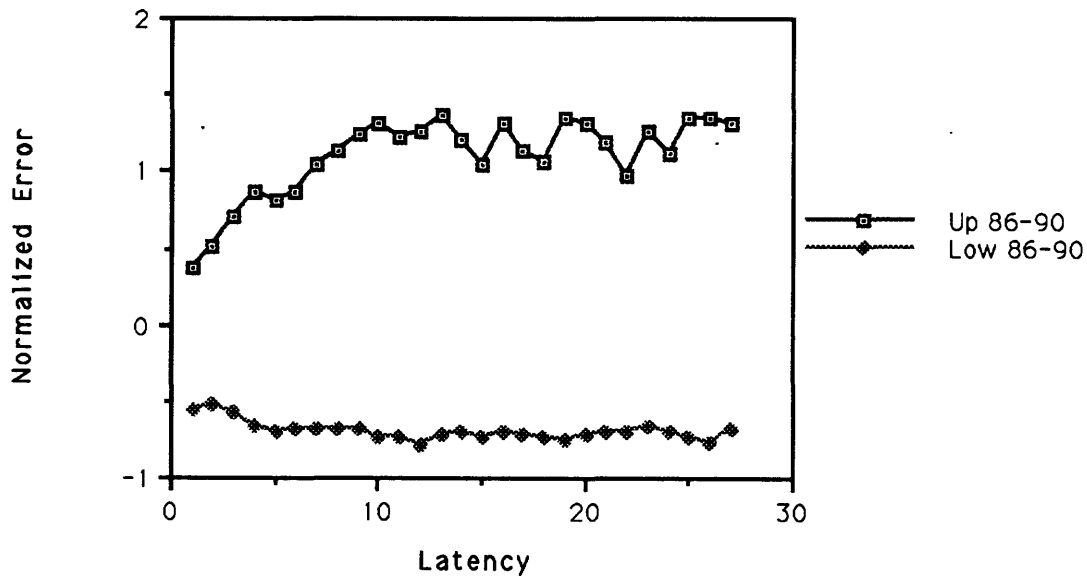

Figure 5.1. 1986-1990 Upper and Lower Limits of Confidence Interval

is very noisy but the general trend increases as the latency of the forecast increases. This general trend can be viewed in Figure 5.3.

5.4.2 Method 2

The second method uses the most recent year of available solar flux and geo-magnetic data, 1990, to determine the difference between the predicted and actual densities. These errors are normalized and then the confidence interval determined. These bounds could then be used in Equations 5.7 and 5.8.

This method assumes that for missions like LANDSAT 6, where the 11 year solar cycle is declining, the previous year of data would provide a conservative estimate of the current density confidence interval. This method also assumes that the normalized error is accurate for only one year, which is more accurate than the assumption in Method 1. Method 2 should be repeated approximately yearly throughout the mission lifetime to determine the new confidence interval limits using data from the previously completed year so that the method assumptions are not violated and the best results achieved. In actuality, this could be repeated at anytime when it is determined that new limits are needed.

The upper and lower limits of the confidence interval can be viewed in Figure 5.2. This data is even more noisy than that calculated for 1986-1990 in Method 1. This was to be expected since 1990 is near the solar maximum and the errors in the forecast are more extreme. Again, the general trend of the confidence interval is to increase as the latency of the forecasted data increases as was expected. This can be viewed in Figure 5.3.

5.5   Conclusions

As stated previously, the results of both methods can be compared in Figure 5.3.

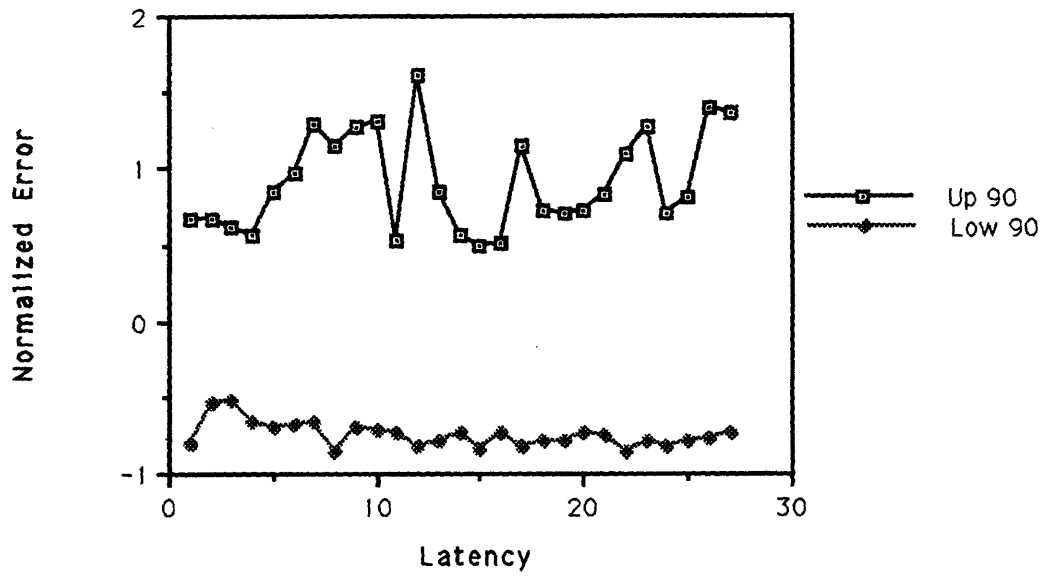The actual equations for these general trends can be found in Table 5.2. where

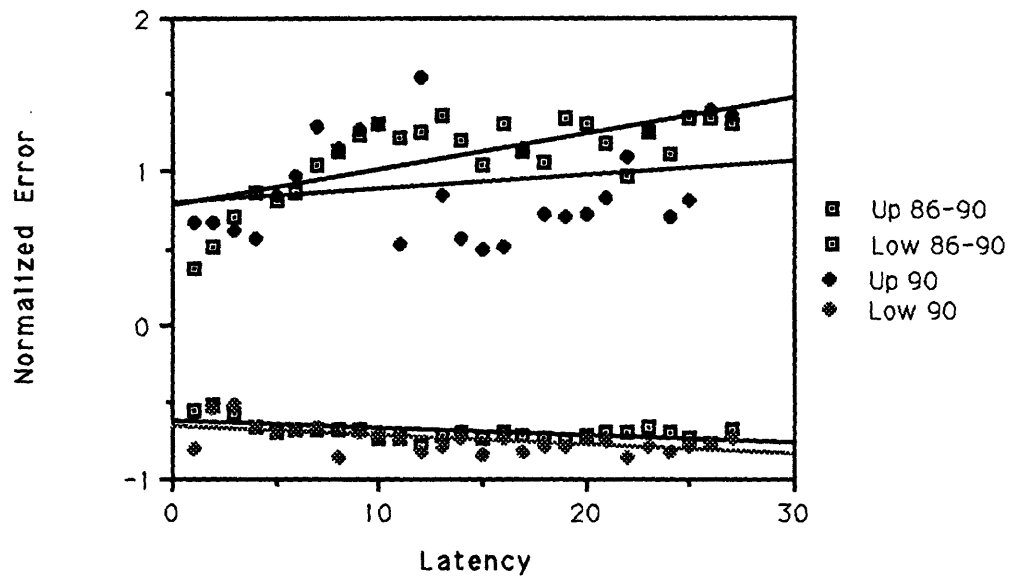**Figure 5.2.** 1990 Upper and Lower Limits of Confidence Interval

Figure 5.3. Upper and Lower Limits of Confidence Interval

117

Table 5.2. Equations for Trends of Upper and Lower Limits

1986-1990	$\epsilon_{up} = 0.77288 + 2.3144 \times 10^{-2}l$
	$\epsilon_{low} = -0.62798 - 4.5675 \times 10^{-3}l$
1990	$\epsilon_{up} = 0.78666 + 8.9609 \times 10^{-3}l$
	$\epsilon_{low} = -0.66662 - 5.5858 \times 10^{-3}l$

l is the latency value of the forecast, $1 < l < 27$. These general trends are better estimations of the actual upper and lower limits of the density since they are smoother and are not dependent on the exact error that might be specific to a certain year.

The confidence interval found for the cumulative years of 1986-1990 in Method 1 gives a slightly more conservative estimate. Although the lower limit for Method 1, is slighlty higher than the lower limit for Method 2, their difference is negligible and the lower limits for both methods are approximately equal. Therefore, it is recommended that the 1986-1990 limits define the confidence interval implemented for LANDSAT 6. If it is found during the mission lifetime that these limits are too conservative, the results from Method 2 could be substituted. It is better to start out the mission with a limit that is too conservative requiring many orbit adjust burns and then switch to a looser estimate. If the initial confidence interval used is too narrow, the bounds of the ground track could be violated and the mission endangered.

Because of the makeup of the Draper Semianalytic Theory Standalone Propagator, it is desired that the upper and lower limits be a constant rather than varying with the forecast latency. In this case, it is advised that the limits for the 27th day of the forecast be used, since these values are the most conservative. Again, these may be changed if they are found to be too conservative during the mission lifetime.

One foreseeable problem with choosing the most conservative confidence interval is that the lower limit might equal approximately zero, causing the lower limit of the

density to be no atmospheric density. This could result in convergence difficulties in the Draper Semianalytic Theory Standalone. If this occurs, it is suggested that a slightly increased lower limit be selected. But in the analyses above, this problem was not encountered, thus the actual lower limit is recommended.

Chapter 6

Results and Conclusions

This thesis provides a starting point for research and development involving maneuver planning with a semianalytic satellite theory. The common orbit constraints of sun synchronous, repeat ground track, and frozen orbit were discussed in the context of maneuver planning. Since drag is the most uncertain acceleration that perturbs these constraints from their nominal positions, a confidence interval for the atmospheric density was determined using solar flux and geomagnetic data in a simple but fairly accurate density model. This chapter concludes this thesis by recommending a density confidence interval for use in a semianalytic satellite theory orbit propagator. In addition, several topics are suggested for further research.

6.1 Maneuver Planning Software Tools

As discussed in Chapter 2, a semianalytic propagation theory combines the speed of an analytic theory but retains the accuracy of a numerical theory. Thus, the semianalytic satellite theory serves as an excellent candidate for application to a maneuver planning process. The Draper Semianalytic Satellite Theory Standalone Propagator is not only fast and accurate, but it is portable to many computing environments.

Program MEANELT is an excellent tool for maneuver planning but has a few problems if the satellite is not in a geosynchronous orbit. This difficulty occurs if the maintained longitude of the ascending node needs to be calculated more than once per day, as in a low altitude satellite. This problem for repeat ground track orbits may be avoided by maintaining the semi-major axis which is the primary variable in the longitude of the ascending node rate.

It is recommended that analytic equations be placed in the Draper Semianalytic Satellite Theory to model the variable thrust throughout the entire burn. These models will be initialized with an impulsive burn and then optimized so that the actual burn achieves the desired change in the orbital elements. Expressions for these impulsive burn parameters can be found in Chapter 4 and the analytic thrust equations can be found in references [67,59].

6.2 Density Confidence Interval

In forecasting the ground track drift, the most uncertain perturbing acceleration is drag. Therefore, in planning an orbit adjust burn, the upper limit of drag must be used to plan when to start the burn so that the eastern ground track limit is not exceeded. The lower limit for drag must be used to determine the magnitude of the burn so that the western ground track limit is not exceeded. It is recommended that atmospheric drag be adjusted using upper and lower limits of the atmospheric density determined from the calculated normalized error from all the available data from previous years. In this case, the years 1986-1990 were used. The upper and lower limits will change for the number of days in the future that the predicted values of solar flux and geomagnetic activity forecast; this is called the forecast latency. This change in the limits for each latency can be fairly noisy, see Figures 5.1 and 5.2. The general trend of the limits for the year of 1986-1990 can be observed in Figure 5.3. The

equations for this general trend are listed in Table 5.2. Since the Draper Semianalytic Standalone Propagator requires a constant value, the most conservative estimate is desired. Thus, the 27 day latency limits for 1986-1990 are recommended. If these values are found to be too conservative in estimating the atmospheric drag on the satellite during the mission, they may be lowered to the limits determined for the year of 1990 alone. It is better to start out too conservative and adjust to lower values to ensure that the ground track boundaries are not exceeded.

6.3 Suggested Further Research

The accuracy and successful application of the Draper Semianalytic Standalone Propagator has been established. But now, it must be applied to the actual LANDSAT 6 mission to prove its success at real time maneuver planning. In addition, the application of repeat ground track and frozen orbits to multiple satellites should be investigated as a simple and accurate means of constellation management.

Program MEANELT needs extensive remodifications to allow it to simulate low altitude orbits, as is common for Earth Observation satellites.

The Soviet density model gives a reasonable first estimate of the confidence interval limits expected for satellites near the LANDSAT 6 altitude of 700 km. These limits could be verified and improved by using the same methodology but applying a dynamic atmospheric model, such as Jacchia-Roberts, to determine the atmospheric density from the forecasted and actual values of solar flux and geomagnetic activity.

Appendix A

Orbital Elements

A.1 Keplerian Orbital Elements

The Keplerian orbital element set, often called the classical orbital elements, are the commonly used to describe an orbit. These parameters, stated in Table A.1 allow the orbit to be 'seen' graphically. Sometimes the true anomaly, f, is used instead of the mean anomaly, M.

Table A.1. Keplerian Orbital Elements

a	= semi-major axis
e	= eccentricity
i	= inclination of the orbit with respect to the equatorial plane
ω	= argument of perigee measured from the line of nodes in the orbital plane
Ω	= longitude of the ascending node measured from the vernal equinox in the equatorial plane
M	= mean anomaly measured from perigee to mean satellite position in orbit, as if the satellite had constant velocity throughout the orbit period

The semi-major axis, geometrically, is half of the major axis of the elliptical orbit. The semi-major axis determines the size of the orbit, while the eccentricity determines the shape of the orbit. The range of values for the semi-major axis and eccentricity

Table A.2. Ranges of Semi-major Axis and Eccentricity

Conic Type	Semi-major Axis	Eccentricity
Circle	$a > 0$	$e = 0$
Ellipse	$a > 0$	$0 < e < 1$
Parabola	$a = \infty$	$e = 1$
Hyperbola	$a < 0$	$e > 1$

Table A.3. Orbit Types from Inclination·

Orbit Type	Inclination
Polar	$i = 90°$
Equatorial	$i = 0$ or $180°$
Direct	$i < 90°$
Retrograde	$i > 90°$

work together to form the conic shape that the orbit will take. These ranges for the various types of conic orbits are shown in Table ·A.2.

Perigee is the point closest to the occupied focus of the elliptical orbit, ie. the Earth. The line of nodes is defined by the intersection of the Earth's equatorial plane and the satellite's orbital plane. It is at this point that the angle between these two planes is measured to determine the orbital inclination. The inclination is always in the range: $0 < i < 180°$. To avoid any ambiguity of which angle is correct, the inclination is measured as the angle between the perpendiculars of the planes, ie. the z-axis of the Earth and the angular momentum vector for the orbit determined by the right hand rule. Common orbit names determined by the type of inclination are stated in Table A.3.

The vernal equinox, in the equatorial plane, is always defined as the direction to the star of Aries. The Earth Centered Inertial (ECI) coordinate system uses this direction to orient its x-axis. The z-axis is defined to be perpendicular to the equatorial

126

plane and the y-axis is defined to be orthogonal to the other two axes. This common coordinate system is considered sufficiently inertial for satellite systems orbiting the Earth. An illustration of the ECI coordinate system is depicted in Figure A.1.
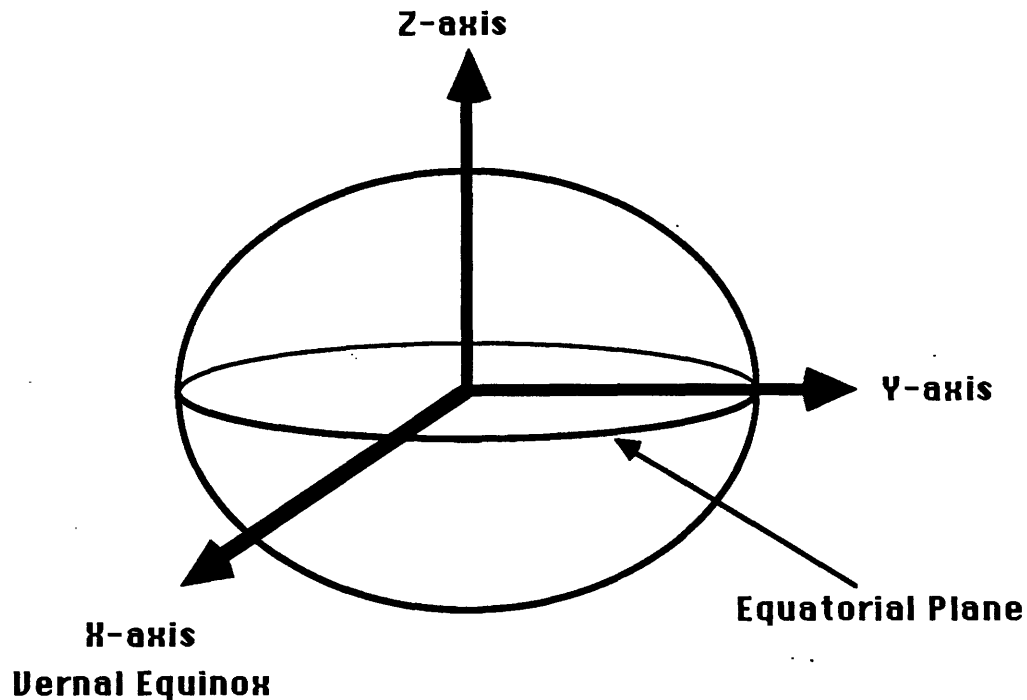
Figure A.1. Earth Centered Inertial Coordinate System

A.2 Equinoctial Orbital Elements

The equinoctial orbital elements, in terms of the classical Keplerian orbital elements are stated in Table A.4. The parameters h and k are the components of the eccentricity vector measured from the vernal equinox in the orbit plane. The variable λ is the 'fast' parameter of the equinoctial element set and is the mean longitude of the satellite. The equinoctial orbital elements are free of singularities in the Variation of Parameters equations of motion. The common Keplerian element set runs into division by zero for values of eccentricity and inclination approaching zero when using these equations. The only complication for the equinoctial element

Table A.4. Equinoctial Orbital Elements

$$a = a$$

$$h = e\sin\left(\omega + I\Omega\right)$$

$$k = e\cos\left(\omega + I\Omega\right)$$

$$p = \tan\frac{i}{2}\sin\Omega,\ I = 1$$
$$\quad = \cot\frac{i}{2}\sin\Omega,\ I = -1$$

$$q = \tan\frac{i}{2}\cos\Omega,\ I = 1$$
$$\quad = \cot\frac{i}{2}\cos\Omega,\ I = -1$$

$$\lambda = M + \omega + \Omega$$

$$I = \pm 1$$

set exists in setting a retrograde factor, I. This retrograde factor can equal positive one for direct equinoctial elements where values of inclination are $0° \leq i < 180°$. The retrograde factor can also have a value of negative one for retrograde equinoctial elements where values of inclination are $0° < i \leq 180°$. The direct and retrograde prefix in the equinoctial element set is motivated by the exact limits of the inclination. This definition is different than the Keplerian element set where the general range of values of inclination determines the prefix.

Appendix B

Porting the DSST Standalone to Non-IBM Mainframe Environments

B.1 VAX

The Draper Semianalytic Satellite Theory (DSST) Standalone is stored in the resident IBM 3090 mainframe at Draper Laboratories in data sets LWE1122.SAST.FORT and LWE1122.EVAL.FORT. This was successfully ported to a VAX 8650 by David Carter [12]. He made several modulations to the program to make the program compatible with VAX FORTRAN.

The VAX VMS operating system is not compatible with file names with the character# in them. For greater portability, it is wise not to use any special characters in source file names.

The VAX default compiler switch for double precision is D_FLOATING. This is not compatible with the exponents stated in the SLP data sets. to avoid this problem, the Standalone *must* be compiled using the /G_FLOATING compiler switch.

In a **CALL** statement, hard coded constants in a calling sequence can not be changed inside of the subroutine.

Instead of using **DEFINE FILE** to define a unit number for an input or output

file, the **OPEN** statement is the correct method to define a file in VAX FORTRAN. Specific to the DSST Standalone, units 14, 38, and 78 are the only direct access files needed to define the minimum standalone package.

Quadruple precision float variables are not supported in standard FORTRAN 77 as they are in the IBM version of FORTRAN. In the Standalone, these variables are stated but not used.

Unique to the Standalone, two subroutines, RDNUMR and QREAD, were deleted since no other subroutine called them and they used quadruple precision numbers.

In the case of reading a direct access file, specifically in subroutines EVAL and TCWF, the IBM apostrophe construction must be replaced by **,REC=** .

All **COMMON** and **EQUIVALENCE** declarations must precede **DATA** statements.

All **BLOCK DATAs** must be named in their definition in every subroutine.

Specific to the Standalone, an **IMPLICIT DOUBLE PRECISION (A-H,O-Z)** in **BLOCKDATA MACHIN** was needed for a successful run of the Standalone.

There are machine specific parameters in the VAX that are different than the IBM mainframe, ie. minimum, maximum, null, etc. In the Standalone, these parameters are in **BLOCKDATA MACHIN** and parameters such as **RELMAX, RELMIN,** and **RELNUL** need to be changed. The values specific for the computer that is worked on can be found in its manual [12].

B.2   IBM PC

David Carter proved that it is a very simple procedure to port a program from an IBM mainframe to an IBM PC using Lahey FORTRAN [12]. To support this port, the following listed modifications along with all of the modifications for the VAX port were needed.

For proper execution, the Lahey FORTRAN necessitates the use of **FILE=...** in the **OPEN** statements.

A file can not be connected in Lahey FORTRAN on the IBM PC unless it has first been opened. In the Standalone, an **OPEN** and **CLOSE** statement were needed in **INREAD** to connect the Newcomb operator file.

If the Extended Memory version of Lahey FORTRAN is used, then there is no need to downsize the **COMMON** blocks. This version of the Standalone will need 1.6 Megabytes to run successfully. The small compiler may be used if the **COMMON** blocks are downsized and this version runs with only 600K [12].

B.3   Sun SPARCstation

The Draper Semianalytic Satellite Theory (DSST) Standalone was ported from the VAX to a Sun SPARCstation 1 (OS version 4.03 Sun4C, F77 Sun release 4.0) by David Carter with help from David Kang. This port took approximately 2 hours. The Standalone default test case output from the Sun was compared with the output from the VAX and the data agreed to the twelfth decimal place. The modifications to successfully port the Standalone are listed in the paragraphs below.

Any **RECL** specifications in direct access **OPEN** statements must be changed from 4-byte convention (required by VAX) to 1-byte convention (standard).

The Sun requires that FORTRAN files end with a .f rather than a .for.

The data files, **SLP1950**, **SLPTOD**, **NEWCOMB**, and **TIMECOEF**, must be rewritten so that they are in the correct Sun form. This is accomplished by running the rewrite programs **writslp.f**, **writtim.f**, and **writnukes.f**. On the Sun, the SLP program can be compiled and linked in one step by typing **f77 writslp.f**, with creates an executable file named **a.out** and can be run by typing its name and pressing **RETURN**. This procedure is repeated for each of the remaining data files

131

needed.

Sun FORTRAN does not allow a block data subprogram to have the same name as its associated **COMMON** block. The name of each **BLOCK DATA** was renamed to end in the character **$**.

All of the subroutines were compiled but not linked by using the wild card command **f77 -c *.f** after temporarily changing the name of the main program, **semi-anal.f** so that is would not be compiled with the others.

Large subroutines may need to be compiled using the compiler switch **-Nq999** if a regular compilation fails because of symbol table overflow. This compiler option allows more symbols.

The main program was compiled and linked with all of the subroutines using the command **f77 *.o semianal.f**. The executable code, **a.out** was renamed **semianal** with the command **mv a.out semianal**. The output from a run was commanded to be printed to a file named **aero.out** by typing **semianal aero.out**.

All of the source code, object files, binary data files, and the executable code was written to a cartridge tape using the command **tar -cv *** [11].

B.4   Macintosh PC

There are many FORTRAN compilers on the market for the Macintosh computer, but the only one found that could manage a large number of subroutines was Absoft's MacFortran II that is used as a tool in the Macintosh Programmers Workshop (MPW) from Apple. Others that failed in handling a large program ported from the VAX were Absoft's MacFortran in MPW and Mactran Plus from DCM Data Products. Mactran Plus by DCM Data Products had several bugs in it that severely limited the number of subroutines and libraries allowed. In addition, their Technical Help Department was not well organized, knowledgeable, nor understandable. MacFortran,

by Absoft, which also runs in MPW like MacFortran II, had bugs that interfered with data stored in common blocks [46].

B.4.1   To Install MPW

The MPW MacFortran II program can be bought from Absoft Corporation for $595.00. To install the application on the hard drive of a Macintosh computer, first copy the Installation Folder from the first disk to the folder named MPW, on the hard drive.

Open the Installation Folder on the hard drive and launch the file **MPW Installer (Launch Me)**

Click the **NO** button at the Update Alert to install MPW.

Insert and confirm each of the remaining MPW disks (all except the first disk) and click the **YES** button at **More MPW Disks** dialogs that will appear. Each file, as it is being copied to the hard drive, is listed and each disk will be ejected automatically.

Click the **NO** button at the **More MPW Disks** dialog after installing the last of the MPW disks.

Click the **OK** button at the **Update Complete!** dialog.

Throw away the Installation Folder by dragging its icon to the trash can. It is OK to throw away the applications in the Installation Folder.

Open the MPW Folder on the hard drive and launch the file **MPW Shell**.

Type **SetupMacFortran** on a line by itself in the Worksheet window followed by pressing **ENTER.**

At the **Remove Build and Project menus?** dialog, click the **NO** button.

Quit MPW by selecting the **QUIT** command in the **FILE** pull down menu [47].

B.4.2 Changes Needed to Port a Program

To port a program from a VAX to the Macintosh, there are a few changes that will be needed to get it running in MacFortran II.

All of the common blocks must be the same size as their associated block data set.

Any **RECL** specifications in direct access **OPEN** statements must be changed from 4-byte convention (required by VAX) to 1-byte convention (standard) as in the Sun SPARCstation.

The reserved unit numbers for standard input and output are listed in Table B.1.

Table B.1. MacFortran II Reserved Unit Numbers

UNIT NUMBER	STANDARD
5	input
6	output
9	i/o
*	i/o

It is easier to manage a large program that will be repeatedly modified if the compile and link statements are kept in a .make file that can be rebuilt any time. To do this, just use the **BUILD** pull down menu and select **MAKE BUILD COM-MANDS...** then double click on the files that you want linked together. This will automatically create the .make file and the compiler and linker options will have to be manually added. This is convenient if a subroutine is modified, since the program can be easily rebuilt by selecting **BUILD** under the **BUILD** pull down menu and typing in the name of the .make file and the .make file will automatically recompile any subroutines that have been modified since the last build and then will relink them together and create executable code or a program application. The only change that

will have to be made to the subroutines to accomplish this is all FORTRAN files must end in .f, not .for as in the Sun SPARCstation.

The block datas in separate files must be listed first in the link line listing whether a manual link or a link in a .make file is being applied.

The compiler options used to successfully port a program from the VAX are listed in Table B.2. Checking the array boundaries and enabling the alignment warnings are

Table B.2. Compiler Options

Option	Description
-C	Check array boundaries
-A	Enable alignment warnings
-N8	Autosegmentation
-f	Fold to lower case
-s	Static storage

not necessary but are beneficial to have when first trying to port the program. They ensure that the disk space allocated for the program stays intact and does not overflow into other applications if an array exceeds its boundaries. The autosegmentation is needed for a program with many subroutines of varied lengths. If this option is not used, the linker may give an error of a jump step being too large. The fold to lower case and static storage options are needed by programs ported from the VAX and IBM mainframe. The MacFortran II compiler is case sensitive to the type in variable names unless fold to lower case is used and the storage of variables in subroutines is different from the VAX and IBM mainframe if the static storage option is not used.

One other compiler option that can be used is -N9. This option allows for more checks for the propellor period command to stop executing a program. This option is not compatible if the program contains computed GOTO's.

The linker options that were successfully used are listed in Table B.3.

135

Table B.3. Linker Options

Option	Description
-o *name*	Name of executable file
-d	Suppress duplicate symbol definition
-f	Largest common used
-mf	Use Multifinder memory
-ss 1000000	Segment size maximum
-srt	Sort near/far files

After the program works, optimization options can then be added. These optimizations will increase compiler time but will decrease runtime. The compiler options -C and -A can be deleted to decrease the compiler time after the program works.

Large tools, ie. straight executable code, made by MPW share memory with the MPW application, thus they may not even be able to load - so it is better to make a large program into an application. Also, the default for applications made in MPW is that they are automatically linked with the MacFortran Runtime Window Environment (MRWE). If any data is printed to the screen, a window is automatically opened with save and print menu items at the top of the screen.

A **PAUSE** rather than a **STOP** at the end of the program for the application is helpful if any data is written to the screen. By adding a pause, the window will stay open so that the data can be viewed and either saved in a file or printed by using the menu commands.

If an application is not running correctly, try allocating more memory to the application by using the **Get Info** command.

The debugger SADE is extra. If it is used, SADE can only run under Multifinder but large programs can usually only be compiled and linked under Finder.

Source lines can be shown by clicking on an error message during compilation.

f77 Option-X.f compiles all .f files in the current folder and creates an application.

Option-X matches any string of 0 or more characters. **?** matches any single character.

Search -i/ *word* **/** *file...* searches through files for *word* and prints out the file and line number.

Option-d is the line continuation character for MPW commands typed into the worksheet [46].

B.4.3   Port of DSST Standalone

The Draper Semianalytic Standalone Orbit Propagator (DSST Standalone) was ported from the IBM 3090 to the VAX as discussed above. Downloaded from the VAX, the Standalone was ported to a Macintosh IIci. The DSST Standalone was successfully run using the default test case. The Macintosh IIci output was manually checked with output from the VAX and the values were found to correlate up to the ninth decimal place. The porting was finalized on December 11, 1990 after six month's work of trial and error. Now that a FORTRAN compiler for the Macintosh has been found to work, a port of another program would only take a few hours.

The DSST Standalone and the needed input files can be stored on six high density disks. The Standalone application has been modified to include namelist inputs and this section explains how to install the application in a Macintosh and use it successfully.

B.4.4   Needs for Exporting

After installing MPW version 3.1 and MACFORTRAN II on the computer (four disks), create a new folder inside of the MPW folder and name it **STANDALONE f.** Inside of this folder put:

The five name list files:

NLSTELM   (7K)

NLSTFRC   (7K)

NLSTAVR   (7K)

NLSTSP   (7K)

NLSTDRV   (7K)

The four input data files:

NEWCOMB   (315K)

SLP1950   (977K)

SLPTOD   (977K)

TIMECOEF   (21K)

The application :

STANDALONE (343K)

If the actual FORTRAN files are to be included for modification by the user - be sure to include the build file, **STANDALONE.make** (28K). All of the files needed for exporting and the actual FORTRAN files can be contained on six disks.

B.4.5   How to use .make File to Build Application

This program must be built under Finder (as opposed to Multifinder) or MPW will not be able to run the application.

Double click on the MPW SHELL icon and MPW will open up a window with menus at the top.

Pull down the **DIRECTORY** menu and select **SET DIRECTORY**.

Click once on the folder in which the application is stored (In my setup this

is **STANDALONE f**) and then click once on the **DIRECTORY** button (it is highlighted).

Pull down the **BUILD** menu and select **BUILD**. This can also be done by pressing Propellor-**B**.

MPW will then display a prompt window to name the **.make** file to be built, type **STANDALONE** and then press **RETURN**. This will compile any subroutines that have been changed or do not have existing object files. It will then link the files and create the application **STANDALONE**.

After the build is complete, it will return to the MPW window and just press **ENTER** to start the application within MPW.

B.4.6   How to Run Inside MPW

This program must be run under Finder (as opposed to Multifinder) or MPW will not be able to run the application.

Double click on the MPW SHELL icon and MPW will open up a window with menus at the top.

Pull down the **DIRECTORY** menu and select **SET DIRECTORY**.

Click once on the folder in which the application is stored (In my setup this is **STANDALONE f**) and then click once on the **DIRECTORY** button (it is highlighted).

Once the shell returns you to the window type in the name **STANDALONE** and then press **ENTER**.

The information will be printed out to the screen and you may send this to the printer at the end of the program by pulling down the **FILE** menu and selecting **PRINT WINDOW**.

To exit after the program is finished just press **RETURN**.

B.4.7 How to Run as a Standalone Application

Once again, this program must be run under Finder (as opposed to Multifinder) or this program can not be opened.

Double click on the **STANDALONE** icon and MPW will automatically start up the program.

The information will be printed out to the screen and you may send this to the printer at the end of the program by pulling down the **FILE** menu and selecting **PRINT WINDOW**.

To exit after the program is finished just press **RETURN**.

B.4.8 Input Through Namelists

Any data that needs to be changed from the DSST standard test case setting may be set in the namelist files. A namelist can be opened from the MPW shell window by typing **open** *nameofnamelist* and then pressing **ENTER**. Remember that the directory must first be set to the folder that the namelists are stored in, ie. **STANDALONE f**. A namelist file could also be opened with by pulling down **FILE** menu and choosing **OPEN....** MPW will then open up a dialog window in which the file to be opened may be selected and opened by clicking on the **OPEND** button which is highlighted. For reference to variable descriptions of the variables that may be set in the namelist files see Table B.4. One common variable that will be set is the epoch orbital elements. These are set in namelist **NLSTELM**. The default form is for these orbital elements to be Keplerian. They are stored in an array in the following order, semi-major axis, eccentricity, inclination, longitude of the ascending node, argument of perigee, and mean anomaly.

The namelist input format is of the following form:

$name of namelist

Table B.4. Variable Reference

NAMELIST FILE	VARIABLE DESCRIPTION
NLSTELM	setelm.f
NLSTAVR	setavr.f
NLSTFRC	setfrc.f
NLSTDRV	setdrv.f
NLSTSP	setsp.f

member = value,

member = value,

member = value,

$END

The end of the data must be followed by a carriage return so that the end of the file may be detected when executing.

B.4.9   After Application is Finished

After the application is finished, there is a pause at the end so **RETURN** must be pressed to go back to the MPW Shell window. Before **RETURN** is pressed, this is the only chance to view the output from the execution and either save and/or print it.

To quit the MPW Shell, pull down the **FILE** menu and select **QUIT** [47].

Bibliography

[1] W.S. Adams, L. Rider. 'Circular Polar Constellations Providing Continuous Single or Multiple Coverage Above a Specified Latitude,' *The Journal of the Astronautical Sciences.* Vol. 35, No. 2. April-June, 1987. pp. 155-192.

[2] D. Andrews, S. J. Dodsworth, M. H. Mckay. 'Control and Monitoring of ERS-1,' *ESA Bulletin - ERS-1 Special Issue.* #65. European Space Agency: Netherlands. February, 1991. pp. 73-79.

[3] *A Synopsis of the Navy Remote Ocean Sensing system (N-ROSS).* Briefing. RCA Astro-Electronics: Princeton, NJ. July, 1983.

[4] Richard H. Battin. *An Introduction to the Mathematics and Methods of Astrodynamics.* Ed. J. S. Przemieniecki. American Institute of Aeronautics and Astronautics, Inc.: New York, N.Y. 1987.

[5] Bruce Baxter. Personal memo to Paul Cefola. April, 1988.

[6] R. S. Bhat, R. B. Frauenholz, Patrick E. Annell. *TOPEX/POSEIDON Orbit Maintenance Maneuver Design.* Proceedings of 1989 AAS/AIAA Astrodynamics Conference, Paper AAS #89-408. pp. 645-670.

[7] Leon Blitzer. 'Nodal Period of a Satellite,' *AIAA Journal.* Vol. 2, No. 8. August, 1964. pp. 1459-1460.

[8] A. Bobick. *J2-Squared MACSYMA Working Notes.* Draper Laboratory working paper, July, 1981. (Copy Available from Paul Cefola, CSDL).

[9] George H. Born, Jim L. Mitchell, Gene A. Heyler. 'GEOSAT ERM - Mission Design,' *The Journal of the Astronautical Sciences.* Vol. 35, No. 2. April-June, 1987. pp. 119-134.

[10] J. J. Burger. 'ERS-1 Ready for Launch,' *ESA Bulletin - ERS-1 Special Issue.* #65. European Space Agency: Netherlands. February, 1991. pp. 12-15.

[11] David W. Carter. *Port of Semianalytic Satellite Theory to the Sun.* #EGC-90-149. Charles Stark Draper Laboratory, Inc.: Cambridge, MA. May 25, 1990.

[12] David W. Carter. *The Standalone - Notes on Porting to VAX and PC.* Unnumbered memo. Charles Stark Draper Laboratory, Inc.: Cambridge, MA. July 26, 1989.

[13] D. Carter, W. McClain, P. Cefola. *LANDSAT Orbit Determination Study Technical Report.* #CSDL-R-1952. Charles Stark Draper Laboratory, Inc.: Cambridge, MA. March, 1987.

[14] Paul Cefola. *A Recursive Formulation for the Tesseral Disturbing Function in Equinoctial Variables.* AIAA Paper #76-839. August, 1976.

[15] Paul J. Cefola. *Standalone Semianalytical Orbit Propagator Preliminary User Guide and System Description.* #CSDL-C-5719. Charles Stark Draper Laboratory, Inc.: Cambridge, MA. May, 1984.

[16] Paul Cefola, R. Brouke. *On the Formulation of the Gravitational Potential in Terms of Equinoctial Variables.* AIAA pre-print #75-9. AIAA 13th Aerospace Sciences Meeting: Pasadena, CA. January, 1975.

[17] Paul Cefola, Ron Proulx. *Application of the Semianalytical Satellite Theory to Shallow Resonance Orbits.* Paper #AAS 91-139. AAS/AIAA Spaceflight Mechanics Meeting, Houston, TX. AAS Publications Office: San Diego, CA. February 11-13, 1991.

[18] Paul Cefola, Wayne McClain, Mark Slutsky. *Navy Remote Ocean Sensing System (NROSS) Ephemeris Data Processing Trade Study: Technical Operating Report.* #CSDL-R-1863, Charles Stark Draper Laboratory, Inc.: Cambridge, MA. April, 1986.

[19] Robert Chase, Michael Mundt. 'On Optimizing a Constellation of Altimetric Satellites for Measuring Global Oceanic Mesoscale,' *The Journal of the Astronautical Sciences.* Vol. 37, No. 4. Oct-Dec, 1989. pp. 477-489.

[20] P. R. K. Chetty. *Satellite Technology and Its Applications.* Tab Books Inc.: Blue Ridge Summit, PA. 1988.

[21] E. Cutting, G. H. Born, J. C. Frautnick. 'Orbit Analysis for SEASAT-A,' *The Journal of the Astronautical Sciences.* Vol. 26, No. 4. Oct-Dec, 1978. pp. 315-342.

[22] *Defense Meteorlogical Satellite Program (DMSP): Technical Operating Report: Preliminary study for Navy Remote Ocean Sensing System (N-ROSS).* System Engineering Task #0007-11. DMSP Programs Office, RCA Astro-Electronics: Princeton, NJ. April, 1984.

[23] Jean de Lafontaine. *Orbital Dynamics in a Stochastic Atmosphere and a Nonspherical Gravity Field.* Doctor of Philosophy Thesis. Institute for Aerospace Studies, University of Toronto: Toronto, Canada. 1986.

[24] André Deprit, S. Coffey. *The New Face of Artificial Satellite Theory.* Naval Space Command Astrodynamics Conference, Dahlgren, VA. January 30-31, 1991.

[25] Jeff Dozier. 'Editor's Corner,' *The Earth Observer.* Vol. 2, No. 10. December, 1990. p. 1.

[26] Kenneth I. Duck. *Inclination Biases for Sun Synchronous Spacecraft.* United States Memorandum originally from Goddard Space Flight Center #733:73:KID:blb. General Electric Astro-Space Division: Princeton, NJ. April 24, 1973.

[27] Early, Leo W., Jr. *Portable Orbit Generator Using Semianalytical Satellite Theory.* Paper AIAA #86-2164-CP. AIAA/AAS Astrodynamics Specialist Conference: Williamsburg, VA. August 18-20, 1986.

[28] *The Early Earth Observing System Reference Handbook: Earth Science and Applications Division Missions 1990-1997.* NASA, Goddard Space Flight Center.

[29] *Earth Observing System: 1990 Reference Handbook.* NASA, Goddard Space Flight Center. US Government Printing Office. 1990.

[30] *EOS: A Mission to Planet Earth.* NASA, Goddard Space Flight Center. February, 1991. (Copy Available from EOS Program Office, NASA Headquarters (Code EE), Washington, DC. 20546).

[31] 'EOS Panels Meet Jointly,' *The Earth Observer.* Vol. 3, No. 1. January, 1991. p. 7.

[32] David L. Farless. *The Application of Periodic Orbits to TOPEX Mission Design.* Paper AAS #85-301. AAS/AIAA Astrodynamics Specialist Conference: Vail, CO. AAS Publications Office: San Diego, CA. August 12-15, 1985.

[33] James W. Finney. 'Ground Track Repeat Analysis,' *Navy Remote Ocean Sensing System.* 4th NROSS Spacecraft Final Review. Ed. L. Gomberg. RCA Astro-Electronics: Princeton, NJ. March 19, 1985.

[34] Jim Finney. 'N-ROSS Repeating Ground Track Report,' Internal Design Note #DN-N-ROSS. RCA Astro-Electronics Division, Jan 22, 1985.

[35] R. Francis, G. Graf, P. G. Edwards, M. McCraig, C. McCarthy, P. Dublock, A. Lefebvre, B. Pieper, P.-Y. Pouvreau, R. Wall, F. Weschler, J. Louet, R. Zobl. 'The ERS-1 Spacecraft and Its Payload,' *ESA Bulletin - ERS-1 Special Issue.* #65. European Space Agency: Netherlands. February, 1991. pp. 26-48.

[36] A. C. Fraser-Smith. 'Spectrum of the Geomagnetic Activity Index A_p,' *Journal of Geophysical Research.* Vol. 77, No. 22. August 1, 1972. pp. 4209-4220.

[37] E. M. Gaposchkin, A. J. Coster. *Evaluation of New Parameters for Use in Atmospheric Models.* Paper AAS #87-555. Proceedings of 1987 AAS/AIAA Astrodynamics Conference: Kalispell, Montana, MT. AAS Publications Office: San Diego, CA. August 10-13, 1987. pp. 1669-1682.

[38] E. M. Gaposchkin, A. J. Coster. *Evaluation of Recent Atmospheric Density Models.* Paper AAS #87-557. Proceedings of 1987 AAS/AIAA Astrodynamics Conference: Kalispell, Montana, MT. AAS Publications Office: San Diego, CA. August 10-13, 1987. pp. 1669-1682.

[39] *Geomagnetic Indices Bulletin.* National Geophysical Data Center: Boulder, CO.

[40] N. Giescher, W. Schäfer. *The Precise Range and Range-Rate Equipment (PRARE) - A Tool for Enhanced Orbit Determination and Geophysical Applications.* #IAF-84-418. 35th Congress of the International Astronautical Federation: Lausanne, Switzerland. October 7-13, 1984.

[41] 'Go-Ahead for ERS-2,' *ESA Bulletin*. No. 63. European Space Agency: Netherlands. August, 1990. p. 81.

[42] P. J. Hassett, R. L. Johnson. *LANDSAT-5 Orbit Adjust Report*. Contract #NAS 5-27888. Computer Sciences Corp. June, 1985.

[43] R. G. Hopkins. *A User's Guide to Program MEANELT*. Aerospace Technical Memorandum #87(9975)-62. Aerospace Corp.: El Segundo, CA. September 9, 1987.

[44] R. G. Hopkins. *Description of the Astrodynamics Department MEANELT Stationkeeping and Orbit Propagation Capabilities*. Aerospace Technical Memorandum #87(9975)-23. Aerospace Corp.: El Segundo, CA. January 27, 1986.

[45] R. G. Hopkins. *Long Term Eccentricity Control Through Stationkeeping*. Aerospace Technical Memorandum #87(9975)-41. Aerospace Corp.: El Segundo, CA. June 17, 1987.

[46] Carole A. Jablonski. *Porting of a FORTRAN Program from the VAX to the Macintosh Computer*. #EGA-91-09. Charles Stark Draper Laboratory, Inc.: Cambridge, MA. February 12, 1991.

[47] Carole A. Jablonski. *Use of Draper Semianalytic Satellite Theory Standalone on a Macintosh II*. #EGA-91-08. Charles Stark Draper Laboratory, Inc.: Cambridge, MA. February 12, 1991.

[48] Peter E. Jasper. *LANDSAT-D Ground Trace Control*. LANDSAT-D Memo #2040. November 16, 1981. .

[49] Peter E. Jasper. *LANDSAT-D Orbit Adjust Criteria*. #SVS-10265. February, 1982.

[50] Nicholas L. Johnson. *The Soviet Year in Space: 1990*. 10th Edition. Teledyne Brown Engineering: Colorado Springs, CO. February, 1991.

[51] Jean-Patrick Rene Kaniecki. *Short Periodic Variations in the First Order Semianalytical Satellite Theory*. MIT Masters of Science Thesis. Charles Stark Draper Laboratory, Inc.: Cambridge, MA. August, 1979.

[52] Haans K. Karrenberg, E. Levin, R. D. Lüders. 'Orbit Synthesis,' *The Journal of the Astronautical Sciences*. Vol. 17, No. 3. Nov-Dec, 1969. pp. 129-177.

[53] C. C. Kilgus, J. L. MacArthur. *The GEOSAT Mission Radar Altimeter Satellite Program*. IGARSS Presentation, Johns Hopkins University Applied Physics Laboratory. 1984. pp. 787-790.

[54] Joseph C. King. *Swathing Patterns of Earth Sensing Satellites and their Control by Orbit Selection and Modification*. Paper AAS #71-353. Published AAS/AIAA Astrodynamics Specialists Conference: Fort Lauderdale, FL. AAS Publications Office: San Diego, CA. August 17-19, 1971.

[55] *LANDSAT 6 Mission Support Critical Design Review: Volume 2 - Software Design Document*. #EGA-91-021, #L6/MSN-91-015, revision 0. Charles Stark Draper Laboratory, Inc.: Cambridge, MA. March 21, 1991.

[56] Raymond J. Leopold. *Low-Earth Orbit Global Cellular Communications Network.* Presented/Published Mobile Satellite Communications Conference: Adelaide, Australia. August 23, 1990.

[57] A. C. Long, J. O. Cappellari, Jr., C. E. Velez, A. J. Fuchs. *Goddard Trajectory Determination System (GTDS) Mathematical Theory.* Revision 1. #FDD/552-89/001, #CSC/TR-89/6001. Computer Sciences Corporation: Lanham-Seabrook, MD. July, 1989.

[58] Jack B. Lyle. *LANDSAT 6 MSN Functional Requirements Specification.* GE Astro-Space Division: Princeton, NJ. Draft March 31, 1990.

[59] Wayne D. McClain. *Analytic Thrust Model for the Orbital Motion of LANDSAT 6.* #EGB-91-054, #L6/MSN-91-003. Revision A. Charles Stark Draper Laboratory, Inc.: Cambridge, MA. February 20, 1991.

[60] Wayne D. McClain. *A Recursively Formulated First Order Semianalytic Artificial Satellite Theory Based on the Generalized Method of Averaging.* Volume 1. #NASA-CR-156782, #N78-28147, revision 1. July, 1989.

[61] Wayne D. McClain. *Eccentricity Control and the Frozen Orbit Concept for the Navy Remote Ocean Sensing System (NROSS) Mission.* Paper #AAS 87-516. AAS/AIAA Astrodynamics Specialist Conference: Kalispell, Montana, MT. AAS Publications Office: San Diego, CA. August 10-13, 1987.

[62] Wayne D. McClain. *Impulsive Model for Targeting LANDSAT 6 Orbit Plane Maintenance.* #EGB-90-368, #L6/MSN-90-028. Charles Stark Draper Laboratory, Inc.: Cambridge, MA. December 21, 1990.

[63] Wayne D. McClain. *Impulsive Models for Targeting LANDSAT 6 Frozen Orbit Maintenance Burns.* #EGB-91-009, #L6/MSN-91-001. Charles Stark Draper Laboratory, Inc.: Cambridge, MA. January 8, 1991.

[64] Wayne D. McClain. *Impulsive Models for Targeting LANDSAT 6 Groundtrack Maintenance Burns.* #EGB-91-062, #L6/MSN-91-005. Charles Stark Draper Laboratory, Inc.: Cambridge, MA. February 27, 1991.

[65] Wayne D. McClain. *LANDSAT 6 Post Ascent Orbit Determination Study Summary Report.* #CSDL-R-2223, Charles Stark Draper Laboratory, Inc.: Cambridge, MA. January, 1990.

[66] Wayne D. McClain. *Performance of the Finite Burn Propagator over an Extended Burn Interval.* #EGB-91-099, #L6/MSN-91-018. Charles Stark Draper Laboratory, Inc.: Cambridge, MA. April 3, 1991.

[67] Wayne D. McClain. *Thrust Modeling in the Mean Element Propagator.* #EGB-90-260, #L6/MSN-90-006. Charles Stark Draper Laboratory, Inc.: Cambridge, MA. September 20, 1990.

[68] Jim L. Mitchell, George W. Hepburn, Harley E. Hurlbert, Donald R. Johnson, John C. Kinde, J. Dana Thompson. *Recommendations for Orbit Determination Requirements for the Navy Remote Ocean Sensing System (N-ROSS).* Ocean Sensing Division, National Space Technology Laboratories: MS. April 14, 1986.

147

[69] *Monitoring Earth's Ocean, Land, and Atmosphere from Space - Sensors, Systems, and Applications.* Ed. Abraham Schnapf. Vol. 97: Progress in Astronautics and Aeronautics. AIAA: New York, NY. 1985.

[70] *MSN Functional Requirements Specification Update.* General Electric Astro-Space Division LANDSAT #1870, GE Astro Space Division: Princeton, NJ. Nov 12, 1990.

[71] *Navy Remote Ocean Sensing System (N-ROSS).* Ed. J. C. Wilkerson. Naval Research Laboratory: Washington, DC. June, 1985.

[72] 'NASA selects Payload for First EOS Satellite,' *The Earth Observer.* Vol. 3, No. 1. January, 1991. pp. 1-5.

[73] *Navy Statement of Work: DMSP Block 6 Risk Reduction (Phase 2).* RFP #F04701-89-R-0029. Attachment 3. Dec. 3, 1990.

[74] 1st Lt. Philip M. Nostrand. *Forecast Verification of the 10.7 Centimeter Solar Flux and the A_p Daily Geomagnetic Activity Indices.* AFIT Master's Thesis. # AFIT/GSO/PH-OS/84D-2. Air Force Institute of Technology. 1984.

[75] Major Robert D. Prochaska. *Regression versus Forecaster in Predicting Solar 10.7 Centimeter Flux.* Student Report #84-2090. Air Command and Staff College: Maxwell, AFB, AL. March, 1984.

[76] Ron Proulx. *Mathematical Description of the Tesseral Resonance and Resonant Harmonic Coefficient Solve-for Capabilities.* #IOC NSWC-001-15Z-RJP. Charles Stark Draper Laboratory, Inc.: Cambridge, MA. April 13, 1982.

[77] Ron Proulx, Wayne McClain, Leo. W. Early, Jr., Paul Cefola. *A Theory for the Short Periodic Motion Due to the Tesseral Harmonic Gravity Field.* Paper #AAS-81-180. AAS/AIAA Astrodynamics Conference: Lake Tahoe, NV. August, 1981.

[78] E. A. Roth. 'Nodal Period of a Satellite Perturbed by the Earth's Oblateness,' *ESA Journal.* Vol. 7. 1983.

[79] Bruce Shapiro. 'The GEOSAT Orbit Adjust,' *The Journal of the Astronautical Sciences.* Vol. 36, No. 4. Oct-Dec, 1988. pp. 407-424.

[80] Mark Slutsky. *First Order Short Periodic Motion of an Artificial Satellite Due to Third Body Perturbations.* #IOC AOD/SD-021-15Z-MS. Charles Stark Draper Laboratory, Inc.: Cambridge, MA. November, 1982.

[81] Mark Slutsky. *Zonal Harmonic Short Periodic Model.* #IOC PL-016-81-MS. Charles Stark Draper Laboratory, Inc.: Cambridge, MA. November 30, 1981. (see also AIAA Paper #80-1658, 1989).

[82] *Solar Indices Bulletin.* National Geophysical Data Center: Boulder, CO.

[83] Stephen Paul Taylor. *Semianalytical Satellite Theory and Sequential Estimation.* MIT Masters of Science Thesis. #T-757. Charles Stark Draper Laboratory, Inc.: Cambridge, MA. September, 1981.

[84] Robert H. Thomas. *Polar Research from Satellites*. Joint Oceanic Institute, Inc.: Washington, DC. 1991.

[85] M. I. Voiskovskii, I. I. Volkov, N. I. Gryazev, B. V. Kugaenko, V. M. Sinitsyn, P. E. El'yasberg. 'An Aspherical Model for the Upper-Atmosphere Density,' *Cosmic Research*. Vol. 11, No. 1. January-February, 1973. pp. 70-79.

[86] I. I. Volkov, Ye I. Knyazeva, B. V. Kugayenko. 'Refining a Model of Atmospheric Density for Ballistic Calculations,' *Nablyudeniya Iskusstvennykh Nebesnykh Tel (Moskva)*. No. 80. Soviet Union. 1982. pp. 126-135.

[87] Elaine A. Wagner. *Application of the Extended Semianalytical Kalman Filter to Synchronous Orbits*. MIT Master of Science Thesis. #CSDL-T-801. Charles Stark Draper Laboratory, Inc.: Cambridge, MA. June, 1988.

[88] Elaine A. Wagner. 'The Extended Semianalytical Kalman Filter and its Application to Synchronous Orbits,' *The Journal of the Astronautical Sciences*. Vol. 34, No. 2. April-June, 1986. pp. 147-159.

[89] K. F. Wakker, B. A. C. Ambrosious, L. Aardoom. *Precise Orbit Determination for ERS-1*. ESOC Contract #5227/82/D/IM(SC). Delf University of Technology: Delf, Netherlands. August, 1983.